Engineering Synthetic Biology Routes for Protein Analysis using Microfluidic Systems

Thesis by

Bárbara Schlicht

In Partial Fulfilment of the Requirements for the

Degree of Doctor of Philosophy

Glasgow, Scotland

‘This thesis is the result of the author’s original research. It has been composed by the author and has not been previously submitted for examination which has led to the award of a degree.’

28th September 2016

.

To my parents, Rita and Peter and my adoring sister Berthe, for their love, support, inspiration and the values they have taught me.

Abstract

Microfluidics is increasingly being used in many areas of biotechnology and chemistry to achieve reduced reagent volumes, improved performance, integration, and parallelism, among other advantages. The sub-millimetre dimensions of micro-channels tend to reduce reagent consumption and waste production, consequently leading to cost savings and permitting precious samples to be relished and divided up for additional assays. Furthermore, the system allows for parallelisation, this way many identical reactions or assays can be replicated on a single microfluidic chip hence increasing throughput, a quality very much desired by pharmaceutical companies. Different steps in a complex process can be combined into a single chip to enhance ease of use, portability and reducing human error—for example, in medical diagnostic devices.

Membrane proteins are of great importance as subjects of physiological study, drug targets in high-throughput assays for drug discovery and drug safety screening[1]. Microfluidic devices can be used for manipulating and analysing proteins, greatly benefiting many of the applications mentioned. The ability to produce artificial membranes within a microfluidic platform is crucial for the realization of these advantages. Current methods of producing and studying artificial cell membranes are typically low-throughput and not automated.

This thesis presents the development of a fully integrated microfluidic system for the production of artificial lipid bilayers based on the miniaturisation of droplet-interface-bilayer (DIB) techniques. The platform uses a microfluidic design that enables formation, alternation, controlled positioning and long-term storage of arrays of droplet-interface-bilayers (DIBs) to mimic cell membrane processes. By encapsulating the desired cocktail of liposomes and metabolites into phospholipid-

stabilized water-in-oil (W/O) droplets, hundreds of DIBs were characterized. To ensure robustness of operation, we have investigated how lipid concentration, immiscible phase flow velocities and the device geometrical parameters affect the system performance. Finally, proof-of-concept data is shown where diffusive transport of molecules and ions across on-chip DIBs can be studied and quantified using fluorescence-based assays. The ability to quantitatively identify DIB permeation values demonstrates the suitability of our system for investigating processes occurring across an artificial lipid bilayer in a miniaturised and scalable format.

Acknowledgements

I would like to thank all of the people that have assisted me in completing this work. I want to thank my supervisor Dr. Michele Zagnoni for the opportunity to carry out this research in his lab, for the constant open door, and for the hours spent advising me and shaping me into a better scientist. I am grateful to Dr. Cheryl Woolhead for advising me on the molecular biology part of this thesis and for letting me work in her lab.

I want to thank the whole of CMP for the all the support over the years, for all the teachings, the lunchtime conversations, the parties and for making me laugh making the last years very special.

My most sincere thanks to Dr. Ania Dudus, Dr. Kay McMillan, Dr. Ralf Bauer, Dr. Graham Robertson, for being by my side in every step of the way, for the kind words, all your help and encouragement. A special thanks to the whole of the microfluidics group (which is much bigger than when I started), I wish you all happiness and success in your endeavours.

Contents

List of Figures

List of Tables

List of Equations

Abbreviations

α-HL	α-haemolysin
AD	alzheimer's disease
AFM	atomic force microscopy
AMS	4'-acetamido-4'-maleimidylstilbene-2,2'-disulfonic acid
ATP	adenosine triphosphate
BLM	black lipid membrane
BTFB	1, 3 bis-trifluoromethyl benzene
CFTRs	cystic fibrosis transmembrane conductance regulators
CHO	chinese hamster ovary
CLC	chloride ion channels
CLIC1	chloride ion channel 1
CMC	critical micelle concentration
CNS	central nervous system
DAPI	4',6-diamidino-2-phenylindole filter
DDM	n-dodecyl-β-d-maltopyranoside
DIB	droplet-interface-bilayer
DHB	droplet-on-hydrogel bilayer
DNA	deoxyribonucleic acid
DPhPC	1,2-diphytanoyl-sn-glycero-3-phosphocholine
DTT	dithiothreitol
E. coli	*escherichia coli*
EDTA	ethylenediaminetetraacetic acid
EIS	electrochemical impedance spectroscopy
ER	endoplasmic reticulum
FDA	Food and Drug Administration
FITC	fluorescein isothiocyanate
FSEC	fluorescence size exclusion chromatography
GABA	gamma-aminobutyric acid
GPCR	g protein coupled receptors
GPCR	g-protein coupled receptor
GST	glutathione s-transferase
GUV	giant unilamellar vesicle
HEPES	4-(2-hydroxyethyl)-1-piperazineethanesulfonic acid
IND	Investigational New Drug

IPTG	isopropyl-β -d-1-thiogalactopyranoside
IVTT	*in vitro* transcription and translation
LB	luria-bertani
LOC	lab-on-a-chip
Luk	leukocidin pore protein
LUVs	Large unilamellar vesicles
MEMS	Micro-electro-mechanical system
MQAE	N- (ethoxycarbonylmethyl)-6-methoxyquinolinium bromide
mRNA	Messenger Ribonucleic Acid
NDA	New Drug Application
NEM	N-Ethylmaleimide
PA	Phosphatidic Acid
PAGE	Polyacrylamide gel electrophoresis
PAMPA	Parallel artificial membrane permeability assay
PBS	Phosphate-buffered saline
PC	Phosphatidylcholine
PCR	Polymerase chain reaction
PDB	Protein Data Bank
PDMS	Polydimethylsiloxane
PE	Phosphatidylethanolamine
PEG	Polyethylene glycol
PFT	Pore forming bacterial toxins
PGMEA	propylene glycol monomethyl ether acetate
PI	Phosphatidylinositol
PMMA	polymethyl methacrylate
POPC	1-palmitoyl-2-oleoyl-sn-glycero-3-phosphocholine
POPE	1-palmitoyl-2-oleoyl-sn-glycero-3-phosphoethanolamine
PTFE	polytetrafluoroethylene
psW/O	phospholipid stabilized water in oil
RNA	Ribonucleic Acid
ROS	reactive oxygen species
SDS	sodium dodecyl sulfate
SEM	scanning electron microscope
SLB	supported lipid bilayers
TMD	transmembrane domain
TRIS	tris(hydroxymethyl)aminomethane
tRNA	Transfer Ribonucleic Acid
µTAS	micro total analysis systems
UV	Ultraviolet
W/O	Water in oil

Thesis Overview

Objectives

This research aims to develop a fully integrated microfluidic system for ion channel experimentation with potential for medium/high-throughput drug screening on artificial membrane constructs. The device should be capable of stable and robust phospholipid stabilized water-in-oil (W/O) droplet generation, droplet alternation and trapping with the objective of creating long-lived droplet-interface-bilayers (DIBs) for membrane protein studies.

Novelty Statement

The ability to form artificial lipid membranes in a reliable, high-throughput lab-on-a-chip format has the potential to advance membrane protein studies and the development of sensitive molecular biosensors, ultimately impacting on the development of novel and low-cost synthetic approaches to drug screening. Existing methods are limited in terms of their automation, throughput and ease of use. Here, a microfluidic system has been developed, that allows the formation, alternation, desired positioning and long-term storage of arrays of droplet-interface-bilayers (DIBs). By encapsulating the desired cocktail of liposomes and metabolites into phospholipid-stabilized water-in-oil (W/O) droplets, hundreds of DIBs were characterized using fluorescence-based assays.

These miniaturised systems based on DIBs have the potential to be used as sensitive tools for artificial cell mimicry, leading to new approaches for healthcare and for drug screening systems. To the best of our knowledge this is the first fully integrated, passive structure capable of simultaneous DIBs formation and assay parallelisation in a high-throughput fashion.

Overview of Research

Chapter 1 provides a general introduction to the role of the lipid membrane environment in the function of biological membranes and their integral proteins. An overview of model lipid bilayer systems is given. A number of membrane models such as vesicles, suspended, supported and droplet bilayers are reviewed in terms of formation techniques and bilayer characteristics. The alternative use of BLMs instead of cell models for drug screening is proposed, and advantages brought by miniaturization and microfluidics in this field are highlighted.

Chapter 2 introduces microfluidic techniques presenting the basic elements of microfluidics, focusing on droplet-based modules that are applicable to the development of a platform for high throughput membrane protein studies. Droplet microfluidics is presented and some of the most important papers are reviewed. Finally, existing miniaturized bilayer platforms are discussed for their amenability to automation and future drug screening platforms.

Chapter 3 provides a detailed description of the materials and methods used in this thesis.

We have developed a fully closed microfluidic device for DIB formation, which is presented in **Chapter 4**. Here, droplet shift registers are introduced as a droplet trapping geometry for the formation of arrays of DIBs. This chapter focuses on the characterization of the device with respect to a variety of parameters which affect droplet trapping and coalescence within the shift register elements.

In **Chapter 5**, the DIBs network is presented, and focus is given to the validation of the bilayer constructs via membrane permeation assays to confirm successful lipid bilayer formation. Using fluorescence microscopy to assess the leakage of fluorescein through the membrane, we were able to assess the suitability of this device as a platform for drug permeation studies similar to the parallel artificial membrane permeability assay (PAMPA). Furthermore, the DIBs formed in our

devices have been characterized in terms of ability to host a fully functional peptide pore. The pore forming protein α-haemolysin, a lipid bilayer-spanning toxin, which forms a heptameric beta-barrel structure, was utilized to detect diffusive Ca^{2+} flux by fluorescence imaging.

Chapter 6 focuses on the ability to use this system to study a pharmacologically relevant human ion channel. Initially the studies focused on the structural and molecular characterization of the protein CLIC1 to identify which parameters were required for the protein to incorporate into liposomes. Once the parameters for channel incorporation into liposome bilayers were identified attempts were made to incorporate the ion channels into DIBs.

In the last chapter, **Chapter 7**, first the results described in this thesis are summarized, followed by general considerations for future developments and discussions on other possible applications for the microfluidic platform developed in this work.

Published Work originating from this PhD studentship

Peer-reviewed Journal Articles

1. Schlicht, B. & Zagnoni, M. Droplet-interface-bilayer assays in microfluidic passive networks. *Sci. Rep.* **5,** 9951 (2015).
2. Bai, S., Debnath, S., Gibson, K., Schlicht, B., Bayne, L., Zagnoni, M., Ulijn, R.V. Biocatalytic self-assembly of nanostructured peptide microparticles using droplet microfluidics. *Small* **10,** 285–93 (2014).
3. Chen, S., Oliveira, M., Sanz, A., Kemppainen, E., Fukuoh, A., Schlicht, B., Kaguni, L., Jacobs, H. A Cytoplasmic Suppressor of a Nuclear Mutation Affecting Mitochondrial Functions in Drosophila. *Genetics* **192,** (2012).

Peer-reviewed Conference Proceedings

1. Schlicht, B. & Zagnoni, M. A high-throughput microfluidic system for the simultaneous formation of droplet-interface bilayer arrays. *17th International Conference on Miniaturized Systems for Chemistry and Life Sciences (MicroTAS 2013).* p. 946-948 3 p. (2013).
2. Schlicht, B. & Zagnoni, M. A microfluidic platform for serial formation of Droplet-interface-bilayers for membrane protein studies. Proceedings of the 4th European Conference on Microfluidics - Microfluidics 2014 - Limerick, December 10-12, 2014 (µFLU 2014).

Chapter 1

Biological Membranes

This chapter presents the current understanding of biological membranes with respect to their molecular composition and ion channel transporters. It aims to highlight the importance and complexity of membrane proteins and to show the necessity for creating membrane models using the microfluidic device proposed in this thesis. The fundamental properties of lipid membranes and their constituents are summarized, followed by an overview of model membrane systems that form the basis of the Droplet Interface Bilayer (DIB) system employed here.

1.1 Cellular Membranes

Membranes are an essential component of all cells, where they function as selectively permeable barriers. They consist of a rich mixture of lipid molecules and proteins (Figure 1.1). In mammalian cells, the plasma membrane physically separates the intracellular components from the extracellular environment[2]. Moreover, intracellular membranes are used to form distinct compartments within the cell that perform highly-specialised functions (e.g. mitochondria – oxidative phosphorylation; lysosomes – protein degradation)[2]. All biological membranes are primarily composed of a thin layer of amphipathic molecules called phospholipids (which have polar hydrophilic head groups and hydrophobic tails)[3]. In an aqueous environment the phospholipids spontaneously assemble into a phospholipid bilayer with the hydrophobic tails sandwiched between the two hydrophilic headgroups[3,4] (Figure 1.1). This bilayer structure serves as a permeable barrier around aqueous volumes such as cells and organelles.

Membrane permeation is controlled by proteins, which are either membrane 'associated' or embedded within the lipid bilayer. These proteins enable nutrient uptake and waste disposal by the cell, thus aiding cell survival. Many membrane proteins have evolved highly specialized functions, such as the capability for energy storage and to mediate the passing of information between the cell and its immediate surroundings by creating gradients of ions.

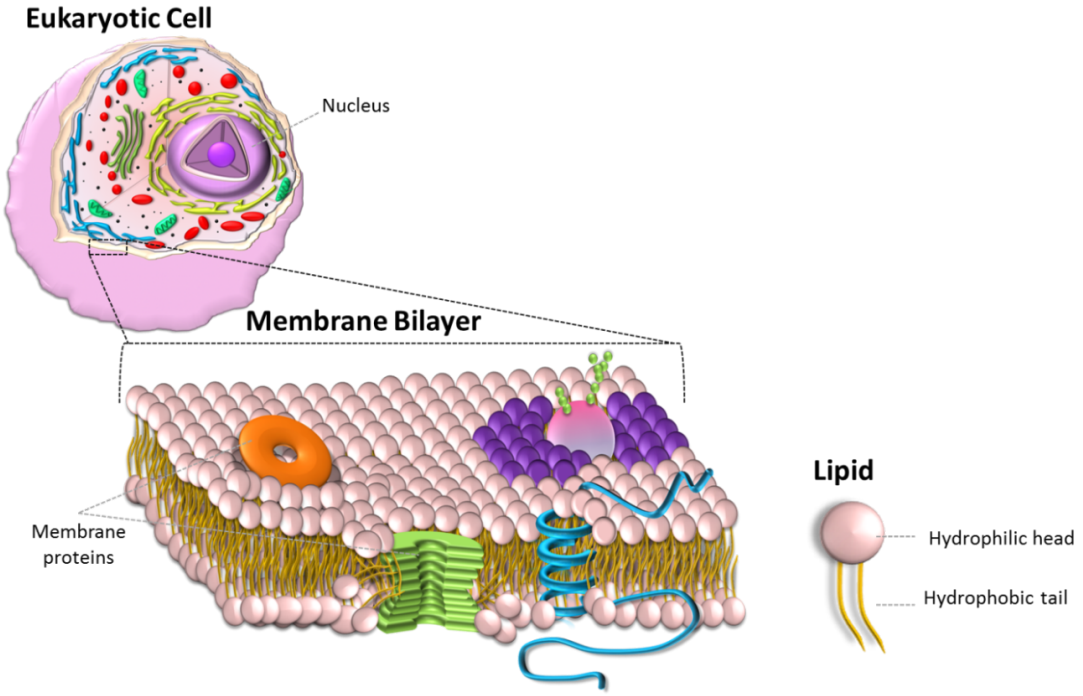

Figure 1.1 Schematic representation of a mammalian plasma membrane. Higher-eukaryotic membranes are a rich mixture of lipid molecules and proteins. Peripheral and integral membrane proteins are located at and in the phospholipid bilayer, respectively. Mammalian membranes are distinct from those found in bacteria, lower eukaryotes and plants in that they contain cholesterol (which gives the membrane increased rigidity)

Although mammalian cell membranes are primarily composed of phospholipids, they also contain sphingolipids, glycolipids and cholesterol[4] (Figure **1.2**). In their simplest form, phospholipids consist of a glycerol backbone to which two fatty acids and a phosphate group are connected. Mammalian cells make a range of related phospholipids (phosphatidyl-choline, -ethanolamine, -serine, -glycerol and -inositol) by attaching different head groups to the core phosphate moiety (Figure **1.2**). Many different fatty acids (including both saturated and unsaturated versions) can be added to the glycerol backbone. The biophysical properties of the fatty acid that are attached influence both the thickness and fluidity of the membrane[5]. Sphingolipids have a similar overall structure to phospholipids except that they have a sphingosine rather than a glycerol spine. Certain phospho- and sphingo-lipids located on the extracellular face of the plasma membrane have short carbohydrate chains attached to them and are called glycolipids (Figure **1.2**). The biophysical properties of the fatty acid influence both the thickness and fluidity of the membrane[5].

Cholesterol, for example, (Figure 1.2) is a major component of mammalian membranes, exclusively found in higher eukaryotes. High concentration of cholesterol with the membrane decreases fluidity as this bulky four-ringed structure restricts the movement of the fatty acids in neighbouring phospholipids[6]. The restriction in the movement of lipids and proteins within the membrane leads to the formation of micro-domains or rafts. Although, the membrane is 'fluid', the movement of molecules is not completely uniform as previously believed[3,7].

1.1.1 Domains and Rafts in Biological Membranes

In 1972 the Fluid—Mosaic Model of membrane structure was proposed by Singer and Nicolson, based on thermodynamic principles of the organization of membrane lipids and proteins, and available evidence of asymmetry and lateral mobility within the membrane matrix[3]. Also termed the two-dimensional continuum fluid model, it describes proteins that match the hydrophobic thickness of a perfect bilayer, diffusing freely in a uniform fluid medium of lipid that is mostly exposed to the aqueous environment. However, it is now known that membranes are much less uniform than previously thought. Developed by Karnovsky et al. (1982)[8], the idea that isolated domains with different lipid phase characteristics and functional roles can co-exist in biological membranes has caused much discussion, with many questioning not only the size and robustness of these domains but also their very existence[9].

Inhomogeneous regions within the mammalian membranes that have high local concentrations of cholesterol and sphingolipids form domains called lipid rafts[2,10,11]. Rafts are more ordered and tightly packed than the surrounding bilayer and float freely in the membrane. They function as specialised membrane micro-domains that enable certain signalling and trafficking events at the cell's surface to be compartmentalised[4,5,11,12].

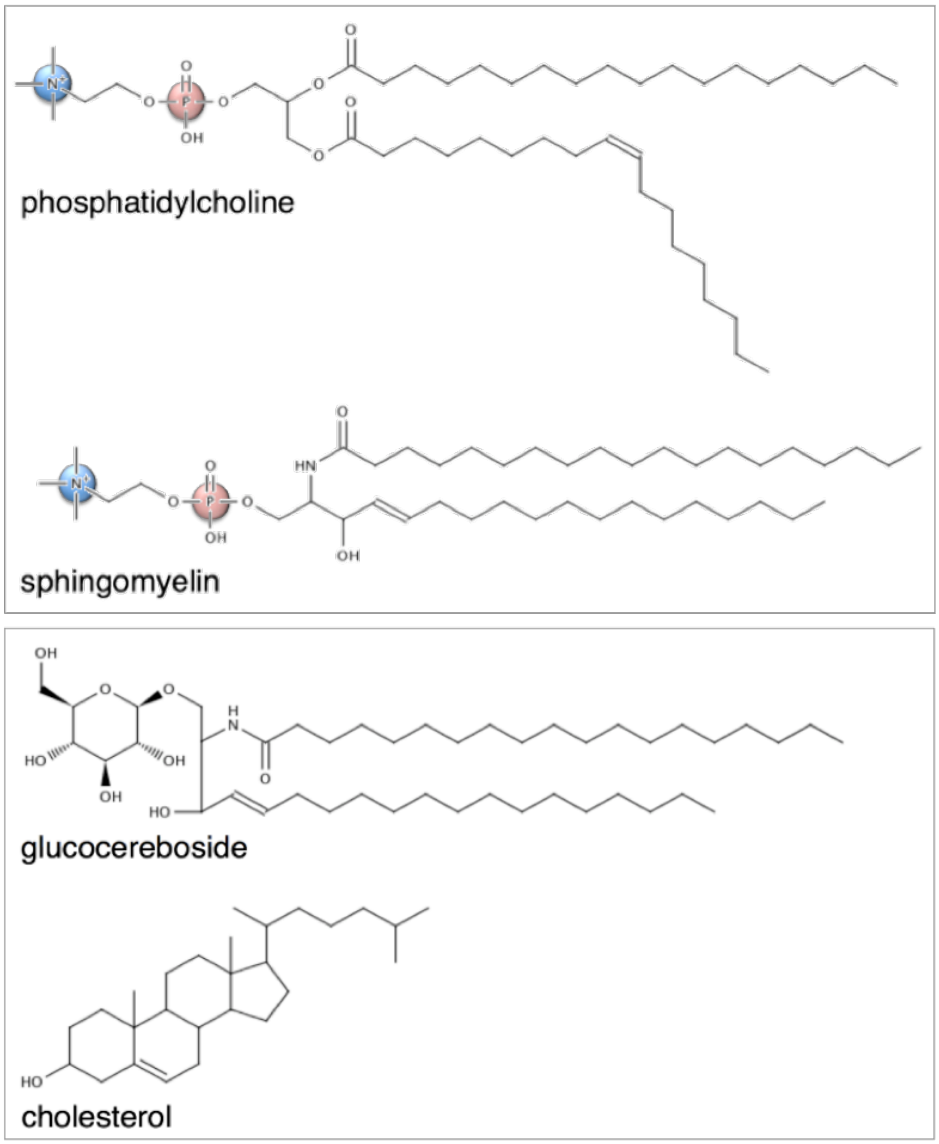

Figure 1.2 Chemical structures of selected lipids found in mammalian membranes. Higher-eukaryotic membranes contain four different kinds of lipid namely phospholipids (for example-phosphatidylcholine), sphingolipids (sphingomyelin), glycolipids (glucocereboside) and cholesterol

Despite many developments in the field of membrane biology, the Fluid Mosaic Model remains relevant for describing the basic nano-structures of membranes of many eukaryotic and prokaryotic cells. However, over the years the importance and functions of large specialized domains such as lipid rafts and glycoprotein complexes have rendered the model partially inadequate. The model fails to describe how macrostructures influence the dynamics and functions of cellular membranes, as well as the roles of the cytoskeleton and extracellular matrix structures in limiting the lateral diffusion and the range of motion of membrane proteins.

New data on membrane biology still build on the fundamental principles of the Fluid Mosaic Model, however it has since been restructured adding new layers of complexity. It is clear that membranes are far more irregular than previously assumed. We now know that membrane proteins are extremely large, dwarfing the phospholipids and that they can cluster to form functional domains. Lipid rafts are chemically and physically distinct from the surrounding membrane. They contain many proteins, and a mixture of lipids particularly cholesterol and sphingolipids, bound tightly together through ionic interactions to resist chemical disruption[7].

Moreover, the hydrophilic heads of phospholipids also associate with membrane proteins. Due to their relatively large sizes, membrane proteins can spread out over the surface of a membrane, allowing the hydrophilic head group of phospholipids to form non-covalent bonds with hydrophilic regions of proteins. This interaction distorts the phospholipids from the idealized planar configuration suggested by the original model and hints that membrane thickness is far from uniform. Data acquired from membrane protein structures shows that the extent of the hydrophobic surface area varies, not only between proteins but also within a single protein, so either the protein or the lipid bilayer has to distort to ensure the enclosure of hydrophobic regions[7]. Given the relative stiffness of protein transmembrane regions[13] compared to lipid bilayers[14], it is more likely that a lipid bilayer would get distorted, either expanding or compressing[15,16], rather than the proteins.

1.2 Membrane Proteins

Membrane proteins make up around 30% of the open reading frames in sequenced genomes[17,18]. They can be classed either as peripheral or integral according to the way that they attach to the membrane[3]. Peripheral membrane proteins are located at the surface of membranes where they are anchored either directly by interacting with the lipid bilayer or indirectly via contact with an integral membrane protein. Peripheral membrane proteins can usually be released from the membrane by washing with a

buffer of high ionic strength. In contrast, integral membrane proteins span the entire membrane, and consist of hydrophilic regions, exposed on either side of the membrane, separated by hydrophobic regions buried within the membrane core (Figure 1.1). These proteins can only be released from the lipid bilayer by treating the membrane with a detergent that will replace the lipids, thus enveloping the protein. This makes them considerably harder to work with when compared to either soluble or peripheral membranes proteins. As even mild detergents are denaturants, it is not uncommon for the protein to lose its functional activity during this purification stage[19].

Membrane proteins such as receptors and ion channels are key regulators of cellular function. The G protein-coupled receptors (GPCRs) are the largest, most versatile, group of membrane receptors and also the most pharmaceutically relevant, accounting for over 45% of all human drug targets[20] and acting as therapeutic targets for a wide range of disease conditions including cancer, cardiovascular, metabolic, CNS and inflammatory diseases. Ion channels represent another important group of membrane protein drug targets and account for about 10% of the current drugs[20].

1.2.1 Secondary and Tertiary Structure of Proteins

Integral membrane proteins are the most abundant type of membrane proteins found. They are incorporated into the membrane by a variable number of hydrophobic α-helices that span the bilayer. Channel proteins also contain α-helices, but are defined by the formation of an aqueous channel surrounded by a variable number of homologous domains within a single polypeptide chain, or by independent subunits[21]. Transmembrane helices in larger membrane proteins are connected by flexible loops, which give the protein movement by varying the position of the helices with respect to each other. Big conformational changes of the protein backbone define the function of many ion channels, enabling gating i.e. the reversible opening and closing of the channel through the interior of the protein[22].

Following translation, proteins fold first into a series of defined secondary structures from which a 3-dimensional shape is eventually formed. There are two main

types of secondary structure found in all proteins called α-helix and β-sheet, both of which are formed by hydrogen bonding between the carbonyl and amine groups of the protein backbone (Figure 1.3)[21]. α-helices are the most common secondary structure found in integral membrane proteins. They require a minimum of 17-20 residues to span the bilayer[21], are energetically stable and have a right-handed coiled conformation. The majority of the amino acids that occur within membrane-spanning helices tend to be hydrophobic in nature[23] and the presence of proline and/or glycine residues in a helix can cause it to kink (as was observed in the structure of rhodopsin)[24]. By having several helices that traverse the membrane in opposite directions linked by loop regions, it is possible to create a diverse range of membrane proteins including transporters, ion channels and receptors.

The G protein-coupled receptors (GPCRs) are the largest, most versatile, group of membrane proteins involved in cell signalling at the cell surface, of which around 800 unique human full-length variants are known. Due to their common topology, they are also referred to as seven-transmembrane helix receptors and most mediate transmembrane signalling by a conformational change upon binding of small signalling molecules, such as cyclic-AMP, on their extracellular domain.

The other main type of secondary structure is the β-sheet. It consists of neighbouring β-strands (stretches of polypeptide where the backbone has an almost fully-extended conformation) that are hydrogen bonded to each other (**Figure 1.3**). Where the β-strands all have a similar orientation, the β-sheet that is formed is denoted parallel. Where the β-strands have alternating orientations, the β-sheet is described as anti-parallel[25].

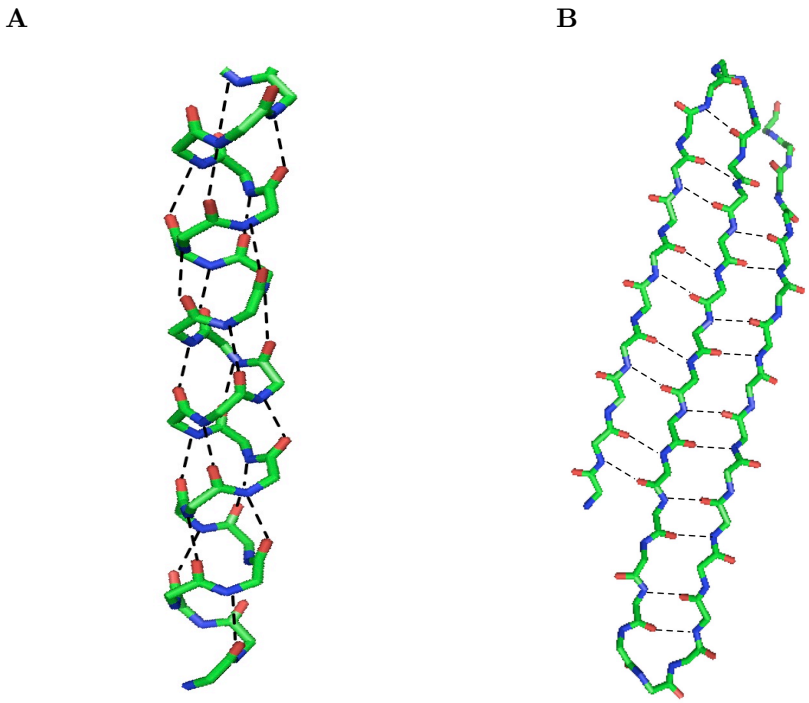

Figure 1.3 Representation of the two main types of protein secondary structure. Figure A shows an α-helix in which every backbone N-H group donates a hydrogen bond to the backbone C=O group of the amino acid four residues previous. There are 3.6 amino acids per turn of helix. (B) Shows an anti-parallel β-sheet with hydrogen bond "bridges" between neighbouring β- strands. Hydrogen bonds are shown as black broken lines.

Porins are a class of channel proteins primarily found within the outer membranes of bacteria, mitochondria and chloroplasts[26]. The transmembrane domain consists of a large β-sheet that has been twisted and coiled to form a closed structure called a β-barrel[26]. β-strands in β-barrels are arranged in an anti-parallel fashion with the first-strand hydrogen bonded to the last[21,26]. Unlike transmembrane α-helices that are largely composed of aliphatic amino acids, the β-sheets that make up β-barrels do not have obvious long hydrophobic regions, which makes their identification from primary sequence analysis alone difficult[26]. The structure formed is a rigid aqueous pore that allows unselective passive diffusion of hydrophilic molecules. The insertion mechanism of porins is not fully understood, but individual insertion of β-strands is highly unlikely. Therefore some type of post-translational chaperoning mechanism must exist. Cytolytic toxins, such as α-haemolysin and gramicidin, are thought to insert spontaneously into the membrane through inter-domain concerted interactions between monomers loosely associated to the membrane in a pre-pore complex, leading to a conformational change that forms the pore[27,28].

Membrane proteins play many fundamental roles in cellular function, from adhesion to cell proliferation, signal transduction, energy storage and muscle excitation. Hence it is unsurprising that nearly 70% of all known drug targets are membrane proteins[17,18,22,29,30]. Surprisingly, out of nearly 60,000 entries on the Protein Data Bank (PDB) only 700 are structures of integral membrane proteins. The number of integral membrane protein structures solved to date does not reflect either their importance in biology or indeed their natural abundance (with 30% of the genes in a typical genome encoding membrane proteins)[31,32]. The slow rate at which membrane proteins are considered reflects the difficulty of isolating these proteins from the membrane without destroying their physiological environment and thus their integrity, resulting in membrane proteins being far less studied than their soluble counterparts. Nevertheless, membrane protein structure determination is now progressing faster, as demonstrated by the rising number of structures in the PDB database[33].

It is becoming clear that oligomerisation is a highly common mechanism in membrane proteins[7] but many hurdles remain to be overcome before current biophysical methods can be reliably used to detect the oligomeric state of proteins and before distinguishing between dimers and higher order oligomers will become trivial[34]. The process often involves the removal or substitution of the natural membrane environment and this disruption can have a large effect on the protein structure and function. Dowhan and Bogdanov[35] have demonstrated that even changes in the net charge of the lipids at the membrane surface can result in similar changes in the topological organization of a membrane protein, changing protein structure and potentially varying protein function. This not only increases the complexity of membrane proteins but also highlights the need for newer, less disruptive methods to study these molecules.

Given the importance of membrane proteins for drug discovery, the ability to interrogate and characterise the behaviour of membrane proteins in a reliable and scalable manner is essential. It is necessary to use either live cells or to create a

simplified environment capable of mimicking a natural cellular membrane. Microfluidic solutions are already commercially available (e.g. from Fluxion, Nanion Technologies, Sophion and Ionera). These use electrophysiology techniques to measure the activity across biological membranes, either using whole live cells[36] or by incorporating ion channels within artificial membranes[37]. The latter approach is particularly interesting as it allows cellular parameters (e.g. membrane lipid composition, pH and ion channel selection) to be individually investigated, enabling novel experimentation, advancing biological knowledge and facilitating the design and testing of more effective drugs.

1.2.2 Transport Across Membranes

The structure and function of cells are critically dependent on membranes, which not only separate the interior of the cell from its environment but also define the internal compartments of eukaryotic cells, including the nucleus, mitochondria, endoplasmic reticulum (ER) and other cytoplasmic organelles.

To transport large amounts of molecules quickly across the membrane, e.g. the release of neurotransmitters into the synaptic cleft, vesicles can fuse with membranes to release their content. In order to exchange larger or hydrophilic molecules, the cell membrane contains proteins to mediate or drive this permeation entirely. Specialized, transmembrane channel proteins form hydrophilic pores to facilitate the diffusion of ions across these lipid membranes[21].

All transport of hydrophilic molecules (e.g. sugars, amino acids, nucleotides) and ions is facilitated by membrane proteins. They are needed to excrete waste, regulate ion concentrations, maintenance of intracellular pH and many other functions. They can be divided into two main classes: transporters and channels. Transporters can undergo conformational changes, which facilitate the transfer of molecules to the other side. When coupled to an energy source, e.g. ATP, transporters can also move molecules against concentration gradients. Channel proteins are specialized for specific molecules, e.g. Ca^{2+}, and do not couple to an energy source.

Therefore, only passive transport is possible through channels and molecules are only transported down a concentration gradient.

1.2.3 Membrane Permeation

Passive permeation is the primary route of absorption of most drugs in the human body, especially in the intestine. Here, the biological membrane is mainly a physical (hydrophobic) barrier for permeating molecules. Hence, the rate of diffusion through a lipid bilayer depends on the charge, size and the polarity of the molecule. Currently, the most commonly used high-throughput permeation assays are the Caco-2 assay and the parallel artificial membrane permeation assay (PAMPA).

Caco-2 Assay

The Caco-2 assay employs a chamber divided by a membrane on which a monolayer of Caco-2 cells grows to confluence (Figure 1.4 Left). When this occurs, neighbouring cells form tight junctions, which can force compounds from one compartment (apical) to travel through the Caco-2 cell membranes into the neighbouring compartment (basolateral) in order for transport to occur. This method is commonly used by drug companies, but relies upon the culturing of Caco-2 cells, which can often take weeks and requires regular feedings. Furthermore, the tightness of junctions formed by cells in the monolayer can vary within and across test chambers, which can result in leaks of compounds across compartments.

Parallel Artificial Membrane Permeability Assay (PAMPA)

Many pharmaceutical industries have implemented high throughput Patch Clamping technologies in their screening process. However, since Patch Clamping techniques are still very expensive, the pharmaceutical industry has shown preference for parallel artificial membrane permeability assays (PAMPA) (Figure 1.4 Right). PAMPA assays employ artificial membranes made of a mixture of lipid and inert organic solvents supported by a hydrophobic filter. It has become a standard in industrial settings because its assay format is compatible with multi-well plates. In PAMPA permeability of substances is determined from a donor compartment, through a lipid-

infused artificial membrane into an acceptor compartment. The assay is prepared from two plates: one containing a porous filter at the bottom of each well and filled with an organic solvent with lipids. The other is a reservoir plate that is precisely moulded to sit under the filter plate so that contact between the two occurs at the filter. Upon contact an artificial membrane forms in between the wells of the two plates. The wells of one plate are then filled with donor solution (i.e., drug), and the other with acceptor solution (i.e., buffer). The drug concentration in the donor and acceptor wells is then determined by fluorescence measurements, and permeability is calculated[38,39].

PAMPA offers some advantages over Patch Clamp and the Caco-2 assays, such as not needing to culture cells, being able to modify the types of lipid in the hydrophobic membranes, and the absence of other proteins type, which may affect the quality of the data. Major difficulties with the PAMPA assays include the thickness of the lipid membranes, the large incubation time (often hours), and the binding of compounds to the hydrophobic fitler[40]. PAMPA membranes are also much thicker than cellular membranes, often at least 100 μm thick[41], while cell membranes are typically about 4 nm-5 nm thick[7].

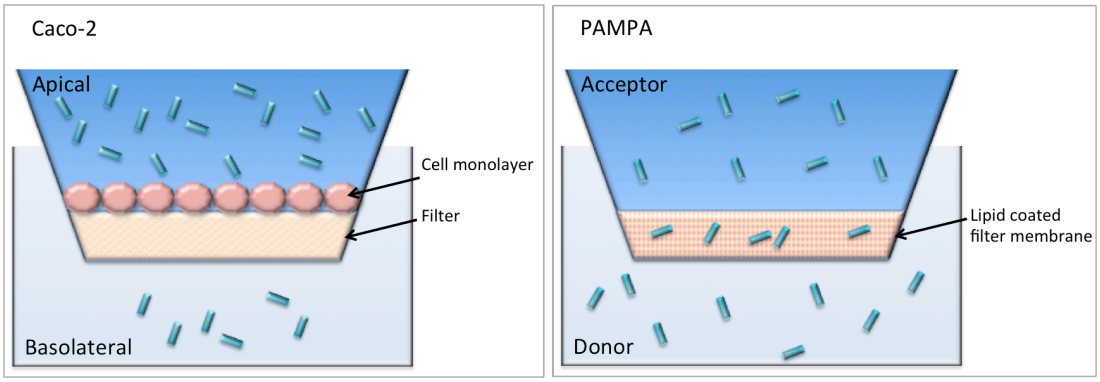

Figure 1.4 Membrane permeability assays. Caco-2 uses compartments of different volumes separated by a monolayer of cells grown on a filter. Compounds must permeate through a monolayer of cells; drug permeability is calculated from the change in receiver compartment concentration over time. PAMPA, however, uses chambers separated by a filter coated with lipid in organic solvent. The compound then diffuses through the membrane into the acceptor compartment where samples are taken and analysed. The time-concentration profile indicates how quickly the compound permeates through the membrane. These results can then be translated to predict compound uptake into the body.

1.2.4 Channel Proteins

A common class of channel proteins found in almost all animals forms are gap junctions which form channels between two adjacent cells connecting their cytoplasm[42]. Both gap junctions and porins, the channel-forming proteins of the outer membranes of bacteria, mitochondria, and chloroplasts (discussed in more detail in Chapter 4) have relatively large and very permeable pores which are continuously open[43].

Pore forming bacterial toxins (PFT) such as α-haemolysin connect the cytoplasm of a cell to the extracellular environment in order to induce cell lysis. When a pore is formed, the tight regulation of what enters or leaves a cell is disrupted. Ions and small molecules, such as amino acids and nucleotides present within the cytoplasm flow out, while water from the extracellular space enters the cell. The loss of these small molecules disrupts protein synthesis as well as many other vital cellular processes. The loss of ions, especially calcium, inaccurately activates and deactivates many cell signalling pathways. The uncontrolled uptake of water into the cell causes the cell to swell uncontrollably causing the cellular membrane to burst.

In contrast, most channel proteins in the plasma membrane of animal and plant cells that connect the cytosol to the cell exterior necessarily have narrow, highly selective pores that can open and close. The function of these proteins is to transport specific inorganic ions; therefore, they are referred to as ion channels. Since these channels cannot be coupled to an energy source to perform active transport, the transport that they mediate is always passive. Thus, the function of ion channels is to allow specific inorganic ions—primarily Na^+, K^+, Ca^{2+}, or Cl^-—to diffuse rapidly down the concentration gradients across the lipid bilayer. The ability to control ion fluxes through these channels is crucial for many cell functions.

Ion channels have many distinct features that make them of interest for biophysical and physiological study. Apart from being highly ion selective, ion channels are very dynamic proteins, which exhibit unique responses under particular

conditions. At resting potential, the channels are completely closed and impermeable to ion flow. However, the channels can undergo a conformational change and open in response to a specific stimulus. The main types of stimulus include a change in voltage across the membrane (voltage-gated channels), the binding of a ligand (ligand-gated channels) or a mechanical stress (mechanically gated channels) (Figure 1.5). The ligand can be either an extracellular mediator, e.g. a neurotransmitter, or an intracellular mediator, such as an ion. The activity of many ion channels is regulated, in addition, by protein phosphorylation and dephosphorylation[44].

1.3 Recording of Ion Channel Activity

Ion channels embedded in cell membranes play important roles in a wide range of physiological processes[45–48]. A better understanding of how ion channels work and how they respond to various stimuli, including drugs, is essential to the development of accurate models of cellular activity and drug discovery.

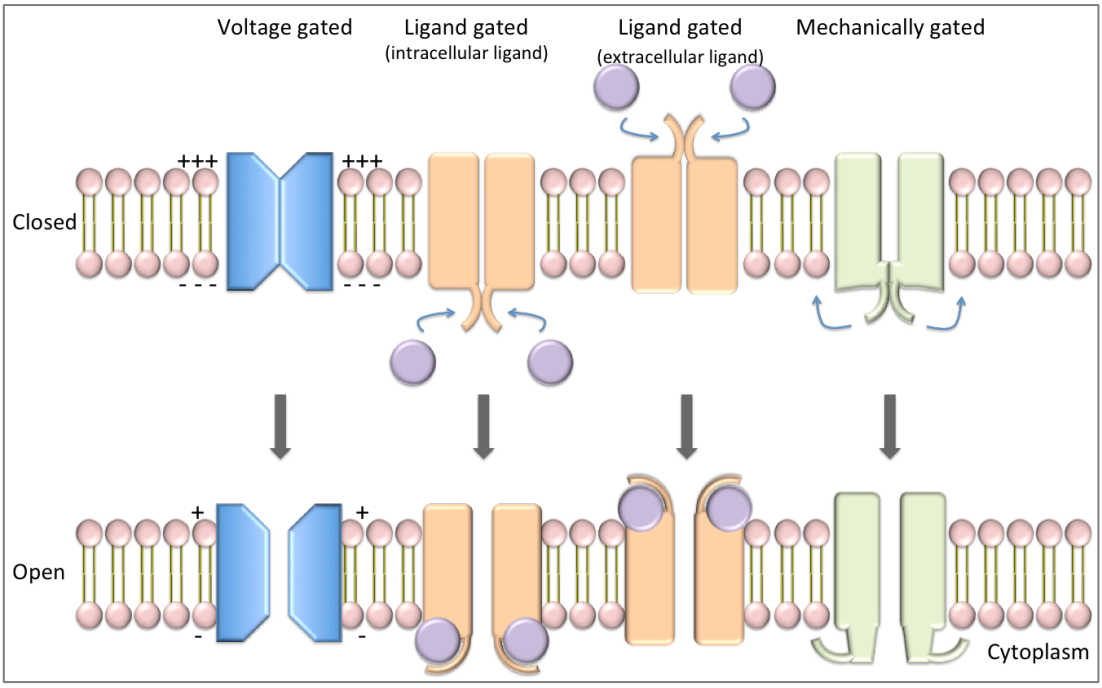

Figure 1.5 Different types of ion channels. The schematic shows how different ion channels have different gating mechanisms in response to a stimulus. Voltage gated channels respond to a change in membrane potential, ligand gated channels are controlled by binding of a ligand and mechanically gated channels respond to a mechanical force on the membrane.

High throughput studies of soluble proteins are well established and are frequently used in academic studies as well as in pharmaceutical research. However, ion channels are typically incompatible with the most common high throughput, non-cell based study methods due to their hydrophobic nature. Additionally, studies which focus on ion channel activity and behaviour need the proteins to be embedded within lipid membranes[49]. Moreover, high-throughput screening generally requires cloning of the target protein and overexpression in a heterologous system in a form that resembles the wild type. For ion channels this is challenging since accurate reproduction of native functional and pharmacological properties is dependent on efficient expression, localization, folding and assembly. As a consequence, there is potential for protein mis-folding and for assembly errors when ion channels are over-expressed. Furthermore, ion channels are poorly tolerated when over-expressed often destabilising intracellular ionic balance. For example, toxicity often occurs when calcium-permeable channels are overexpressed since they can perturb calcium homeostasis within the host cell.

Technological advances in electrophysiology and molecular biology have led to great progress in ion channel research. Advances in the development of functional ion channel assays over the years have enabled a more systematic approach to study this important protein class. All of these assays rely on the fact that activation of ion channels results in an ion flux across a cellular membrane.

Patch clamp electrophysiology directly measures ion channel activity by recording currents across cell membranes, whereas indirect assays examine flux of ions or local changes in the membrane potential. Indirect assays are higher in throughput when compared to patch clamp techniques however, they lack information on the ion channel function, and only analyses the effect of tested compounds in an on/ off manner. Limitations on ion channel studies in the form of the extremely low throughput assays for functional assays, has been overcome by the employment of multi-well plate format screening strategies. These combine optical and electrophysiological techniques to monitor ion flux and have significantly impacted

drug discovery leading to major developments in the establishment of automated electrophysiology.

1.3.1 Manual Patch Clamp

Most of the electrophysiological characterization of ion channels is done using patch clamp technology[50–52]. It can be employed to study single ion channel behaviour in detached cell patches and in intact patches of live cells providing detailed insight into the function and the behaviour of channels spanning the outer membrane of the cell[53,54].

The major trade-off that researchers must make when using manual patch clamp is that they must patch on to a single cell at a time. The method is very labour intensive. It requires glass pipettes to be heated, pulled, and fractured to yield pipette openings that can be as small as a few microns in diameter. The tips must be made smooth to avoid problems with sealing the glass pipette tip with a cell membrane. The pipette itself needs to be carefully positioned with a microscope and micromanipulators. A light vacuum must be applied to seal the pipette tip with the cell membrane, and resistances of at least 1 GΩ between the inner pipette solution and the bath solution must first be obtained before accurate measurements of ion channel currents and precise voltage clamping of the cell membrane is possible. These requirements alone make manual patch clamp an impractical method for electrophysiological studies (Figure 1.6).

1.3.2 Automated Patch Clamp

Automated electrophysiology platforms have evolved from glass pipette through to planar-patch and lateral-patch substrate-based systems (Figure 1.6). These advances have brought with them significant gains in throughput but this has come at the cost of the quality of the biophysical data that are generated. Consequently, none of the current planar- and lateral-patch automated electrophysiology platforms is sufficient in isolation to support ion channel screening.

Currently, a combination of higher-throughput, lower-quality "loose-seal" platforms for hit identification (e.g., IWQ or IonFlux) with lower-throughput, high-quality giga-seal platforms for supporting medicinal chemistry (e.g., PX or QPatch) provides the best available screen sequence. However, in spite of the recent advances in this technology, there remain serious limitations. Tests of 10,000-30,000 compounds per day are not atypical in labs that conduct high throughput drug screens. A typical automated patch clamp system can successfully test 100s of compounds per day, while the latest systems can theoretically test several thousands of compounds per day. The success rates of forming giga-seals with patches of cells in the latest generation of such systems can be as low as 50%. Moreover, only a limited number of ion channels can be studied as it is not possible to access intracellular channel proteins and only channels in the plasma membrane can be reached[55]. The need for even greater experimental throughput at lower cost necessitates the consideration of alternative technologies for conducting high throughput studies on ion channels, while overcoming cytotoxicity due to overexpression in live cells.

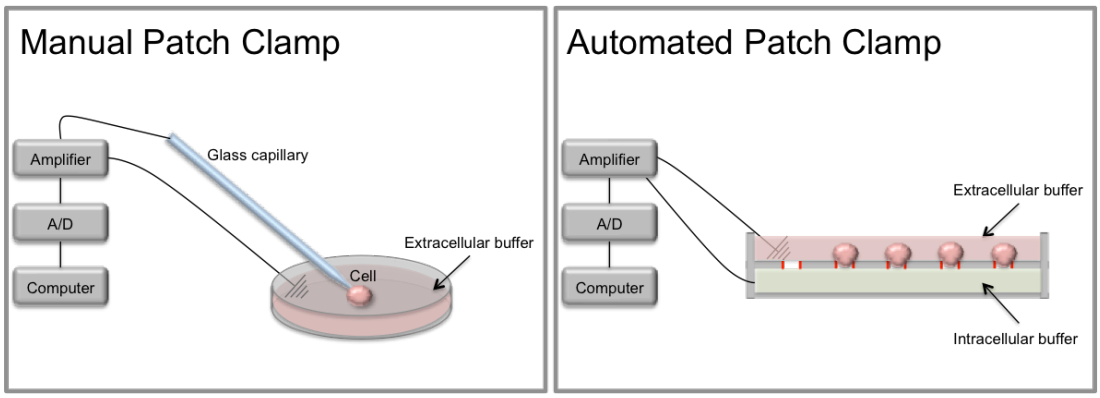

Figure 1.6 Patch Camp techniques. In Manual Patch Clamp an electrode-containing glass micropipette is positioned onto the surface membrane of an individual cell. Mild suction is then applied to form a high resistance electrical seal and to pull away the piece of plasma membrane enclosed by the pipette tip. This gives electrical continuity between the pipette electrode and the inside of the cell allowing the membrane potential to be precisely controlled. Currents passing across the entire cell membrane, representing the overall activity of all channels expressed in the plasma membrane can then be recorded with reference to a second electrode positioned in the external medium. In Automated Patch Clamp the pipette is replaced with a multi-well plate. Each well contains a microscopic recording aperture upon which suction is applied and a cell becomes trapped forming an electrical seal so channel activity can be recorded.

1.4 Model Membranes

Model lipid membranes are simplified mimics of a cell membrane. Instead of using a variety of lipids, one or only a few types of lipids are used to form a model membrane, which allows the study of the biophysical and thermodynamic properties of a particular lipid in the cell membrane and how it interacts with a particular protein. This also gives the possibility to examine the functional interaction between a specific lipid type and a particular protein. Development of model membranes broadened the knowledge about the cellular processes down to the molecular level.

Made from either natural or synthetic lipids, these systems exist in many conformations (Figure 1.7). The first type of model membrane system to be developed was the black lipid membrane (BLM) used 1960s[56]. Since then different types of model membrane systems have been developed. These will be discussed further.

Model membrane systems have been used to study a variety of cellular processes such as transport of ions and molecules across the cell membrane, protein structure and function, and the relationship between membrane and integral proteins. As well as to exploit the nature of cellular processes such as cell signalling for biotechnological applications.

1.4.1 Planar Lipid Bilayers

The first model bilayer method was developed by Mueller *et al.* in 1962[56]. This method forms planar bilayers typically for electrical interrogation across an aperture of approximately 100 µm in diameter, pierced through a synthetic hydrophobic substrate (either polytetrafluoroethylene (PTFE) or Teflon) placed between two aqueous chambers.

Another method, namely the Lipid painting[57–59] technique, is based on lipid bilayers that are formed by physically spreading or 'painting' lipids dissolved in an organic solvent on an aperture in a hydrophobic substrate before or after filling the surrounding chambers with aqueous solution to immerse the aperture. The lipid

molecules self-assemble to form a monolayer at the solvent-water interface. This process is accompanied by optical blackening of the suspended film across the aperture due to destructive interference, in contrast to the area where the bilayer is not formed. Hence, the resulting planar bilayer is also referred to as a black lipid bilayer (BLM).

In the Montal-Mueller[56,60] method the substrate is positioned above an aqueous phase with the aperture orthogonal and above the surface. Lipids are mixed within the aqueous phases and self-assemble into a monolayer at the water-air interface with the heads oriented toward the water and the tails oriented in the air. When the aqueous phase rise, the hydrophobic tails fold onto the hydrophobic substrate and form a monolayer on the substrate. As the aqueous level passes over the aperture, the hydrophobic tails of the lipids on either side of the aperture will contacts forming a bilayer (Figure 1.7-F). This method is also referred to as 'lipid folding'.

A further method is the Langmuir-Blodgett[57,59,61,62] technique that uses a procedure similar to the Montal-Mueller method, but the substrate is instead hydrophilic. The lipids are spread across the surface of an aqueous phase and self-assemble into a monolayer at the water/air interface. The substrate is immersed perpendicular to the aqueous phase and slowly removed. As the substrate is pulled out of the aqueous phase, the heads of the lipids will adhere to the hydrophilic surface of the substrate, forming a monolayer on the surface. The substrate is then turned 90° degrees and placed on the monolayer on the surface of the aqueous phase, thus forming a bilayer between the substrate and the aqueous volume.

1.4.2 Supported Lipid Bilayers

The main limitation of planar bilayers is that they are difficult to image using common characterization methods such as single molecule fluorescence and atomic force microscopy (AFM). This encouraged the development of horizontally aligned bilayers, commonly known as supported lipid bilayers (SLB) (Figure 1.7-A).

SLBs can be coupled to many different substrates, such as gold, glass or silicon dioxide, to form tethered bilayers (t-SLB) (Figure 1.7-B). They are commonly formed either by vesicle fusion[63] or Langmuir-Blodgett deposition[61]. In vesicle fusion, surfaces are incubated with vesicles. Vesicles adhere to surfaces and rupture to form continuous planar bilayers (Figure 1.7- C). In Langmuir-Blodgett deposition, bilayers are transferred to solid substrates from Langmuir monolayers at the air-water interface in a two-step process.

SLBs are widely used for structural studies and for the study of mechanism of formation and lipid-surface interactions. However, the use of SLBs for practical application, e.g. single channel recordings of the development of biosensors, is limited. This is mostly due to insufficient space between the bilayer and the substrate restricting, for example, the insertion of membrane proteins, which are likely to denature or unfold upon interaction with substrate surface. It is difficult to achieve a suitable electrical seal between the two sides of the bilayer, as a deposited membrane has open ends and often contains defects that occur during deposition. Many methods have suggested the decoupling of the lipid bilayer from the substrate, providing enough space for a lower reservoir, rendering the bilayer suspended.

1.4.3 Suspended Lipid Bilayers

Suspended lipid bilayer membranes[64–66] are planar lipid bilayers supported horizontally over small hydrophobic apertures between two aqueous environments. Their formation is simple and rapid and results in bilayer that are often more stable than the conventional BLMs described earlier[67].

An advantage of this system as well as the BLM configuration is that both sides of the membrane are typically accessible, therefore salt gradients across the membrane and other asymmetric conditions can be created.

1.4.4 Droplet-Interface-Bilayer (DIB)

Droplet interface bilayers (DIBs) are typically formed by depositing a water drop into a solution of lipids in an alkane, such as hexadecane, and allowing the lipids to self-assemble in a monolayer at the oil-water interface. When two such droplets are brought into contact, the oil between the monolayers is displaced and a droplet-interface-bilayer forms spontaneously (Figure 1.8). By piercing the droplets with an electrode, a configuration similar to a Montal-Mueller bilayer is achieved.

Alternatively, the droplet can be used in conjunction with planar supporting hydrogels to form bilayers between water droplets and hydrogels[68–71]. This technique is called the droplet-on-hydrogel bilayer (DHB) (Figure 1.7- E). Hydrogels can form a monolayer of lipids using the lipid-out technique when placed in the solvent because the hydrogel is hydrophilic, and the heads of lipids are attracted to it. A droplet placed in the solvent will form a monolayer and a bilayer can be formed between the droplet and the hydrogel.

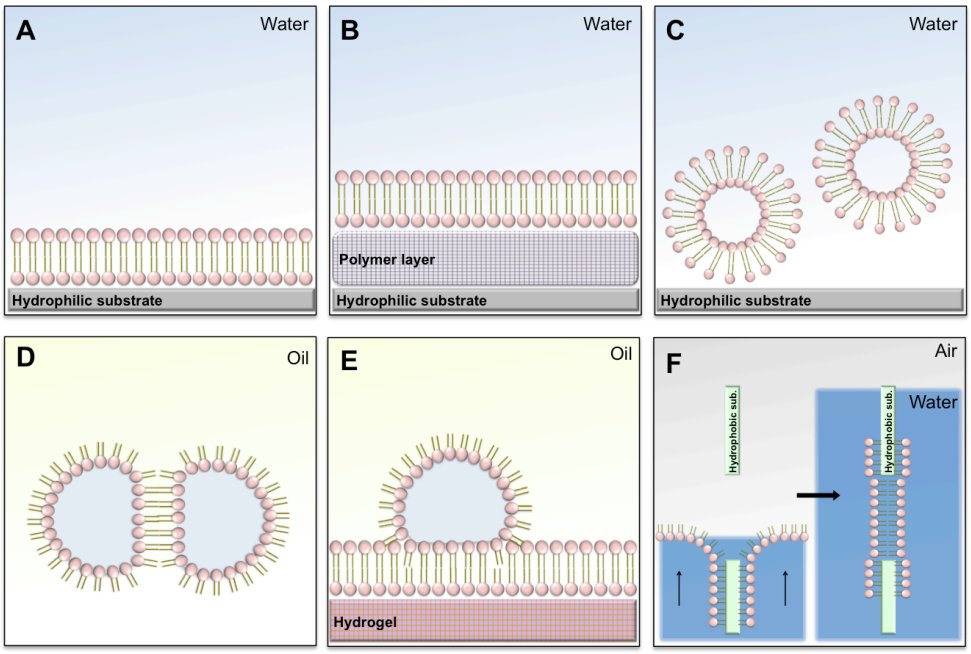

Figure 1.7 Model bilayer systems. (A) Solid supported lipid bilayer (s-SLB). (B) Tethered supported bilayers (t-SLB), are supported on a substrate but separated from it with a hydrophilic polymer layer. Tethers can consist of spacers such as DNA, functionalized lipopolymers or thiolipids interfacing with a gold surface. (C) Vesicles. (D) A Droplet Interface Bilayer (DIB). (E) A droplet hydrogel cushioned bilayer (DHB). (F) Montal-Müller BLMs, which are solvent-free, being created across a vertical aperture.

Droplet-Interface-Bilayers (DIBs)[57,62,72–74] were proposed as a way to study bilayers without the need of a solid support. DIBs are effectively a liquid supported system. Bilayer lipid membranes formed on solid supports have several disadvantages, as discussed by Bayley *et al.* 2007[67], including the formation of solvent lenses and poor bilayer longevity. Droplet interface bilayers, address many of the shortcomings encountered by SLBs, ensuring a tight electrical seal by completely enclosing the aqueous volumes on either side of the bilayer in an oil phase. Another drawback of solid supported membranes is the decrease in membrane fluidity. Fluidity is a factor that can severely affect membrane permeability. For example it has been reported that water molecules are highly permeable to liposome membranes in the fluid phase state, but much less permeable to them in the gel phase[75–77]. Liquid supported systems such as DIBs permit the lipid bilayers to have similar fluidity to biological membranes. Given the higher stability and smaller volumes, DIBs have an exceptional potential to be used in high throughput assays for membrane protein investigations.

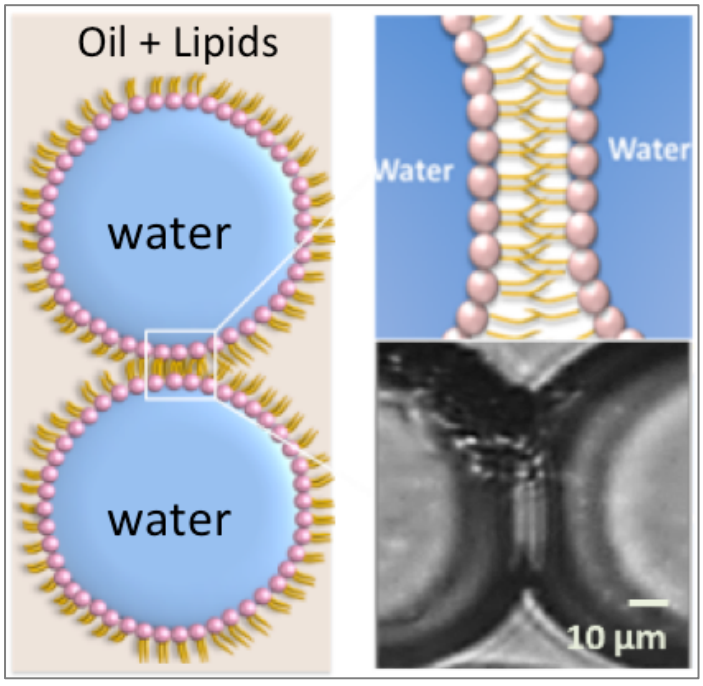

Figure 1.8 Droplet interface bilayer (DIB). A lipid monolayer self assembles at an oil/water interface, with the hydrophobic lipid tails facing towards the oil phase and the hydrophilic heads facing towards the aqueous phase. As the tails of two lipid monolayers come into contact, a DIB is formed.

1.4.5 Membrane Protein Reconstitution

Model membrane systems have been used extensively to study membrane proteins[78,79]. However, despite the versatility of model membranes significant difficulty lies in the techniques used to transfer membrane proteins into the lipid bilayers where they are investigated. Membrane proteins and ion channels can either be integrated into the bilayer by self-assembly from solution or by fusion of proteoliposomes with the bilayer[37].

Fusogenic proteins including β-barrel bacterial pore forming toxins (PFTs) such as α-haemolysin (α-HL), alamethicin and gramicidin[1,80,81] are a highly diverse set of soluble proteins, which can be assembled *in situ* from monomers[82] or as pre-formed protein pores stabilized by a low level of detergent such as sodium dodecyl sulphate (SDS) or n-dodecyl-β-D-maltopyranoside (DDM)[83]. For such proteins, spontaneous insertion can be sufficient for electrophysiological studies, as only a small number of functional pores are needed for measurements.

For non-spontaneously inserting proteins, incorporation of the protein into the bilayer relies in membrane fusion[84–88]. Membrane fusion is a common process in nature. Within a cell, new membrane proteins are delivered to the plasma membrane by exocytosis, which involves the fusion of vesicles with the membrane. Intracellular transport between organelles is also based on fusion of vesicles. For vesicles to fuse the lipid bilayers need to be brought into close proximity. When they are adjacent within 1.5 nm, they can join and lipids are able to diffuse from one membrane into the other. To bring lipid bilayers this close together, strong hydration forces have to be overcome, i.e. water molecules need to be removed from the polar heads of the lipids. This process is energetically very unfavourable and as a consequence fusion is not a passive process in biological systems.

Zagnoni *et al.* 2007[37] were amongst the first who investigated the addition of membrane proteins to suspended bilayers by proteoliposome fusion in a microfluidic device[37]. The technique for protein insertion was adapted from an earlier report by de

Planque *et al.* 2006[89] and Bear *et al.* 1992[90], *who* used a nystatin/ergosterol technique to assist the fusion of proteoliposomes (with the potassium channel KcsA incorporated), with the bilayer subjected to a salt concentration gradient. Within the microfluidic device, membranes with incorporated with channels were shown to remain intact for $1.5 - 2$ h and were stable enough to exchange the solution on one side of the membrane. In a different approach, the potassium channel KcsA and Leukocidin pore protein (Luk) have been inserted mechanically in a controlled manner by touching an agarose-tipped probe containing purified protein directly to the bilayer[91]. While biophysical and electrophysiological procedures involving suspended and supported BLMs have been developed and studied considerably in the laboratory, micro systems and lab-on-a-chip approaches have been popularized, promising novel systems for membrane-based applications. These systems are based on microfluidics and the manipulation of micro emulsions through channels in a high-throughput manner. Such microfluidic approach enables alternative methods for the study of membrane proteins in a cell-free system, as outlined in the next chapter.

1.5 Drug Discovery in Industry

A drug discovery programme initiates because of an unmet clinical need for a medical product to be used in the treatment of a disease or clinical condition. The initial research often occurs in academia and generates data to develop a hypothesis that the inhibition or activation of a protein or pathway will result in a therapeutic effect in a disease state. The outcome of this activity is the selection of a target, which may require further validation prior to progression into the lead discovery phase in order to justify a drug discovery effort (Figure 1.9).

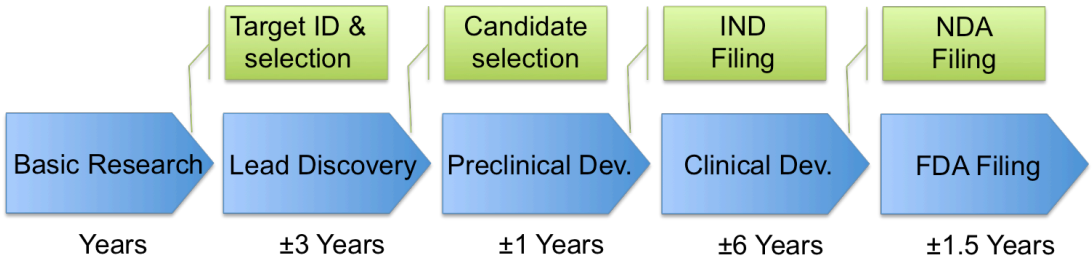

Figure 1.9 Drug discovery process from basic research to target ID and validation through to filing of a compound and the approximate timescale for these processes.

During target identification the aim is to identify a target for a potential therapy. Targets include receptors, ion channels, DNA, enzymes, hormones etc. The focus in lead discovery is to identify a drug-like small molecule or biological therapeutic, termed a development candidate that will interact with the target and have the potential to impact the disease studied. After screening many compounds, researchers focus on whether the molecule binds to a target protein. Every year pharmaceutical companies identify hundreds of thousands of compounds that may be useful new drugs. The process of finding a new drug that affects a chosen target for a particular disease usually involves high-throughput screening (HTS), in which large libraries of chemicals are tested for their ability to modify the target. This process enables researchers to conduct millions of biochemical, genetic or pharmacological tests and rapidly identify those that modulate a particular biomolecular pathway.

When a "lead" has been identified, the next stage is to find compounds that are similar to it, that might bind even better (optimization). This can involve 'similarity search' to find compounds previously made, or available commercially for purchase. To assess similarities, the following properties are analysed: absorption, distribution, metabolism, excretion, toxicity (ADMET).

1.5.1 Screening Throughput

High-Throughput Screening (HTS) has become a standard method for drug discovery in the pharmaceutical industry. It is basically a process of screening and assaying a large number of biological modulators and effectors against selected and specific targets. It is used not only among industrial scientists but also among academic

researchers. HTS assays are used for screening of different types of libraries, including combinatorial chemistry, genomics, protein, and peptide libraries. It is of vital importance, because parallel and combinatorial chemical synthesis generates a vast number of novel compounds. High-throughput screening methods are also used to characterize metabolic, pharmacokinetic and toxicological data about new drugs. HTS technology can reduce the costs of drug development[92–96] . HTS consist of several steps such as target identification, reagent preparation, compound management, assay development and high-throughput library screening[96].

HTS is capable of accelerating drug discovery by screening large libraries often composed of hundreds of thousands of compounds (drug candidates) at a rate that may exceed 10,000 compounds per day. HTS screening is often aided by the use of large liquid handling robots; medium and low throughput assays can often assay thousands or hundreds of compound per day respectively[97,98].

Ultra-high-throughput screening (UHTS) technologies are also emerging and increasing in popularity (testing of 100,000 compounds/day). Such high throughput can be achieved either with high-end liquid handling robots or by using droplets microfluidics technology as described by Agresti et.al. 2010[99–101]. In Table 1.1 types of screening modes are presented.

Table 1.1 Types of screening modes.

Screening mode	**# Samples tested/day**	**Examples**
Low-throughput screening (LTS)	1–500	Animal models, assays for cyp-mediated metabolism combined with LC/MS/MS
Medium-throughput screening (MTS)	500–10,000	Fluorescent cellular microscopic imaging assay, assays for determination of catalytic activities of oxygen-consuming enzymes
High-throughput screening (HTS)	10,000–100,000	Fluorescent enzymatic inhibition assay, luciferase reporter gene assays
Ultra-high throughput screening (UHTS)	>100,000	B-lactamase cell reporter assay, assay for quantification of 5-HT_{2c} receptor editing

1.5.2 Membrane Based Screening Assays

Pharmaceutical companies spend hundreds of millions of dollars developing drugs to be administered orally, which is why it is unacceptable for a compound to demonstrate low oral absorption in clinical trials. To prevent this problem, drug candidates are screened for their oral-absorption potential early in the discovery and development phase as a filter to remove poor performers and identify candidates that need to be modified.

The two most common assays for permeability studies in industry are PAMPA and Caco-2 (Section 1.2.3). In industry PAMPA is often used as a pre-screening tool in early drug discovery, where number of new molecular entities (NMEs) is large and after screening the molecules through PAMPA, they are finally tested with Caco-2 model. The use of 96-well microtiter plates for PAMPA assays coupled with the rapid quantification by a spectrophotometric plate reader allows this system to screen a large array of compounds in a relatively short period of time, typically 650 compounds per week (three plates/day in duplicate)[102]. Alternatively, the compound analysis can be performed with fast and sensitive LC/MS by pooling the samples together. Both the spectrophotometric and mass spectrometric methods can be used for low-solubility compounds since the limit of quantitation can reach nanomolar concentrations. The major advantage of PAMPA is that it is much less labour intensive than cell culture or in vivo studies that have similar predictive power.

It is generally accepted that the Caco-2 model is most helpful during early lead optimization in the pharmaceutical setting. This type of early screening provides medicinal chemists with guidance in choosing the more favourable chemotypes. When the Caco-2 system is teamed up with high-throughput liquid chromatography–mass spectrometry (LC/MS), a group of 1 or 2 scientists could screen 50 compounds per week (two plates/ day in duplicate)[102]. In addition, using 24-well or even 96-well plate systems coupled with LC/MS, significantly reduces the amount of compound required to perform permeability experiments with this model[103].

The pharmaceutical industry is motivated to shorten research timelines and discover increasing numbers of clinical candidates. Research efforts are focusing on how to identify high-quality lead compounds that are less likely to fail in pre-clinical testing and HTS laboratories are ideally placed to assist in this regard.

Much of the infrastructure that has been established for running a primary screen at high throughput (particularly laboratory automation, assay development, and data analysis systems) is being applied to downstream needs in drug discovery. Many HTS departments are shouldering the responsibility for running preliminary ADME-Tox screens, and the tendency toward automating assays that have traditionally been run in low throughput is likely to continue.

Miniaturization has decreased the cost of individual screening campaigns, but the abundance of new targets generated by genomics approaches (for which HTS is often the only feasible option for leads discovery) has driven running costs even higher. As a consequence of financial considerations, in the future, we are likely to observer a mutual relationship between HTS (in vitro screening) and synthetic (in silico) screening.

HTS and synthetic screening are complementary approaches for leads discovery: they can be employed independently of each other or in combination[102]. HTS methods (both of random libraries and focused compound collections) will continue to play a pivotal role in systematic discovery as high-throughput approaches are progressively applied to accelerate the identification of new clinical drug candidates.

1.6 Chapter Summary

Research on both membrane permeation and drug screening on ion channels can benefit from miniaturization approaches such as microfluidics. Much progress has been made to integrate membranes into microfluidic devices and different platforms have

been proposed. However, none of these technologies satisfy all criteria required for industrial application such as high throughput, low cost and high recording quality.

For membrane permeability studies, alternative methods have been established, such as the parallel artificial membrane permeability assay (PAMPA) or diffusion assays across cell monolayers, e.g. Caco-2. Cell-based assays such as Caco-2 are more application relevant but they allow only limited throughput and are very labour-intensive. Additionally, the drugs have to pass through the cells and may be metabolized during the process. PAMPA is a cost-efficient and commonly applied method in which a solution containing the drug is separated from an initially drug-free buffer by an artificial membrane, however the artificial membrane formed is too thick in comparison with a biological membrane and residual solvent in the membrane, may influence the permeation kinetics. For ion channel studies and drug screening applications, the development of automated patch clamp platforms has considerably improved throughput. Yet, the data quality acquired is still limited for primary screening. Consequently, there exists a role for novel technologies combining these key features, ideally working with a cell-free model.

Chapter 2

Miniaturization of BLM Systems

This chapter aims to present the basic elements of microfluidics focusing on droplet-based modules that are applicable to the development of a platform for high throughput membrane protein studies. We introduce the physical phenomena that are most important for the experiments in this thesis and review a large number of microfluidic systems for lipid membrane research that have been developed in recent years.

2.1 Microfluidics

Of particular interest for both drug discovery and basic research is the ability to interrogate and characterise the behaviour of membrane proteins in a fast, reliable and miniaturised manner. Therefore, it is essential to find ways to mimic biological membranes and design approaches where some guiding principles from nature are extracted in order to provide a basis for creating new technological devices in order to solve complex problems. Microfluidics technology offers such opportunities.

Microfluidics systems are characterized by the ability to manipulate fluids in channels with dimensions of less than 1 mm. Miniaturization of the fluidic processes to the micro-scale offers many important advantages, some stemming directly from the reduction in size - reduced sample usage, portability, lower costs- and others as a result of the ability to integrate at this scale. Additionally, the decrease in dimension leads to new phenomena and permits entirely new applications that are not accessible to traditional platforms.

The concept of microfluidics originated in 1970 when the first gas chromatograph based on micrometre size channels was developed[104]. Miniaturized systems became popularized by Manz et al.[105] with the concept of micro total analysis systems (μTAS) where they proposed that it was possible to perform complex analytic experiments in microchannels with the advantages offered by the decrease in size.

The use of soft lithography techniques using polydimethylsiloxane (PDMS) for the rapid prototyping of microstructures by Duffy *et al.* 1998[106] allowed microfluidics to become more widely adopted by research groups. Polymers are an attractive alternative to the silicon and glass, which were previously used, as they are inexpensive and more robust and fabrication techniques are faster and cheaper.

Simplified device fabrication and the possibility of integration have helped microfluidics to expand into a universal technology, initially with applications in fields which included: electrophoretic separation systems[107], DNA amplifiers[57], chemical microreactors[108], and enzymatic screening. More currently the technology has

proposed applications in the field of tissue engineering[109], organ-on-a-chip[110] and point-of-care diagnostics[111]. By detecting cellular analytes, electrical activity, physical and chemical signals transmitted by the cells or proteins, biosensors can provide insights into cellular activities and responses in real time.

2.1.1 Physics at the Micro Scale

When channels are downscaled to micrometre size, interesting and unexpected phenomena occur compared to those in the macro-world. Surface effects become very important because of the high surface-to-volume ratios, flows are typically laminar rather than turbulent, and gravitation has mostly negligible effects[112].

Reynolds Number

The Reynolds number (Re) is an important dimensionless number in fluid mechanics and describes whether a fluid is influenced more by viscous or by more inertial forces. Re is defined as:

$$Re = \frac{\rho U l}{\mu}$$

Equation 2-1 Reynolds Number

where U (m/s) is the characteristic velocity, l (m) is the characteristic length scale, ρ (kg/m^3) is the density of the fluid and μ (kg/(m · s) is its dynamic viscosity.

The Reynolds number denotes the ratio of the magnitude of inertial forces in the flow to viscous forces in the flow. At low Reynolds number (Re$< 10^{-1}$), inertial forces – the property of an object to continue at a constant velocity, unless an external force acts on it – are very negligible with respect to viscous forces, thus an object will start or stop almost instantaneously with the flow. In contrast, an object with a large inertia will resist strongly to a change in velocity, being difficult to start or stop its movement.

The non-linearity caused by large inertia creates oscillations in the flow. As a consequence, at large Reynolds numbers when inertial effects are dominant, the flow

can get turbulent. For small Reynolds number, on the other hand, the flow is always non-turbulent, i.e. laminar.

The resistance of a fluid to flow under the influence of an applied external force is its viscosity. Viscosity is the source of drag on objects moving through the fluid. While inertia strives to keep the object going, viscosity tries to stop it.

Fluid Flow

Fluid flow in microfluidic devices can be considered by the Navier–Stokes equation for incompressible fluids:

$$\frac{\rho(\delta\vec{u})}{\delta t} = -\rho\vec{u}\nabla\vec{u} - \nabla p + \eta\nabla^2\vec{u}$$

(Rate of change of momentum) = (convective forces) + (pressure) + (viscous forces)

Equation 2-2 Navier–Stokes

where u is the velocity of the fluid, ρ (kg/m^3) is the fluid density, η (kg/(m · s)) is the viscosity and p (Pa) is the pressure in the system. The left-hand side of Equation 2-2, with the inertia related terms, describes the change in momentum of the fluid. This could be a change in velocity or an acceleration of the fluid (e.g. due to a flow constriction). The right-hand side takes the forces acting on the fluid into account.

For an incompressible fluid within a micro-channel, the flow is typically laminar for small Reynold numbers, resulting in negligible inertial effects. Hence, the equation above can then be simplified to:

$$\nabla p = \eta\nabla^2\vec{u}\bigtriangledown$$

Equation 2-3 Navier–Stokes Simplification

The simplified equation now contains no time derivatives because at the microscale (not considering temperature effects), all motion is symmetric in time. Thus, if the pressures or forces exerted on the fluid are inverted, the motion in the fluid is completely inverted[113]. This equation shows that driving pressure and viscous forces are balanced in a laminar, stationary flow.

Diffusion

Due to the low Reynolds numbers and therefore the absence of turbulence in microfluidic channels, diffusion is the main transport mechanism to mix fluids. The characteristic diffusion time (t_D) can be written as:

$$t_D = \frac{l^2_D}{2D}$$

Equation 2-4 Diffusion Time

with l_D (m) being the diffusion distance and D (m^2/s) the diffusion coefficient:

$$D_{AB} = \frac{kT}{6\pi r_0 \eta_B}$$

Equation 2-5 Diffusion Coefficient

where A is the diffusing substance, B is the viscous liquid, r_0 is the particle (molecule) radius (m), T (K) is the absolute temperature, η_B ($kg/(m \cdot s)$), the liquid viscosity and k the Boltzmann constant (1.38×10^{-23} $m^2 \cdot kg/(s^2 \cdot K)$). Because of the small length scales in microchannels, the diffusion time t_D is short compared to larger volumes. However, for larger biomolecules, like DNA or proteins, it still takes minutes to cross a distance of 100 µm.

2.2 Droplet Microfluidics

Droplet-based microfluidics involves the generation and manipulation of discrete droplets inside micro devices[114]. It uses immiscible phases to create emulsions of mono-disperse droplets that act as reaction and transport vehicles. This method produces highly mono-disperse droplets in the nanometre to micrometre diameter range, at rates of up to twenty thousand droplets per second[115].

The advantage of generating microscale droplets over the macroscale (> 1 mm in diameter) ones is the larger surface-to-volume ratio. The change in surface-to-volume ratio and the small length scale has a strong impact on mass and heat transfer, often allowing a significant increase in reaction kinetics in comparison to reactions on

larger scales due to faster mixing, an advantage that is also generally applicable to microfluidics.

Particular to drug discovery, droplet microfluidics offers many attractive characteristics including minimal sample consumption, low cross-contamination, fast mixing, miniaturized space, high-throughput capabilities and multiplexed detection[116]. In molecular biology, droplets with homogeneous diameters and controlled content that do not evaporate are important for screening experiments that rely on high reproducibility such as protein crystallization[117], gene mutation[118], and molecular evolution[119].

In droplet-based microfluidic systems, aqueous droplets are dispersed in an immiscible phase, which isolates the aqueous droplet from its environment, thus creating self-contained micro reactors. This offers the ability to perform large number of reactions without compromising device size or complexity. Furthermore, aqueous contact with solid walls is eliminated reducing problems due to adsorption of dissolved components to the channel walls, hence increasing the efficiency of chemical reactions[120].

Surfactants are an essential part of the droplet-based microfluidic technology. They are involved in the stabilization of droplet interfaces, in the biocompatibility of the system and in the process of molecular exchange between droplets. These amphiphilic molecules are commonly used to stabilize the droplet interface and prevent coalescence of droplets[121]. The dispersion of a fluid into another is a system out of thermodynamic equilibrium: the total energetic cost for the formation of the interfacial area is unfavourable and the minimum of energy of the system is a configuration where the two liquids are separated in two phases. The driving force acting towards the homogenisation of the system is balanced by the action of surfactants. Adding surfactants provides an energy barrier to stabilize the dispersion in a metastable state[121,122].

The formation of uniform droplets requires fine control over the size, shape, and mono-dispersity of droplets. The ability to exert such fine control is the essence of droplet microfluidics. Even though the same basic principles and materials are employed, many different techniques have been used for droplet generation.

The two most common droplet formation techniques are the T-junction and flow focussing geometries (Figure 2.1). Even though the size of the opening of the T-junction or flow focussing channel are major contributors to the size of droplets formed, other factors such the immiscible phase viscosity, the surfactant type, and the hydrophobicity of the channel surface can determine the size ranges of droplets formed.

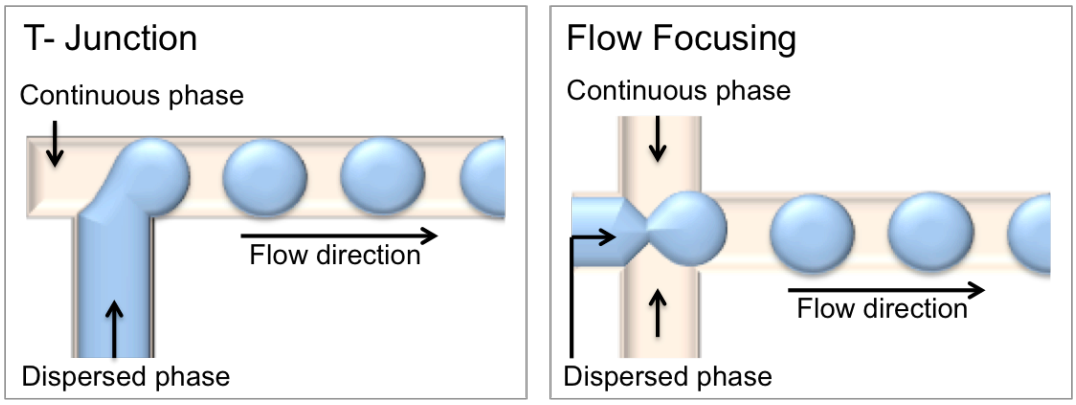

Figure 2.1 The two most common droplet formation geometries. T-Junction and Flow Focusing.

Capillary Number

The dimensionless capillary number, *Ca*, plays an important part in determining droplet dynamics, such as droplet break off[123].

Capillary number describes the relative effects of viscous forces versus surface tension forces acting across an interface between immiscible liquids. In a microfluidic system, when there is flow present, gravity can be neglected and the dominant forces are those related to viscous stress and capillarity. Capillary number is defined as:

$$Ca = \frac{\eta v}{\gamma}$$

Equation 2-6 Capillary Number

where η (kg/(m · s)) is the viscosity of the continuous phase, v (m/s) is the velocity of the continuous phase, and γ (N/m) is the interfacial tension between the oil and water phases. In a microfluidics system, we can anticipate that at small capillary numbers (Ca $<$ 0.01), interfacial tension forces dominate over viscous forces and droplets will be spherical. At moderate capillary numbers (0.01 $<$ Ca $<$ 1), viscous forces dominate over interfacial tension forces and the droplet will be subjected to deformations induced by viscous forces. For high value of Ca (Ca $>$ 1), the droplet becomes unstable and breaks easily.

2.2.1 Droplet Microfluidics for industrial Applications

Droplet microfluidic technology can be a suitable platform for a wide variety of reactions through systems integration with other microfluidic models. Droplet microfluidics has been one of the most applied novel technologies in bioprocess investigations, even though still in laboratory scale, but there are interesting perspectives for commercial applications.

In industrial biotechnology, droplet-based microfluidics major application focus is on analysis in situ, involving determination of cell density, use of sensors to detect any metabolites, and for the high-throughput screen of microbial cells[124]. The employment of the droplet microfluidic technique where droplets acts a compartmentalized microbioreactor was demonstrated by Wang *et al.* 2014[125] for analysing growth and the production and consumption of extracellular metabolites in engineered yeast cells in order to improve the productivity of xylose isomerase (Figure 2.2). This platform also allows for the integration of concentration gradient systems, which are able to promote, for example, the encapsulation and evaluation of enzyme kinetics *in situ*, as investigated by Bui *et al.* 2011[126] (Figure 2.2). As a bioanalytical tool, Piao *et al.* 2015[127] used droplet systems to perform high sensitivity detection of glucose concentration through an enzyme catalytic reaction. Taking into account that multiple factors can be analysed in a fast and reproducibly way in a single platform,

these technologies are relevant as determination methods toward increasing biological processes yield.

Another important advantage of droplet microfluidic systems is the possibility to generate drops at high production rates in a compact system, overcoming limitations for industrial applications[128,129]. The strategy is to develop devices that generate droplets in parallel and through a continuous process, maintaining the same characteristics as the simplified and individual models[128,130] as the higher monodisperse microparticle generator shown by Nisisako and Torii 2008[131] on Figure 2.3. Thus, the possibility to increase production rates using the parallelization of individual units is called amplification, which is attractive for industrial applications.

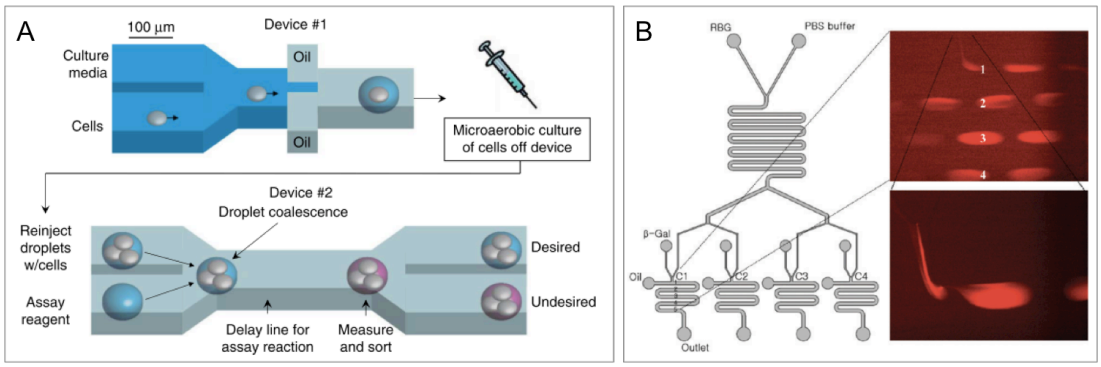

Figure 2.2 Droplet microfluidic platforms for cells investigations: A) Droplet microfluidics integrated with microreactor to cells growth and determination of metabolites consumption and production[125]. B) Droplet microfluidic with gradient system for evaluation of enzyme kinetics in situ[126].

The industrial biotechnology interest in droplet-based microfluidics also concerns its economic value, given the reproducibility and scalability of the process. Further, the microencapsulation technology protects products of high economic value, reuses encapsulated biocatalysts, and produces reactors of continuous process without loss of biological material. Indeed, the amplification approach involves significant technological challenges[128,132]. Nevertheless, the controlled production of droplets in microfluidics, which is much harder to achieve using standard techniques, favours its applications for industrial biotechnology.

2.3 Miniaturization of Model Membrane Systems

Several of miniaturized devices have been developed in the last decade, with primary focus on membrane protein studies. These miniaturised devices are aimed at the creation of automatable, high-throughput and reliable methodologies for drug screening applications and the mimicking of cellular mechanisms[133–135].

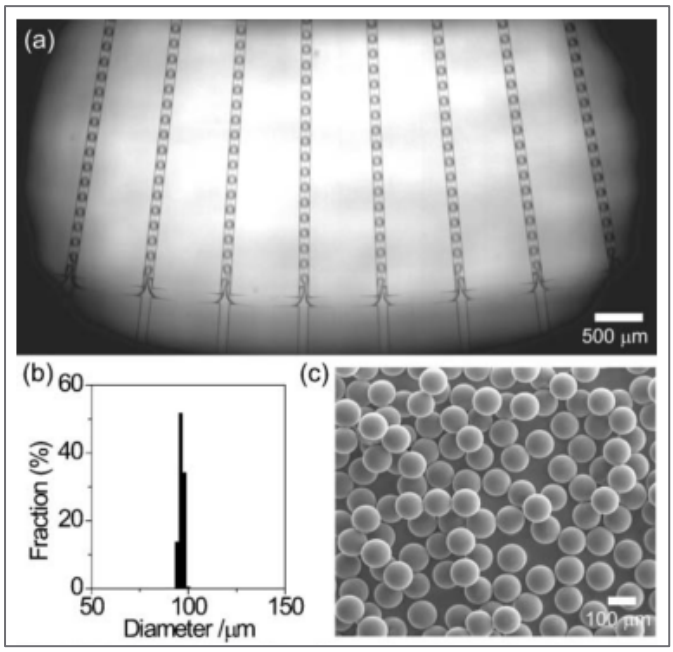

Figure 2.3 Amplified microfluidic platforms with parallelization showing co-flow geometries for scale-up of biphasic Janus droplets[131]

The use of model membrane systems for the analysis of membrane proteins offers two main advantages over conventional assays: first, it allows the study of membrane proteins that are difficult to access by patch clamp, including proteins located in intracellular organelles. Secondly, measurement conditions, such as the composition of the lipid membrane and buffer, can be finely tuned for sensitive analysis and unlike in experiments with live cells, where protein expression levels fluctuate widely from cell to cell, the concentration of membrane proteins in reconstituted membranes can be controlled, permitting more reproducible results. Nevertheless, a number of issues, such as bilayer stability, multiplexing and eukaryotic channel recording, still must be carefully addressed before the technology can be

considered in an industrial setting. These subjects have been the focus of the most recent research on the miniaturization of model bilayers. Furthermore, to gain interest form the pharmaceutical industry microfluidic bilayer platforms must be validated on relevant ion channels, and finally through drug screening.

2.3.1 Bilayer Stability and Miniaturization

Traditional approaches to form model bilayers such as the Montal-Mueller[56] technique are low-throughput processes, which cannot be readily translated into microfluidic and miniaturized devices due to rearrangement of the geometry of the device. Furthermore, like manual patch clamp, studies on ion channels embedded in a membrane can only be carried out in one experiment at a time. Currently, there are no widely available commercial systems that allow for the automated formation of artificial lipid bilayers and ion channels recordings on parallel arrays of artificial lipid bilayers are still in an early stage. Therefore, novel approaches are required to create BLMs in a miniaturized, microfluidic format.

An advantage of miniaturization for bilayer platforms is the possibility to produce micron-sized apertures. It has been shown that stability of BLMs inversely scales with the size of the aperture supporting the bilayers and the lifetime of the lipid bilayers is enhanced if suspended on nanometre sized pores (Figure 2.4). Han et *al.* 2007[136] created lipid bilayers on nanopore arrays by painting and observed the bilayer resistance using electrochemical impedance spectroscopy (EIS) to study the influence of pore dimension and membrane lipid composition on the stability of the planar bilayer. It was found that for a given lipid composition bilayer stability could be improved by a factor of 30 when the pore size decreases from 800 nm to 200 nm (Figure 2.4 A - Right).

It is worth noting that not only the size of the aperture matters, but also the ratio between the height and the diameter of the channels as well as lipid composition. For instance, the stability of suspended bilayers consisting of naturally occurring lipid mixtures could be significantly improved by paying close attention to bilayer and lipid

shape. Suspended bilayers made using phosphatidyl ethanolamine (PE) lipids showed extremely high stability lasting for 6 days whereas bilayers made with phosphatidyl choline (PC) lipids were found to be less stable in the suspended nanopore arrays (Figure 2.4 A - Right). This effect mostly is due to the overall shape of the lipids. Cylindrical PC lipids form stable planar bilayers whereas PEs, which have an overall "conical shape", with a small head group compared to its apolar tail are better suited for the curved bilayers of liposomes[136].

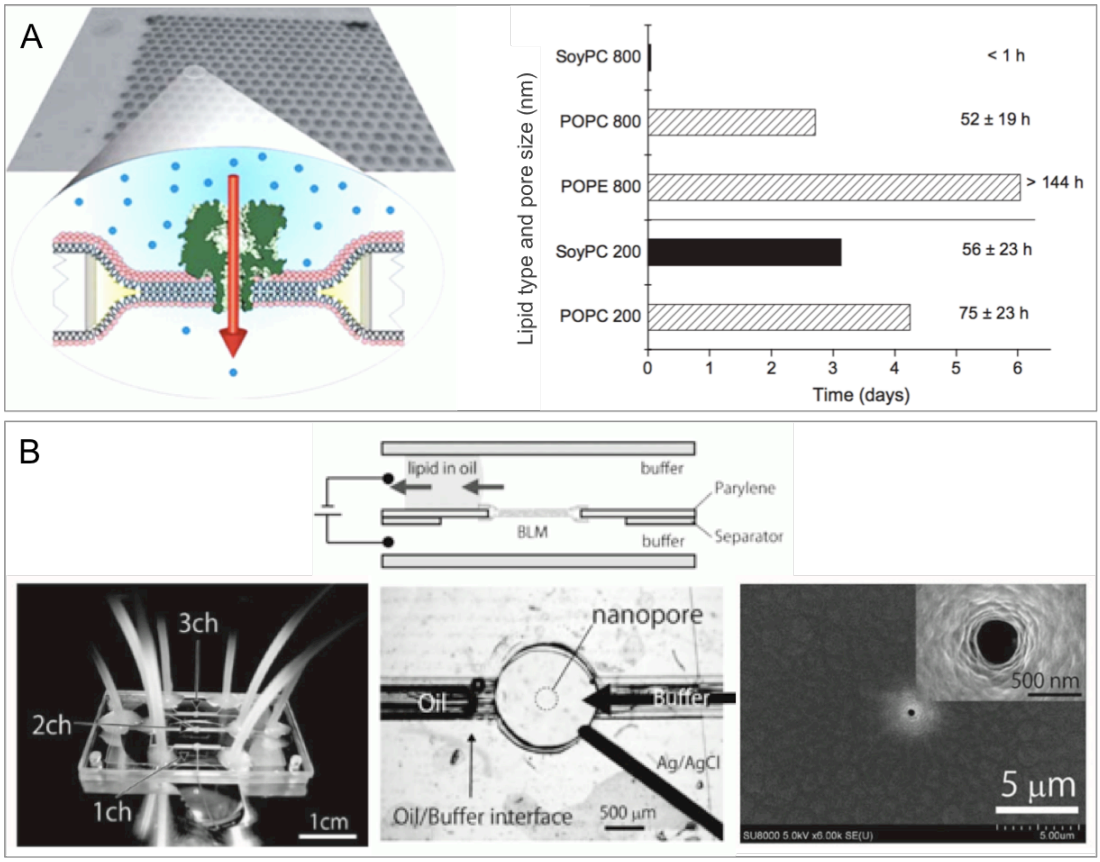

Figure 2.4 Bilayer formation and stability. (A) Left -Spontaneous insertion and pore formation of a-haemolysin in a freestanding lipid bilayer in nanopores[136,137]. Right- Stability of bilayers of different lipids on 800 nm and 200 nm pores. From four separate preparations, the longest period (in days) is displayed and the mean ±1 S.D. (3 best preparations) is given (in hours). (B) A fully closed microfluidic device with three nanopores in parallel (left). Two fluidic layers are connected by a 400 nm pore in parylene (middle and right[138])

Kawano *et al.* 2010[138] advanced the system to use nanometre-sized pores in combination with microfluidics depositing parylene onto micropores (Figure 2.4 B). Here, several milestones for BLM integration into microfluidic devices were achieved. First, a low-cost fabrication technique was presented; second, the membrane remained

stable for several days; third, solution exchange was possible without rupture of the membrane. In a complementary study, the same group reported that the device could be multiplexed to an array of pores for small molecule detection[139].

Supporting the bilayer with hydrogel (DHB) or a droplet (DIB) greatly increases the bilayer mechanical stability and lifetime, those being extended from days to weeks[14,135]. The bottleneck found with DIB models is the difficulty to perfuse liquid into the droplet compartments once the bilayers have been created. Two solutions have recently been proposed: Firstly by connecting the droplets to independent microfluidic channels enabling solution replacement[140] and secondly by separating the droplets and reconnecting them to other droplets filled with a different buffer solution (Figure 2.7 A)[135,141].

2.3.2 Multiplexing of BLMs

Another common challenge often faced by conventional BLMs methods is the ability for multiplexing. Miniaturized platforms often have a more malleable geometry, which can be designed to allow parallelisation and multiplexing of assays, thus allowing higher throughput of experiments.

Many of the current designs proposed for multiplexing bilayer experimentation comprise of two fluidic compartments, which are separated by the bilayer formed across a micro aperture. This format has the potential to be extended by arraying the cavities and the bilayers. Osaki *et al.* 2010[142] proposed a microarray system permitting simultaneous monitoring of ionic currents across transmembrane α-haemolysin pores arrayed in bilayer lipid membranes. The fast and reproducible self-assembly of bilayers was achieved in a semi-automated manner by painting lipids dissolved in solvent across micro chambers with microfluidics handling, a technique previously proposed by Suzuki *et al.* 2006[143]. Electrodes were integrated for electrophysiological recordings and parallel monitoring of eight wells was accomplished (Figure 2.5 B).

Using a similar bilayer formation protocol, Ota *et al.* 2011[144] have shown a fully enclosed microfluidic device hosting an array of BLMs. In this approach, the

buffer and the lipid–solvent mixture were sequentially injected in the microfluidic device, forming an array of BLMs between a main channel and an array of micro chambers on either side. Within the chambers, α-haemolysin monomers were added to form nanopores in the membrane and calcium flux was recorded optically to probe the functionality of incorporated ion channels (Figure 2.5 A). A clear drawback of this configuration is that all bilayers must be tested under the same experimental conditions.

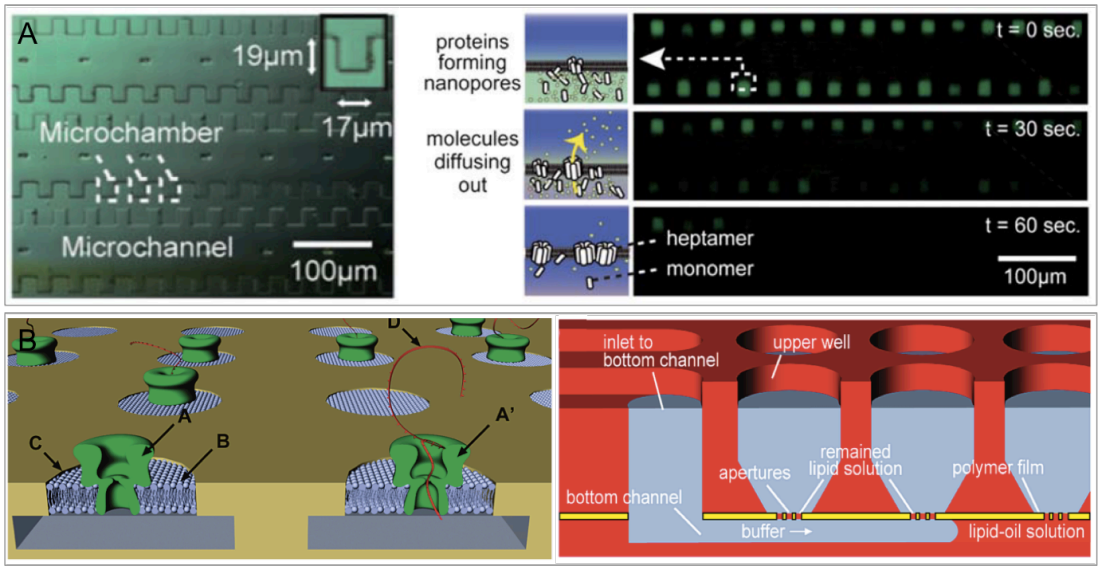

Figure 2.5 Ion channel detection using a microfluidic system. (A) Left- Magnified view of the device. Right- Time-lapse images showing successful incorporation of α-haemolysin channels demonstrated by rapid decrease in fluorescence intensity in the micro chambers across the lipid membranes. (B) Left- A system enabling parallel detection of single molecules using α-haemolysin (α -HL) pores -A present in a bilayer -B suspended in micron sized nanopores-C. Right- cross-sectional image of the device

Using droplet microfluidics, Stanley *et al.* 2010[145] showed that droplet interface bilayers (DIBs) can be made quickly and in a high-throughput format by storing droplets in a capillary adjacent to each other. Bilayer formation was successfully validated using a fluorescein permeation assay (Figure 2.6).

2.3.3 Channel Recording in BLMs

Channel incorporation into microfluidic bilayer platforms has mainly been tested using self-inserting pores such as alamethicin, gramicidin and alpha-hemolysin[138,142,144] by dissolving the purified pores in the aqueous phase. However, large transmembrane

channels do not usually reliably self-insert into planar membranes and different techniques are required to ensure channel reconstitution into a BLM.

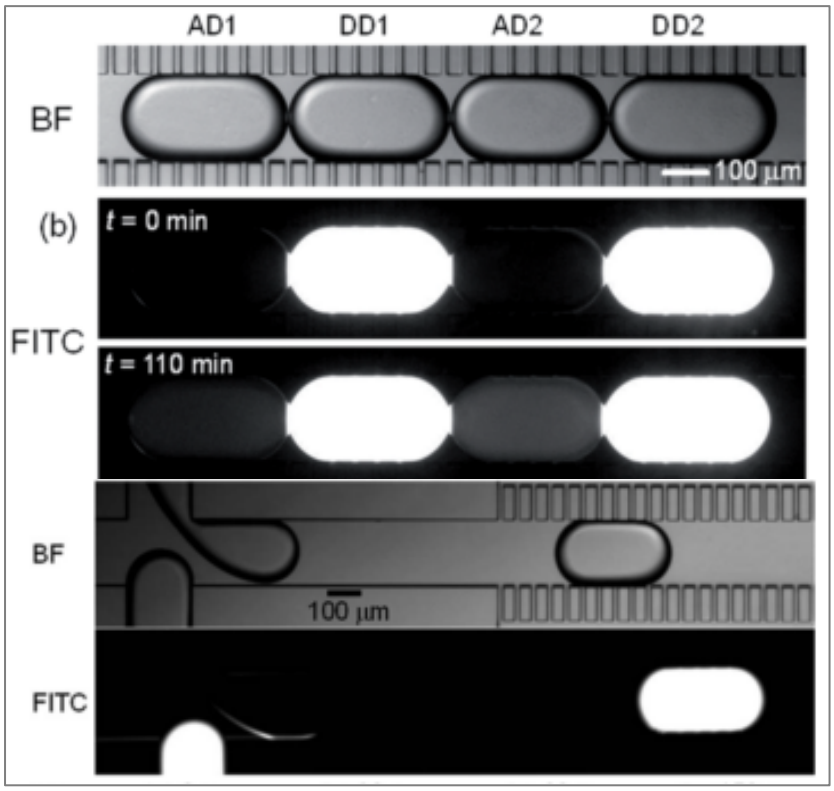

Figure 2.6 Formation of DIBs at the interface between two stationary aqueous droplets (top). Exchange of fluorescein from a donor droplet (DD) containing fluorescein to an acceptor droplet (AD) containing buffer only, is observed overtime[145].

In a pioneering report, Funakoshi *et al.* 2006[57] built microfluidic chips in which a bilayer is formed between two aqueous streams surrounded with hexadecane (Figure 2.7 A). The formation of a true DIB was confirmed by capacitance measurements of the bilayer and voltage-clamp recording indicating incorporation of α-haemolysin pores. This DIB system was proved to be useful in investigation of other proteins, for example bacterial potassium channels[140,146] or eukaryotic mammalian menthol receptor or equinatoxin[147–149] where the channels were incorporated into the DIB by proteoliposome fusion.

Syeda *et al.* 2008[141] showed that membrane proteins freshly synthesized by *in vitro* (cell-free) transcription and translation (IVTT) inside a droplet can be incorporated into the bilayer in a functional form. Channel incorporation is made

possible due to the closely coupled membrane protein expression and reconstitution because expression happens in the vicinity of the DIB. The viral potassium channel, Kcv, was produced by IVTT and screened by serially contacting droplets containing Kcv to drug-containing droplets. DIBs were formed between the two lipid monolayer confined droplets, one of which is filled with the in vitro (cell-free) transcription and translation (IVTT) mixture, while channel blockers were encapsulated in the other. The currents flowing through individual Kcv channels were recorded as the channels became incorporated into the bilayer. The Kcv containing droplet was then disconnected from the buffer droplet and connected to a droplet containing a blocker. Conductance values were recorded and seemed to demonstrate channel inhibition (Figure 2.7 B).

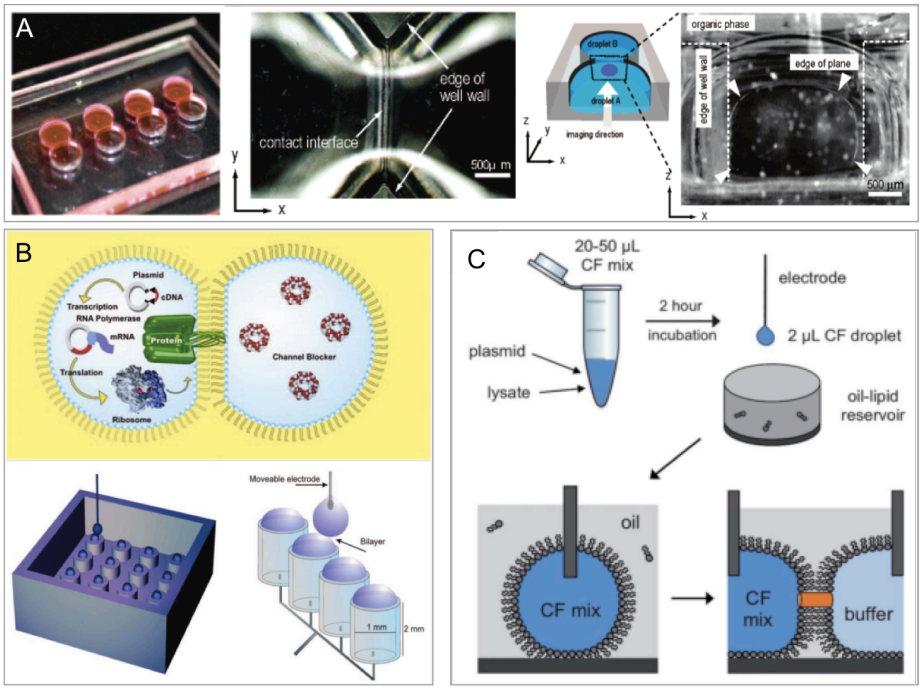

Figure 2.7 DIB platforms. (A) Left-Photo of the double well chip with two different colour droplets (red and clear). The droplets do not mix as the lipid bilayer forms at the interface. Middle- Microscopic images of the bilayer interface viewed from the top[57]. (B) Schematic representation of cell-free transcription and translation (IVTT) to form polypeptides within the aqueous droplet used to form a DIB (top). Simplified schematic of the chip used for ion-channel screening. Each well holds 1.5 µL of solution and presents a convex surface under the oil. A droplet containing the desired IVTT mixture is suspended from an Ag/AgCl electrode. A DIB is formed between the IVTT droplet and the control well to verify normal channel function. Subsequently, the DIB is separated and the droplet is moved to the next well, and so on[141]. (C) Left- Schematic representation DIBs exposed to a cell-free expression reaction mixture[150].

In a similar approach Friddin *et al.* 2013[150,151] used IVTT to express and record KcsA channels in droplet lipid bilayers. The IVTT reaction mixture was placed at the tip of an agar- coated Ag/AgCl electrode, which was subsequently immersed in a reservoir of decane oil with solubilized asolectin lipids, leading to the formation of a lipid monolayer at the aqueous–oil interface. Bilayers were formed by manually moving the electrodes towards each other (Figure 2.7 C).

Finally, and most importantly, several recent articles have demonstrated the capability of droplet interface platforms for the establishment of IC_{50} curves using potassium channels, which is clearly indicates that this microfluidic bilayer approach can be utilized for drug screening application on ion channels[147,152].

2.3.4 Synchronization of Droplet Production

The ability to produce droplets in the ABAB format is very important for membrane protein assays. Membrane protein studies require an external input to elicit a response causing a change to the internal environment of the cell or vice-versa. The assays performed in this thesis will have one droplet representing the interior of the cell and the other representing the external environment. Droplet pairing can be achieved either by alternating droplet formation, or synchronization of two separate droplet streams. Passive methods of alternating droplet formation mainly utilize the hydrodynamic coupling effects at multiple droplet generators[153–158].

Zheng *et al.* 2004[153] demonstrated the alternating droplet formation at two opposing T-junctions. These droplets did not appear to be cross-contaminated even though the solutions A and the solutions B came into proximity during the formation of the droplets. Generation of droplet ratios of two reagents was not observed under all conditions, and the coalescence of droplets was a problem at low flow rates. Coalescence and droplet alternation was characterized as a function of Capillary number (Ca). In the first regime ($Ca < 0.001$, Figure 2.8 A, top), surface tension dominates. The aqueous streams reached the inlet junction head to head and coalesced. Droplets containing a mixture of the colourless and dark red aqueous

streams formed. In the second regime ($0.001 < Ca < 0.05$, Figure 2.8 A, middle), the aqueous streams snapped-off cleanly and did not coalesce. The two streams took turns to form droplets and a steady array of alternating droplets was generated in the main channel. In the third regime ($0.05 < Ca < 0.13$, Figure 2.8 A, bottom), shear forces became larger and there was a competition between shear force and surface tension.

Hung *et al.* 2006[159] improved this design by adding two triangular wings between the inlets and the T- junctions in order to reduce the flow instability and prevent reagents from back flowing (Figure 2.8 B). Chokkalingam *et al.* 2008[160] also presented a self-synchronizing pairwise production of droplets with two step-emulsification devices sharing the continuous phase (Figure 2.8 C). In addition, Frenz *et al.* 2008[156] studied a microfluidic dual nozzle for the production of droplet pairs (Figure 2.8 D). Droplets are paired by the hydrodynamic coupling of two nozzles, and the size ratio between paired droplets is directly controlled by the flow rates of the dispersed phase. All of these hydrodynamic coupling droplet generators suffer from problems with irregular fluid flow rates and pressure fluctuations, which could disrupt the droplet formation.

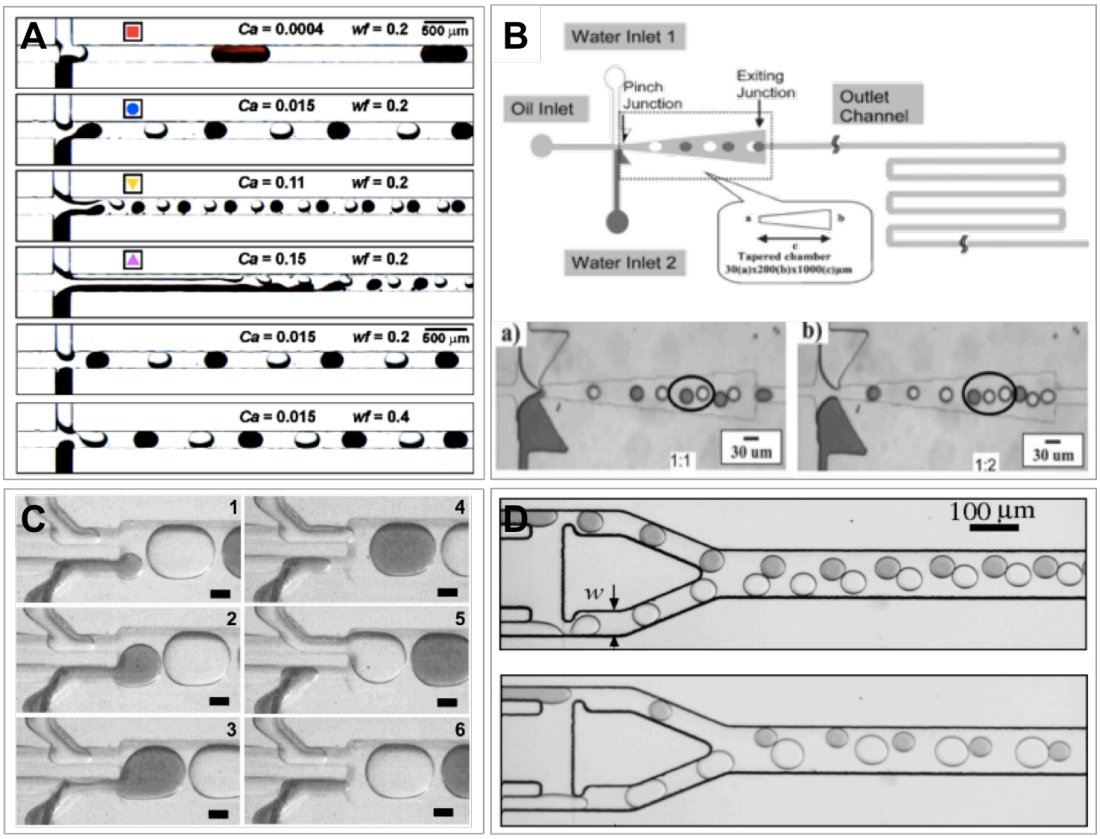

Figure 2.8 Droplet alternation geometries. (A) Formation of alternating droplets by Zheng et al. 2004[153]. Four regimes observed for the formation of alternating droplets as a function of the capillary number Ca. Microphotographs of the four regimes observed as the capillary number (Ca) varied. (B) Schematic diagram of the micro channel geometry demonstrated by Hung et al. 2010[159]. (C) Time series of optical images displaying the droplet formation mechanism presented by Chokkalingam et al. 2008[160]. (D) Pairing module. Two aqueous phases are injected by the outer channels and synchronously emulsified by the central oil channel studied by Frenz et al. 2008[156].

Ahn et al. 2011[161], presented a ladder structure for droplet synchronization, in which a top and a bottom channel were connected with a ladder network and experimentally studied the synchronization efficiency as a function of droplet length and droplet generation frequency (Figure 2.9). The droplet synchronization mechanism is based on the change in velocity within the channel due to an increased net flow of the continuous phase towards the least resistive channel, thus decreasing the velocity with in the more resistive channel. This velocity gradient makes it possible to diminish the distance between droplets and achieve droplet synchronization. The synchronization efficiency can reach up to 95% when the droplet generation frequency

difference in two streams is minimized, but can drop dramatically when the generation frequency difference is high.

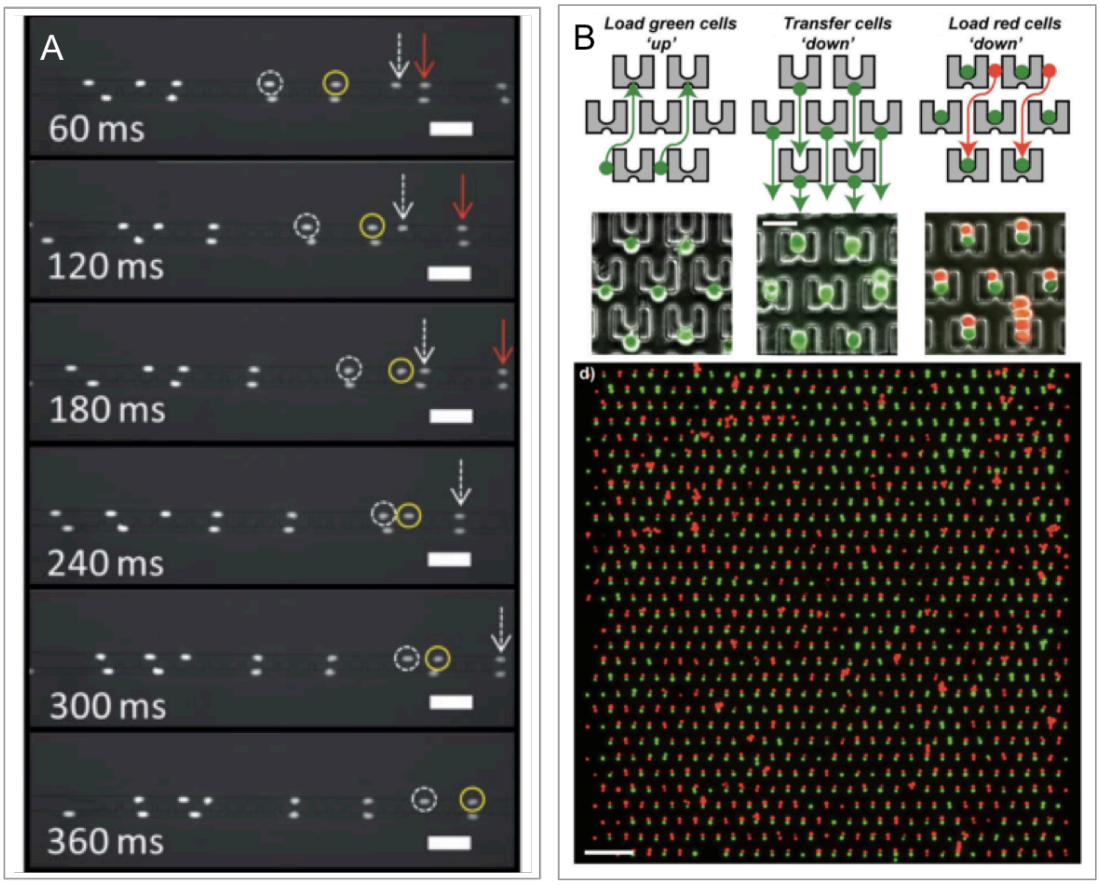

Figure 2.9 Droplet synchronization. (A) A fluidic ladder network for droplet synchronization reported by Ahn et al. 2011[161]. Four different droplets are marked. At 60 ms the solid arrowed droplet is the unpaired droplet and the others are matched. At 120 ms the following droplet (dotted arrowed droplet) is catching up with the unpaired droplet and the droplet paring is switched. (B) Microfluidic device for cell capture and pairing presented by Skelley et al 2009[162]

Skelley *et al.* 2009[162] presented another microfluidic device to pair different cell types in a high throughput manner using flow-induced cell trapping as shown in Figure 2.9, and later improved the design by using flow-induced deformation of cells[163]. Since the cells were randomly trapped, many cells bypassed the pillars without getting trapped leading to a pairing efficiency of approximately 70%.

2.3.5 Droplet Storage

The study of DIBs permeation and channel incorporation requires the incubation of droplets in an alternating manner. For this, droplets must be trapped inside micro

channels by adding some narrow constriction geometries or by storing droplets inside a large chamber.

Tan *et al.* 2007[164] first proposed a trap-and release integrated microfluidic system containing a repeated sequence of loops as shown in (Figure 2.10 A) to trap and release selected droplets. Each loop consists of two branches with one branch containing a hydrodynamic trap and the other containing a bypass channel. When the trap is empty, the flow resistance of the trap is lower than that of the bypass channel, allowing one droplet go into the trap. After the droplet gets trapped, the flow resistance of the trap is higher than that of the bypass channel and the following droplets will go through the bypass channel.

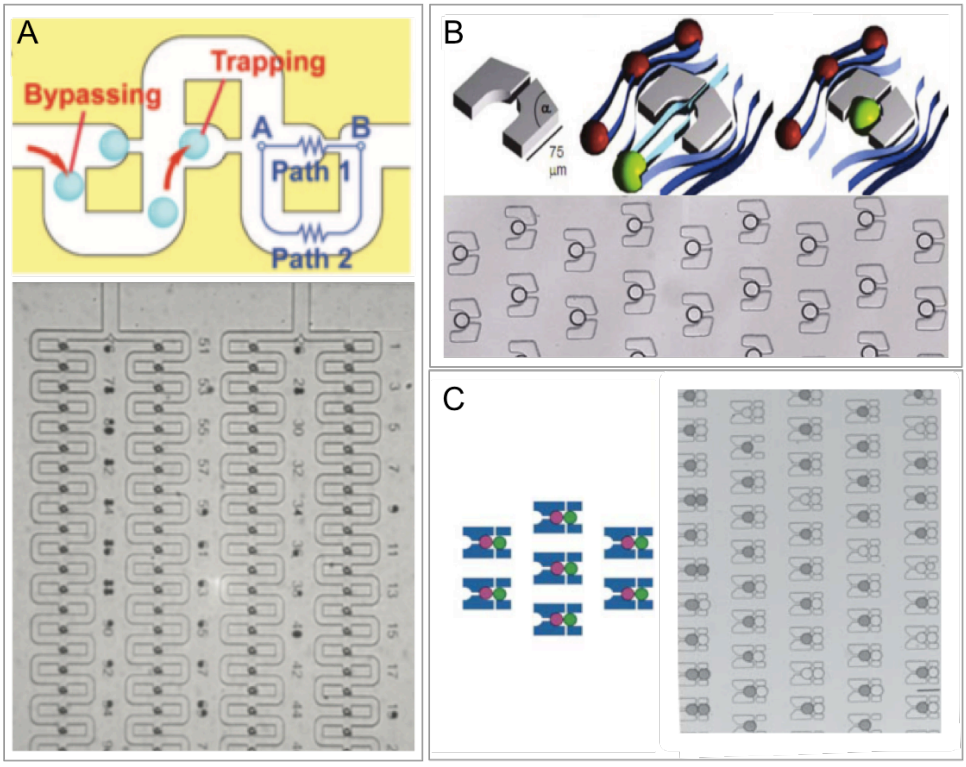

Figure 2.10 Droplet trapping geometries. (A) Trap-and-release mechanism and experimental setup proposed by Tan et al. 2007[164]. (B) Droplet trapping arrays presented by Huebner et al. 2009[165]. (C) Design by Bai et al. 2010[166] for the trapping of alternating droplet pairs. Droplets were first loaded toward the backside cup of traps. When the direction of the flow was reversed, the droplets were transferred down into the front-side capture cup two rows below. The second droplet was loaded from the top, and captured in front of the first droplet type.

Huebner *et al.* 2009[167] described another droplet trapping geometry (Figure 2.10 B). When a trap is empty, oil is able to flow through the pillars. As long as a

droplet is captured within a pillar, it blocks the exit leading to the termination of fluid flow within the trap and keeping a second droplet from entering the trap. This design just randomly captures droplets flowing through the channel, and most droplets pass through the chamber without being trapped. However, this design is helpful to release trapped droplets by just applying a reverse flow of the continuous phase. Bai *et al.* 2010[166] modified this design to trap a pair of droplets for studying mass transport across a droplet-droplet interface (Figure 2.10 C).

2.4 Summary

The steady development of microfluidic technologies has provided sophisticated methodologies in many areas of science, including the ability to integrate and multiplex bioassays. The creation of biocompatible environments and the laminar flow properties of microfluidic channel networks offer very exciting prospects for future developments of automated and high-throughput synthetic biology platforms.

Miniaturized lipid bilayer technologies perfectly fit membrane studies' needs. Different types of bilayer models have been proposed in recent years. Microfluidic solutions have been developed to create artificial cell membranes using immiscible fluids in silicon and polymer substrates, where suspended lipid bilayers were formed simply by fluid phase manipulation[57,58,144]. Alternatively, lipid stabilised water-in-oil (W/O) droplets have been used to create artificial cell membranes (known as droplet-interface-bilayers[73] - DIBs). Droplet based platforms have been implemented in microfluidic devices with different geometries, characterized by different levels of accessibility to the bilayers, while being compatible with both electrophysiological measurements and high-resolution optical techniques. These platforms meet the key requirements of automation, membrane stability, and throughput required by industry. They have also been successfully applied for recording ion channels and for drug screening assays. Initially, DIB based assays required manually bringing droplets into contact but, in recent years, more efforts have been dedicated to creating similar assays using miniaturised systems that rely on micromanipulators, microgeometries and dielectrophoresis[140,168–170] or by creating droplet bilayers with agarose gel layers

(DHB)[68,171]. These approaches present many limitations due to either a lower throughput than automated patch-clamp systems or necessitate procedures that require manual intervention. To overcome these challenges we have developed a microfluidic solution that integrates the throughput typical of droplet microfluidic systems[115] with the functionalities obtained from passive channel networks[172] into a single device, where artificial cell membrane assays can be developed using fluorescence microscopy. As presented in the next chapters, by designing passive microfluidic networks, the precise and automated positioning of droplets within microchannels is facilitated, offering new solutions for developing DIB assays in an automated fashion.

Chapter 3

Materials and Methods

3.1 Chemicals, Buffers and Equipment

3.1.1 Materials

Table 3.2 List of Materials

Supplier	Material
AbCam Biochemicals (Cambridge, UK)	Fluo-8 K^+ Salt
Avanti Polar Lipids (Alabama, US)	1,2-diphytanoyl-sn-glycero-3-phosphocholine (DPhPC); 1-palmitoyl-2-oleoyl-sn-glycero-3-phosphocholine (POPC); 1-palmitoyl-2-oleoyl-sn-glycero-3-phosphoethanolamine (POPE). Mini Extruder
Bio-Rad Laboratories Ltd. (Hampshire, UK)	Agarose
Diener electronic GmbH + Co (Ebhausen, Germany)	Pico low-pressure plasma system
Dow Corning (Midland, MI, U.S.)	Sylgard 184, Polydimethylsiloxane (PDMS)
Fisher Scientific UK Ltd. (Leicestershire, UK)	Ammonium persulphate (APS); Ethylenediaminetetracetic acid (EDTA);

	Glucose; Glycerol; Glycine; Methanol; Potassium hydroxide (KOH); Sucrose; Tris base
Formedium Ltd. (Norfolk, UK)	Bacterial Agar; Tryptone; Yeast Extract Powder
GE Healthcare (Amersham, UK)	GE His GraviTrap Ni Sepharose Fast Flow column
Integrated DNA Technologies (Leuven, Belgium)	Oligonucleotide primers
Invitrogen Ltd. (Paisley, UK)	PureLink PCR Purification Kit; SeeBlue Pre-stained Standard
Kodak (Hertfordshire, UK)	X-ray film
MicroChem Corp (Newton, MA, U.S.)	SU-8 photoresist
Melford Laboratories Ltd. (Ipswich, UK)	Dithiothreitol (DTT); Isopropyl- -D-thiogalactopyranoside (IPTG)
New England Bioscience Ltd. (Hertfordshire, UK)	10x T4 DNA Ligase Buffer; T4 DNA Ligase; Pre-stained SeeBlue Protein Marker
PPG Industries Inc. (Pittsburgh, PA)	Aquapel
Promega (Southampton, UK)	1 kb DNA Ladder; 100 bp DNA Ladder; Bovine Serum Albumin (BSA); Dithiothreitol (DTT)
Qiagen Ltd. (West Sussex, UK)	Nuclease-free Water; QIAquick Gel Extraction Kit; QIAprep Spin Miniprep Kit
RainDance Technologies (Billerica, MA, U.S.)	EA PFPE-PEG fluorosurfactant
Severn Biotech Ltd. (Worcestershire, UK)	30 % Acrylamide [Acrylamide: Bis-acrylamide ratio 37.5:1]
Sigma-Aldrich Ltd. (Dorset, UK)	Asolectin, Brilliant blue; Bromophenol blue; Calcium chloride ($CaCl_2$); Carboxyfluorescein; Chloroform; n-dodecyl-β-D-maltopyranoside

	(DDM); Ethidium bromide; FC40 fluorocarbon oil; Fluorescein; Hexadecane; Hydrochloric acid; Isopropanol; Lysozyme; Methoxypolyethylene glycol maleimide (PEG-mal); N-(6-methoxyquinolyl)acetoethyl ester (MQAE); Sigmacote, Span 80; Tricine; Tween 20; Tween 80.
Thermo Fisher Scientific Inc. (Waltham, MA, USA)	4-acetamido-4'-maleimidylstilbene-2,2'-disulfonic acid (AMS); NanoDrop spectrophotometer; N-Ethylmaleimide (NEM); Slide-A-Lyzer Dialysis Cassette 3,500 MWCO

3.1.2 List of Buffers

All buffers were prepared with ultrapure water (MilliQ, Millipore Corporation, Germany). A list of all buffers is given on

Table 3.3.

Table 3.3 List of General Buffers

Buffer	Composition	pH
Coomassie Staining Buffer	0.1% (w/v) Coomassie R250 10% (w/v) Acetic acid 40% (w/v) Methanol	7.5
De-staining Buffer	40% (w/v) Methanol 7% (w/v) Acetic Acid	
Dialysis Buffer	40 mM Tris 100 mM NaCl	7.0
Laemmli Sample Buffer	12.5 mM Tris 4% (w/v) SDS 20% (w/v) Glycerol	6.8

	0.02% (w/v) Bromophenol blue	
LB Media	1% (w/v) Bacto-tryptone. 0.5% (w/v) Yeast extract. 1% (w/v) NaCl	7.5
LB Agar	1% (w/v) Bacto-tryptone. 0.5% (w/v) Yeast extract. 1% (w/v) NaCl 1.5% (w/v) Agar	7.5
MES Running Buffer	50 mM MES 50 mM Tris 1 mM EDTA 0.1% (w/v) SDS	7.5
Native Anode Buffer	50 mM Bis-Tris	6.8
Native Cathode Buffer	50 mM Bis-Tris 50 mM Tricine 0.02% (w/v) Coomassie Blue G250	6.8
Native Sample Buffer	50 mM Bis-Tris 10% (v/v) Glycerol 0.05% (w/v) DDM 0.01% (w/v) Ponceau	6.8
Ni^+ Purification Binding Buffer	40 mM Tris 300 mM NaCl 1 mM DTT	8.0
Ni^+ Purification Elution Buffer	40 mM Tris 300 mM NaCl 1 mM DTT 400 mM Imidazole	8.0
Ni^+ Purification Wash Buffer	40 mM Tris 300 mM NaCl 1 mM DTT 40 mM Imidazole	8.0
PBS	137 mM NaCl	7.5

	2.7 mM KCl 10 mM Na_2HPO_4 1.8 mM KH_2PO_4	
PBS-T1	137 mM NaCl 2.7 mM KCl 10 mM Na_2HPO_4 1.8 mM KH_2PO_4 0.1% (v/v)Tween20	7.5
PBS-T3	37 mM NaCl 2.7 mM KCl 10 mM Na_2HPO_4 1.8 mM KH_2PO_4 0.3% (v/v) Tween20	7.5
TAE Buffer	40 mM Tris, 20 mM Acetic acid 1 mM EDTA	
TBS Buffer	40 mM Tris 300 mM NaCl 10% (w/v) Glycerol	8.0
Transfer Buffer	20 mM Tris 190 mM Glycine 20% (w/v) Methanol	8.3
PBS-T1 Blocker	137 mM NaCl 2.7 mM KCl 10 mM Na_2HPO_4 1.8 mM KH_2PO_4 0.1% (w/v) Tween20 5% (w/v) Milk	7.5

3.1.3 Equipment

AKTA Prime Plus System (GE Healthcare Life Sciences)

The protein purification system was used with a Superdex 200 10/300 GL size exclusion column for the purification of CLIC1 monomers and dimers. 100 µl of each protein sample was added into the sample feed loop at a minimum concentration of 2 mg/ml and analysed with an absorbance maxima at 280 nm and 500 µl samples were collected. Using sample standards, Ve/Vo (elution volume/ void volume) was calculated in order to determine the relative molecular weight of protein.

Horiba FluoroLog-3 Spectrophotometer

The equipment was used to measure the fluorescence signature of Trp35 residue when CLIC1 is membrane bound at A295 nm and to detect MQAE flux through CLIC1 channels at A350 nm.

Microfluidic Flow Control System (MFCS) 4C, Fluigent

A MFCS commercially available pressure control system was used to independently drive the phases into the microfluidic device, applying pressure patterns typically in the range 0-150 mbar. The system allowed the prompt generation of on-demand droplets at each T-junction by adjusting the pressure of each phase simultaneously via computer controlled software.

Microscope

An inverted Axiovert A1 microscope from Zeiss was used for all experiments. Objective lenses of 2.5x (0.075 N.A.), 5x (0.13 N.A.), 10x (0.25 N.A.) or 20x (0.45 N.A.) were used. Fluorescence images were acquired using a fluorescein isothiocyanate (FITC) filter (Ex 495 nm, Em 517 nm) or a 4',6-diamidino-2-phenylindole (DAPI) filter (Ex 358 nm, Em 463 nm) for the CLIC1 experiments

Cameras

Images and videos were acquired using either a CMOS Genie HM1024 camera (Teledyne Dalsa) controlled by ab in house written LabVIEW software or an EMCCD LucaR camera (Andor Technologies) via Andor Solis software.

3.2 Microfabrication

3.2.1 Mask Design

All masks were designed in house using CorelDraw (Corel Corporation) and sent for high-resolution (256k dpi) print as chrome on glass transparencies (JD PhotoTools, UK)

3.2.2 Photolithography

Photolithography was carried out in order to fabricate the microfluidic master onto which the PDMS is cast. The aim is to create protruding areas on a silicon wafer in the shape of the desired channel configuration. The masters were prepared as follows:

A circular 4 inch silicon wafer was cleaned in an ultrasonic bath for 3 minutes in each of three separate solvents; acetone, methanol and isopropanol. The ultrasonic bath creates a wave of between 150-400 kHz enhancing the effect of the solvent solution by creating compression waves in the liquid. After cleaning, the silicon wafer is blow dried with nitrogen to remove any excess solvent, dehydrated on a hotplate at 180ºC for 1 hour and oxygen plasma cleaned for 2 minutes at 100% power (200W). A schematic of the process is shown in Figure 3.1.

All our silicon masters were produced using SU8 photoresist (3000 series, MicroChem, US) which crosslinks upon UV exposure. A layer of SU8 3035 was spin-coated at 2500 rpm with a ramp of 300rpm for 30 seconds onto a silicon wafer to produce a uniform film of 50 µm thickness. The coated wafer was then pre-baked on a hotplate in a two-step process: first for 5 min at 65 ºC and then at 95 ºC for 20 min. After cooling to room temperature, the wafer was exposed for 30 seconds to a collimated UV light source through a previously designed photomask. SU8 is a negative resist, so only the portion of the resist exposed to UV light will be cross-linked. After UV exposure, the wafer was baked at 65ºC for 1 min and at 90ºC for 5 minutes, once the images of the mask started to become visible, the heat was turned down and the wafer was left to cool down to room temperature slowly. Once completely cooled, the excess and non-exposed resist was washed off in SU-8 developer

(propylene glycol monomethyl ether acetate (PGMEA)) for 5 min. The completion of the development was tested by washing the wafer with isopropanol, if a milky precipitated appeared, the wafer was developed further in 10-30 seconds increments to prevent over development. Once fully developed the wafer was washed with isopropanol and dried under a nitrogen stream.

The silicon master was then coated with 1H,1H,2H,2H-perfluorooctyl-trichlorosilane for 1 hour under vacuum by adding 50 µl of the silane in a desiccator together with the silicon wafer, after exposure to oxygen plasma for 2 minutes (100W). This procedure was done to create hydrophobic surfaces and prevent PDMS adhesion to the wafer. Micro-patterned channel networks of 50 µm height were successfully generated.

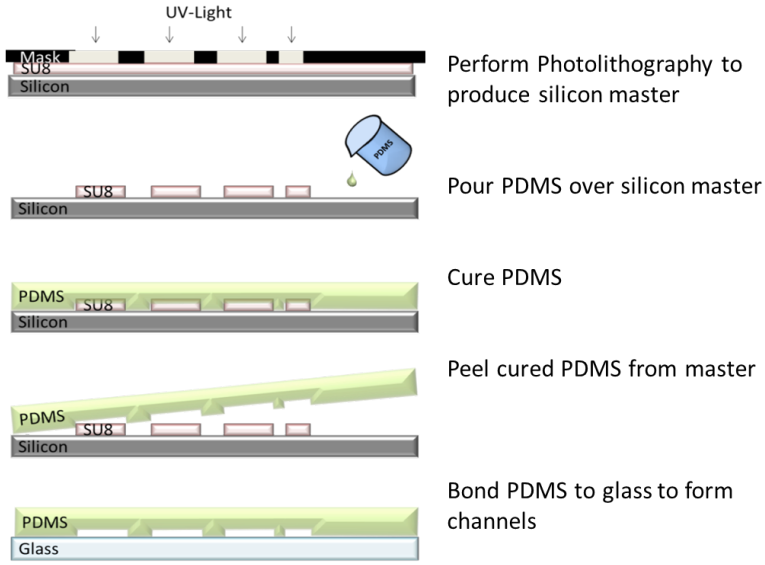

Figure 3.1 Steps in the chip fabrication process. Once a photomask has been designed and printed in high resolution, patterns can be produced onto a silicon wafer using SU8 resin which crosslinks when exposed to UV light. The patterned wafer is referred to as a silicon master. This master is then used as a mould to cast PDMS. A 10:1 mixture of PDMS to curing agent is then poured over silicon master, before being degassed and left to cure for 2 hours at 70°C. The cured PDMS inversion is then peeled off the silicon master, cleaned and bonded to glass to form microfluidics channels on a chip.

3.2.3 Soft Lithography

Polydimethylsiloxane (PDMS) was mixed at a ratio of 1:10 base to curing agent before being poured onto a silicon master, degassed in a vacuum desiccator chamber for 30

min to remove any air in the mixture and cured at 70 °C for at least 2 hours. After baking, the PDMS devices were carefully cut and peeled from the wafer, leaving the microchannels imprinted on its surface (Figure 3.2). The PDMS was cut to the desired size and holes were punched with a needle to obtain the inlet and outlet ports.

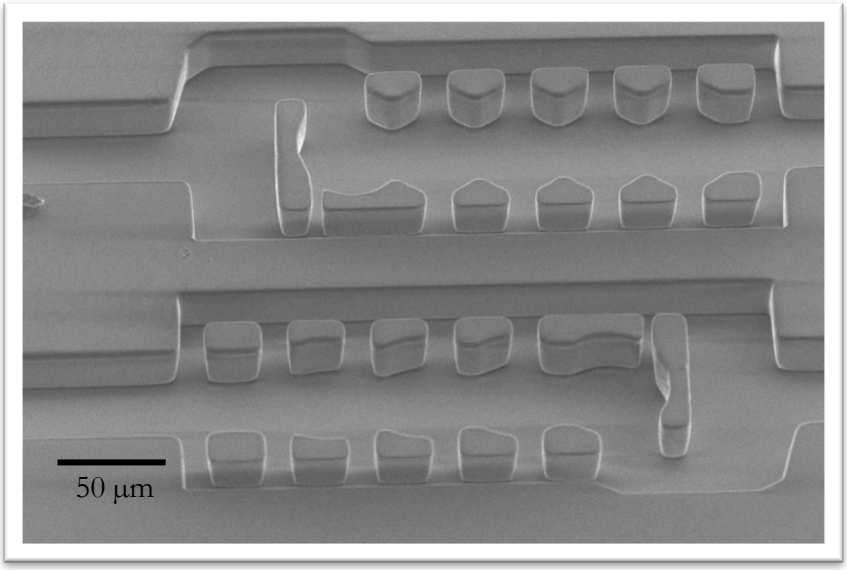

Figure 3.2 SEM image of PDMS after soft lithography. PDMS is poured onto to a silicon master patterned with SU8 and baked for 2 hours. The PDMS mould is then peeled off from the silicon wafer leaving a negative imprint of the microchannel patterns. From the SEM image, it can be noted that our channels have very straight walls and the patterns are not T-topped – this is important for flow calculation and comparison with simulations.

3.2.4 Bonding of PDMS to glass

Prior to bonding, the prepared PDMS and 75 by 26 mm glass slides were cleaned using an ultrasonic bath. To clean PDMS only methanol was used, for the glass, acetone, methanol and isopropanol were use. Both were dried under a nitrogen stream and dehydrated in an oven for 15 minutes at 70ºC.

Both surfaces were oxygen plasma treated. Exposure to oxygen plasma was carried out at 50% power for 18 seconds. The exposure to high-energy oxygen plasma changes the surface chemistry of both the PDMS and the glass, so when the exposed surfaces come into contact a strong irreversible bond is formed. Soon after bonding

channels were flushed with Sigmacote, followed by air to render the channels hydrophobic. To obtain fluorophilic surfaces devices were treated in the same way with Aquapel instead of Sigmacote. The coating allowed organic and fluorinated oils to wet the microchannels.

PTFE tubing with an inner diameter of 0.3 mm and outer diameter of 0.76 mm was then cut before being flushed with water to clear any debris and inserted into the punched holes to form lines to feed in the different liquid phases.

3.3 Microfluidic Methods

3.3.1 Water in oil droplet formation

Mono-dispersed micro droplets were generated by implementing T-junctions in the device design to promote the emulsification of the water phase (Figure 3.3). The immiscible oil phase flows through the main channel while the aqueous phase perpendicularly enters the oil flow forming droplets. In the devices used in this study, the main channel is 100 µm in width while the perpendicular channel is 60 µm with a 40 µm opening at the intersection. Both channels are equal in height, at 50 µm.

Using the MFCS pressure pump, we were able to control the pressures of the fluidic phases. The with typical starter values of 100 mbar for the continuous phase and 90 mbar for the dispersed phase. It is important to note that inside the device, these pressures vary over a wide range for both phases and the pressure in the dispersed phase oscillates synchronous with that of the continuous phase[173].

For a droplet to form at a T-junction the pressure on the dispersed phase must be greater than the pressure on the continuous phase, thus allowing it to overcome the Laplace pressure (P_L) difference (Pa), given by Equation 3-1:

$$\Delta P_L = -\gamma\left(\frac{1}{r_2 - r_1}\right)$$

Equation 3-1 Laplace pressure

where, γ (N/m) is the interfacial tension and r_1 and r_2 (m) is the two principal radii of curvature of the interface.

Droplet formation at the T-junction is generally regarded as consisting of three main stages, namely filling, necking and breaking as illustrated in Figure 3.3. The cycle initiates with the filling period, where the dispersed water phase infiltrates from the side channel into the main flow. This stage is characterized by a build-up in pressure upstream on the main channel and a pressure decrease in the dispersed phase. These changes in pressure force the stream to curve downstream. The droplet grows until it reaches maximum infiltration thus blocking the main channel.

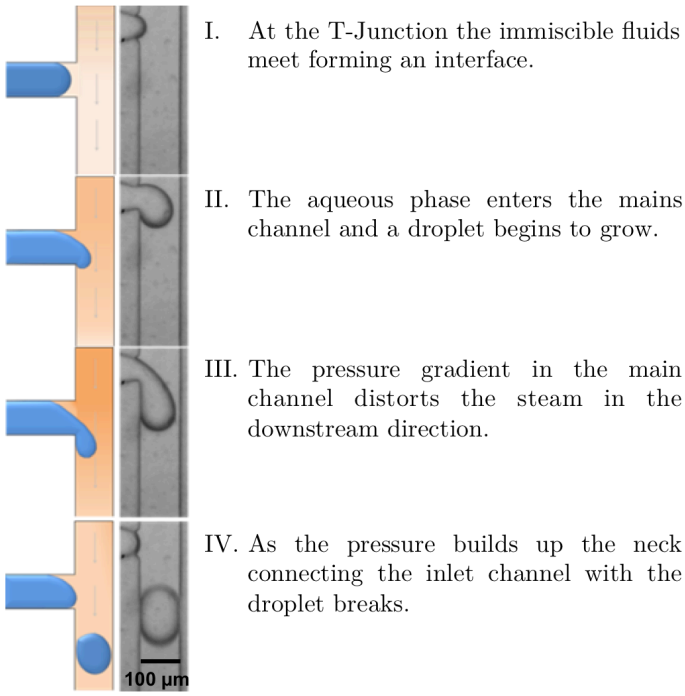

Figure 3.3 Droplet formation in a T-Junction. Due to cyclic changes in pressure on both the continuous phase and the dispersed phase droplets are periodically formed. The channels are planar and have uniform height, with 100 µm width and 50 µm height. Flow along the main channel proceeds from top to bottom. The continuous phase (oil – shown in orange), flows along the main channel, and is supplied with the fluid that will be dispersed (water – shown in blue) via the orthogonal inlet of a smaller width.

The obstruction causes the pressure in the oil phase in the main channel to build, while the dispersed phase remains constant. The continuous phase starts to squeeze the dispersed fluid decreasing the width of the droplet neck. Eventually the width of the droplet neck reaches a critical size resulting in droplet break off. The

newly formed droplet is pushed downstream as the water/oil interface withdraws whilst the pressures go back to the original values and the process repeats.

3.3.2 Numerical Fluid Flow Simulations

Simulations were conducted in COMSOL Multiphysics® to theoretically demonstrate droplet trapping within the droplet shift register described in Chapter 4. The phase field module on COMSOL Multiphysics® uses the incompressible formulation of the Navier-Stokes equations (Equation 2-2) to describe the fluid evolution in the multiphase system.

The Laminar two-phase flow, Phase Field physics module was used to model droplet trapping in three and two-dimensional spaces. In the phase field method, the multiphase flow is described with the help of a variable known as the order parameter represented by the Greek letter ϕ. The disperse phase is defined as the fluid element in which $\phi = 1$, the surrounding media (i.e. continuous phase) is represented by $\phi = 0$. Finally, the set of values $1 < \phi < 0$ represents the interface between both phases, also known as the phase field. For a full description of how COMSOL Multiphysics® describes two-phase flows please refer to Yue *et al.* 2004[174].

The two phases were set to water and FC40, with the necessary fluidic properties e.g. density and dynamic viscosity (shown on

Table 4.7). The simulations were performed both in 2D and in 3D - 3D-simulation yields neat visualization of the droplet formation and trapping, however, 3D-simulations are time-consuming (require several hours of computations), hence 2D-simulations were favoured for its low computation time. The pressures for the two phases were set according with what was generally used in practical experiments and were then altered to see the effect of different ratios. The interfacial tension was set to 11 mN/m.

3.3.3 Capillary Number and Droplet Coalescence

Different combinations of oils and surfactants were studied to understand how this influenced droplet coalescence.

The velocity of the droplets was calculated by video analysis, measuring how many frames were needed for a droplet to travel 100 µm. Equation 3-2 shows how the velocity was calculated.

$$v = \frac{d * n}{f}$$

Equation 3-2 Droplet velocity

where f (Hz) is the acquisition frequency of the camera, d (µm) is the distance travelled and n is the number of frames needed for the droplets to travel that particular distance. All the distance measurements were done using the freely available software ImageJ (National Institute of Health). The same was done for the investigation on the effect of droplet velocity on coalescence.

For the experiments investigating the effect of lipid concentration and droplet velocity on emulsion coalescence (Chapter 4), droplets were formed using different concentrations of lipids either dissolved in hexadecane or in the aqueous buffer, or in both phases. The droplets were forced to come into contact at different velocities in order to find a threshold velocity at which they stopped coalescing. This study was very important to establish a reliable DIB system, where coalescence is undesirable.

3.3.4 Dissolving lipids via chloroform dehydration

A small amount of dry lipid was taken from the container as purchased and added to a previously weighed 2 mL glass vial. The lipid was then dissolved by stirring in a small amount (~100 µL) of chloroform. Subsequently, the chloroform was carefully evaporated using a stream of nitrogen until a waxy film was visible. The vial was then placed under vacuum for a minimum of 1 hour to ensure complete evaporation of chloroform. The dried lipids were dissolved by vortexing vigorously in either

hexadecane or an aqueous buffer to the desired final concentration. The sample was used immediately and kept at room temperature.

3.3.5 Preparation of Liposomes

Liposomes were prepared by extrusion. If the lipids were dispersed in an aqueous buffer the final dissolved solution was extruded 21 times using the Avanti mini extruder or until the solution was translucent through a 100 nm polycarbonate membrane (Avanti Polar Lipids) using the Avanti mini extruder to produce unilamellar lipid vesicles.

For the preparation of N-(Ethoxycarbonylmethyl)-6-methoxyquinolinium bromide (MQAE) - containing liposomes, 250 µM of MQAE dye and 0.5 mg of PC:Chl at a ratio of 10:1 were extruded as mentioned above. The extra vesicular MQAE was separated from the liposomes on gel filtration columns (0.7 cm × 50 cm) containing CL-6B Sepharose equilibrated with 40 mM TRIS, 150 mM NaCl buffer. As the free dye travels faster than the liposomes, fractions containing liposomes with MQAE inside were collected and used within a few hours.

3.3.6 DIB Permeation Experiments

To evaluate the permeation of substances through the droplet-interface-bilayers a donor droplet and an acceptor droplet were produced and trapped in an alternating format within the device. Acceptor droplets contained a non-fluorescent buffer while, donor droplets contained a fluorescent buffer. The droplets were trapped within registers and images where acquired every 5 minutes for 1 hour using a FITC filter. For the passive permeation experiments, 10 mg/ml asolectin was dissolved in the hexadecane and fluorescent droplets contained either 100 mM fluorescein or 100 mM calcein in 10 mM HEPES, 200 mM KCl, pH 7.4 buffer. In the facilitated diffusion studies, droplets were made using 5 mg/mL DPhPC in hexadecane and donor droplets contained 10 mM HEPES, 20 mM EDTA, 1 M $CaCl_2$, 2 mg/ml α-haemolysin at pH7.4, while acceptor droplets contained 10 mM HEPES, 333 mM EDTA, 2 M KCl, 250 mM Fluo-8 at pH 7.4.

To quantify the permeation of solutes through the DIBs we used the apparent permeability index P_{app} (cm/s)[175], which was calculated using the adapted Equation 3-3:

$$P_{app} = \frac{V_R(t)}{A(t) * C_{D0}} \frac{dC_R(t)}{dt}$$

Equation 3-3 Apparent permeability

where C_{D0} (mol) is the initial concentration of the compound in the donor droplet, $C_R(t)$ (mol/s) is the concentration of the compound in the acceptor droplet over time, $A(t)(\mu m^2)$ is the estimated total surface area of the DIB (i.e. taking into account that some droplets had two DIBs) and $V_R(t)$ (pL) is the estimated volume of the acceptor droplet over time. The droplet volumes and DIB surface areas at each time point were estimated from the respective microscopy images by approximating droplets to ellipsoids and DIB areas to ellipses using ImageJ. The calculation takes into account variability in droplet size and bilayer area for all measurements; therefore, temporal changes do not affect the estimate of the permeability coefficient. As the fluorescence intensity is proportional to molecular concentration, the intensity values were used as a proxy for compound concentration. Fluorescence intensity from the droplets was obtained by averaging the intensity values of a region of interest of 50x50 pixels in the centre of the droplet using the Andor Solis software.

3.4 Molecular Biology Methods

3.4.1 Human CLIC1 WT plasmid

Human CLIC1-His 6x was expressed from a pET28a plasmid provided by Dr Louise Brown from Macquarie University, Australia. It was prepared as previously described by Goodchild *et al.*[176,177]

3.4.2 Strains

Escherichia coli strain DH5α (Invitrogen, Paisley, UK) was used for transforming and propagating the recombinant expression plasmids. Protein expression was performed in the *Escherichia coli* strain C41 (Invitrogen, Paisley, UK).

Table 3.4 Bacterial Strains Used

Strain	**Genotype**
DH5α	F– Φ80*lac*ZΔM15 Δ(*lac*ZYA-*arg*F) U169 *rec*A1 *end*A1 *hsd*R17 (rK–, mK+) *pho*A *sup*E44 λ– *thi*-1 *gyr*A96 *rel*A1
C41 (DE3)	F^- ompT gal dcm $hsdS_B(r_B^- m_B^-)$(DE3)

3.4.3 Transformation

1 µl of 20 ng plasmid DNA was combined with 100 µl chemically competent C41 (DE3) *E. coli* cells in a sterile eppendorf tube and allowed to rest on ice for 15 minutes. The cells were then heat shocked for 2 minutes at 42 °C and returned to ice for 5 minutes. Following incubation on ice, 1 ml of sterile Lysogeny broth (LB) was added to transformed cells and placed in a shaking incubator at 37 °C for one hour. Cells were then spread onto sterile LB plates containing 50 µg/mL Kanamycin, dried on the bench for 10 minutes, and placed upside down in a 37 °C incubator overnight.

3.4.4 Small-scale preparation of plasmid DNA (mini-prep)

From the bacterial transformation, a single colony was picked and used to inoculate 5 mL LB broth containing 100 µg/mL of Kanamycin which was then incubated overnight (~16 hours) in a shaking incubator at 37 °C. Plasmid DNA was purified using a Qiagen QIAprep Spin Miniprep kit and its own set of buffers (P1, P2 and N3). The overnight culture was centrifuged at 18,000 x g for 10 minutes to pellet the cells. The pellet was re-suspended in 250 µl Buffer P1 and transferred to a sterile eppendorf tube. Cells were lysed by addition of 250 µl Buffer P2, which was then neutralised after 5 minutes by addition of 350 µl Buffer N3. The sample was then centrifuged at 18,000 x g for 10 minutes and the supernatant transferred to a QIAprep

spin column. The columns were centrifuged at 13,400 rpm for 1 minute, the flow-through was discarded and the column was washed with 750 µl Buffer PE and again centrifuged at 18,000 x g for 1 minute. The flow-through was again discarded and the column spun again at 18,000 x g for 2 minutes to remove residual wash buffer. The plasmid DNA was eluted into a sterile eppendorf by addition of 100 µl nuclease-free water to the column and centrifugation at 18000 x g for 1 minute. Plasmid DNA was then stored at -20 °C.

3.4.5 Protein Overexpression and Purification

Overnight culture was made from transformed CLIC1-His pET28a in C41 (DE3) cells by inoculating 10 ml of sterile LB with a single bacterial colony. 5 ml of overnight culture was added to 500 ml LB and 50 mM Kanamycin containing flasks and placed into 37 °C shaking incubator until A_{600} of 0.4-0.6 was obtained. Overexpression was induced by the addition of sterilized IPTG to a final concentration of 1 mM. Cells were placed back into the incubator and grown for another 2 hours. Cells were harvested by centrifugation at 4,000 x g for 10 minutes. The supernatant was then discarded and the pellets resuspended in 20 ml of TBS buffer combined with one EDTA-free protease inhibitor tablet (Roche Life Science) and lysozyme at a final concentration of 1 mg/ml. Following 15 minute incubation on ice, cells were passed through a French press three times at 600 psi and centrifuged at 27,000 x g for 30 minutes at 4 °C. The supernatant was collected and centrifuged again at 120,000 x g for 50 minutes at 4 °C.

The resulting supernatant was purified through a Ni^{2+} column. GE His GraviTrap Ni Sepharose Fast Flow columns were used to purify the protein by Histidine binding. Following Ni^{2+} column equilibration in 10 ml of binding buffer (40 mM Tris, 300 mM NaCl, 1 mM DTT at pH 8.0) the supernatant was added to the column and the flow through discarded. The column was then washed with 10 ml of wash buffer (40 mM Tris, 300 mM NaCl, 1 mM DTT, and 20 mM imidazole at pH 8.0) and protein fractions were collected following the addition of 3 ml elution buffer (40 mM Tris, 300 mM NaCl, 1 mM DTT, and 400 mM imidazole at pH 8.0). Samples

were examined on a Novex NuPAGE 4-12% SDS-polyacrylamide gel and treated with Coomassie Brilliant Blue stain. Fractions containing CLIC1 (Chapter 6) were dialysed overnight to remove the imidazole and stored at -20°C. Protein concentration was measured using a NanoDrop spectrophotometer (Thermo Scientific), typical concentration values were found to be in the order of 1-3 mg/ml from 1 L of initial culture.

3.4.6 SDS PAGE

To carry out sodium dodecyl sulphate polyacrylamide gel electrophoresis (SDS-PAGE), protein samples were mixed with NuPAGE® LDS Sample Buffer (Invitrogen) before running on pre-cast 12-well 10% NuPAGE® Bis–Tris gel (Invitrogen). Samples were run with MES buffer against SeeBlue Plus2 pre-stained marker for 30-40 minutes at 150 mV to obtain good separation. Protein bands were resolved by staining with staining solution (0.05 % Coomassie R250, 25 % isopropanol, 10 % acetic acid) and destained in 40 % methanol and 10 % acetic acid in water.

3.4.7 Western Blotting

After SDS-Page, the SDS-gel was placed on a blotting cassette and the proteins were transferred to a nitrocellulose membrane for 1 h at 30 mV (Hoefer semi dry transfer unit, Hoefer Inc) in transfer buffer (25 mM TRIS, 192 mM glycine, 20% methanol, pH 8.3). After transfer, the membrane was washed for 5 min in 10 mL PBS buffer, followed by blocking for 1 hour in 10 mL blocking buffer (5% milk powder in PBS-tween (PBS-T)). The membrane was then washed 3 times for 5 min in 10 mL of PBS-T. Once the blocked membrane had been washed it was incubated overnight with the primary antibody, 1 µl of Mouse monoclonal CLIC1 antibody (AbCam, Cambridge, UK) mixed in 10 mL PBS-T. The membrane was then washed three times for 5 min in 10 mL PBS-T and incubated in 10 ml of PBS-T containing 0.5 µl of goat anti-mouse IgG conjugated with horseradish peroxidase secondary antibody, for 1 hour in PBS-T. Following incubation with the secondary antibody the membrane was washed three times for 5 min in 10 mL PBS-T3 (containing 3 ml of Tween 20) and three times for 5 min in 10 mL PBS-T. Protein was detected by incubating the membrane

in enhanced chemiluminescence (ECL) solution (Pierce Chemical, Rockford, IL, USA) for 5 min and then placed in a lightproof cassette, exposed to X-ray film and then processed in a Kodak X-Omat processor for film development.

3.4.8 Gel Filtration/Size Exclusion Chromatography

Size exclusion chromatography was performed using a Superdex 200 10/300 GL Increase column (GE Healthcare Life Sciences, Buckinghamshire, UK) and analysed on an AKTA Prime Plus System (GE Healthcare Life Sciences, Buckinghamshire, UK). 100 µl of each protein sample was added into the sample feed loop at a minimum concentration of 2 mg/ml and analysed at $A_{280.}$ Sample standards of known MW were used to calculate the Ve/Vo (elution volume / void volume) in order to determine the relative molecular weight of the protein.

3.4.9 Tryptophan Fluorescence

The tertiary structure of a protein can be characterized by fluorescence spectroscopy because of the presence of the intrinsic aromatic fluorophores, Tyr and Trp, in most proteins. Fluorescence spectroscopy gives information about the packing and local environment of Tyr and Trp residues, although protein fluorescence spectra are generally dominated by tryptophan emission. Proteins exhibit characteristic fluorescence spectra according to the environment of which the main fluorescing species are packed. Fluorescence emission intensity and wavelength for tryptophan depends on to the polarity of the environment within which the tryptophan is found, and the degree of quenching experienced by the fluorophore as a result of that environment[178]. The greater the exposure of Trp to the polar aqueous environment, the more 'red-shifted' the wavelength of maximum emission will be. Tryptophan can be selectively excited at 295 nm to eliminate any interference from Tyr residues since it absorbs well below this wavelength. CLIC1 has one Trp residue, Trp35, which is located in the putative transmembrane region in the N-terminal domain, acting as a local reporter for that region.

All fluorescence measurements on CLIC1 were performed on a Horiba Jobin Yvon Flurolog-3 Spectrofluorometric. Scan speed was 200 nm/min over a wavelength range of 280-450 nm using a quartz cuvette (Starna) of path length 4 mm at 20 °C. Excitation was at 350 nm (Ex.280) or 295 nm (Ex.295), with excitation and emission slit widths of 1 nm. The fluorescence spectra of soluble and membrane bound CLIC1 were measured and all data were buffer-corrected.

3.4.10 Pegylation

Liposomes made of phosphatidylcholine and cholesterol at a ratio of 10:1 were incubated in buffer with purified CLIC1 to a final concentration of 1 mg/ml in buffers with reducing or oxidizing conditions overnight at 4 °C. The reducing buffer contained 2 mM DTT, and the oxidizing buffer contained 2 mM H_2O_2. The liposomes were centrifuged at 18,000 x g for 10 min at 4 °C and the supernatant was separated. Pellets were then re-suspended on ice in 10 µl of buffer containing 1 mM of either N-Ethylmaleimide (NEM) or 4-acetamido-4'-maleimidylstilbene-2,2'-disulfonic acid (AMS) and incubated at room temperature for 1 hour. Following incubation, 10 µL of buffer containing 2 mM PEG-mal was added to each of the samples and incubated for 2 hours at room temperature. These samples were incubated at room temperature for 10 minutes before again being split in half. The reaction was terminated by addition of 100 mM DTT and incubation for 10 minutes. Samples were centrifuged at 18,000 x g for 15 minutes and following this the pellet and supernatant fractions were split into separate tubes. The pellets were washed with 500 µl cold acetone whilst the supernatant was incubated with 10% TCA on ice for 10 minutes before being centrifuged at 18,000 x g for 10 minutes at 4 °C. TCA pellets were then washed with 1 mL cold acetone and both pellets were then centrifuged at 14,000 rpm for 10 minutes at 4 °C. The supernatants were then discarded and all pellets were dried for 15 minutes. The pellets were then re-suspended in 2x sample buffer and analysed by SDS-PAGE.

Chapter 4

A Microfluidic Platform for DIB Formation

This chapter describes the progress in the development of a fully integrated microfluidic platform suitable for large-scale droplet-interface-bilayer experimentation. The platform permits droplet production, droplet alternation and the formation of artificial bilayer constructs within a single chip. Our investigation has identified the key parameters enabling reliable formation and long-term storage of DIB arrays.

4.1 General Considerations for Designing a DIB Platform

We designed and characterized a microfluidic platform consisting of a passive microchannel network capable of a series of integrated functions, including droplet production, droplet alternation, in-line change of droplet velocity, DIB formation and storage of DIB arrays. The final structure comprises a double T-junction (for droplet formation) and a Y- junction (for droplet alternation) followed by a series of microfluidic shift registers[179] that have been optimised here for DIB formation and their long-term storage. The aim of this chapter is to discuss each module individually and describe the conditions that allowed an integrated system to be ultimately obtained.

4.1.1 Pressure Driven Systems

Both syringe pumps and pressure control systems have been widely used to pump fluids in droplet microfluidic systems. Syringe pumps produce a constant flow rate output, while a pressure control system provides a constant pressure source. Syringe pumps lead to short term oscillations in the output caused by the stepper motor. Korczyk *et al.*[172] demonstrated the oscillation in the generated droplet volume when using syringe pumps and the uniformity of the generated volume when using a pressure control system instead. Therefore, in this study, a high-precision microfluidic pressure control system (MSFC 4C, Fluigent) was used to pump fluids. This system can control up to 4 output channels at the same time with a maximum pressure of 1 bar and accuracy of 0.5 mbar. The value of flow rate produced by a pressure control system depends on the value of the resistance of micro-channels and by periodic fluctuation caused by droplets forming and leaving the site of formation.

In a fluidic system where the Reynolds number is small ($\leq 10^{-1}$), fluid flow is analogous to the flow in an electric circuit. Therefore, the Hagen-Poiseuille's law corresponds to Ohm's law, where the pressure drops, ΔP (Pa), is analogous to the voltage drop, the flow rate, Q (m^3/s), to the current and the hydraulic resistance, R_H, to the electric resistance. Fluidic resistance also depends on the geometry and crossectional area of the channel shown in Equation 4-1 below, where a is a

dimensionless geometric constant, L (m) is the length of the channel, η (kg/(m · s)) is the viscosity of the fluid, W (m) is the channel width and H (m) the channels depth[180,181].

$$R_H = \frac{\Delta P}{Q} = \frac{a\eta L}{WH^3}$$

Equation 4-1 Fluidic Resistance

4.1.2 Issues with PDMS

All the devices used were made of PDMS. While it is a very versatile polymer in terms of ease of use and fast prototyping (Chapter 3.2), it is worth noting that PDMS easily absorbs solvents and also water vapours, a problem, which can adversely impact droplet microfluidics procedures. In all experiments, droplet shrinkage occurred over time, due to fluid absorption through the PDMS walls (both hexadecane and aqueous phase). To minimise this effect all devices were immersed in water for at least one hour prior to experimentation, obtaining a 16% droplet area decrease after 40 minutes (Figure 4.1).

Attention should be paid to the type of carrier fluid and device material used. In our work, except for minor advantages in reducing PDMS swelling with respect to other solvents, hexadecane was primarily used for the formation of DIBs as it has been consistently reported that increasing the n-alkane chain length of the oil increases the chances of obtaining oil-free conditions within a lipid bilayer[71], thus forming DIBs with a more similar environment to that found in natural cell membranes. Further advantages can also be gained by fabricating the microfluidic devices with transparent materials that do not absorb solvents and are not gas and water permeable, such as poly-methyl-methacrylate, polystyrene or glass, resolving the issues associated with temporal droplet volume variation when performing long-term assays.

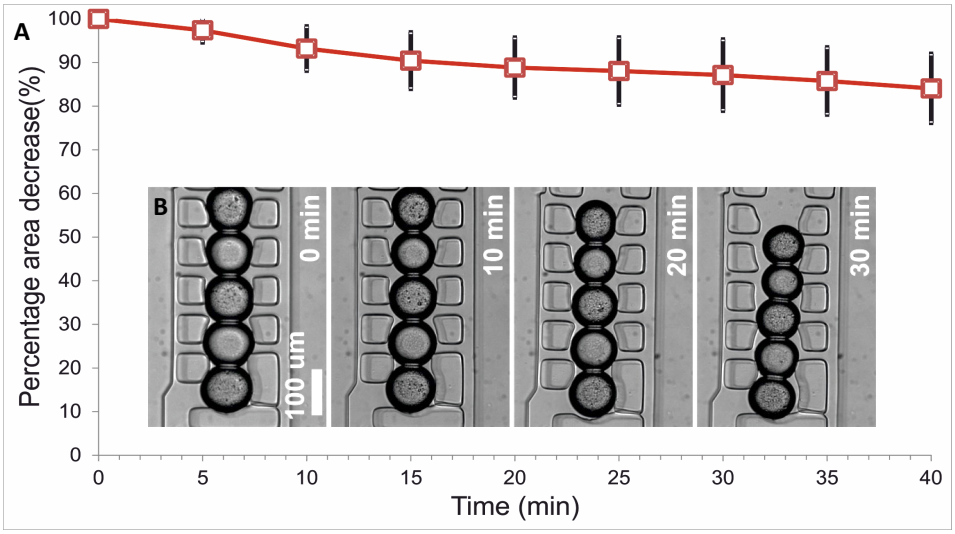

Figure 4.1 Droplet shrinkage within registers. (A) The graph shows droplet shrinkage as a function of time. The error bars represent the standard deviation resulting from a set of 15 measurements. (B) Microscope images showing droplet shrinkage over time. Here, hexadecane was used as the oil phase and the aqueous phase comprised of a 10 mM HEPES, 200 mM KCl, pH 7.4 buffer. Droplets were produced as described on Chapter 3, section 3.3.1, once the droplets were trapped both the aqueous and the oil flow were stopped, and the droplet size was monitored by taking pictures at 5 minutes intervals. The light source was only on to capture the images and subsequently turned off to minimise heat production.

4.1.3 Droplet Alternation

The ability to produce alternating droplets in the ABAB format is of vital importance for membrane protein studies, where one droplet has to mimic the internal environment of the cell and the other the extracellular environment. We have tested and adapted various microchannel geometries to achieve droplet alternation and assessed their suitability to the developed system (Table 4.5).

Figure 4.2 right, shows an adaptation of the train track geometry first proposed by Ahn *et al.* 2011[161] as a method for synchronizing droplets. Droplets are generated on separate T-junctions upstream from the train track geometry. The size of the droplets must be larger than the microfluidic channel to prevent the flow of the continuous flow past the droplets. The small channels connecting the two main channels only allow the oil phase through. Due to the identical dimensions of the top and bottom channels they experience the same hydraulic resistance. The same is true for when droplets are synchronized. Thus, once the droplets are synchronized, they stay synchronized and flow towards the outlet with the same velocity. The droplets

synchronization mechanism is based on the change in velocity within the channel due to an increased net flow of the continuous phase towards the least resistive channel, thus decreasing the velocity in the more resistive channel. This velocity gradient makes it possible to diminish the distance between droplets and achieve droplet synchronization. In our adapted version one channel is slightly longer than the other, this way one droplet will always be ahead, and droplet alternation can be achieved.

Table 4.5 Design iterations for the droplet alternator geometries

Train Tracks (Figure 4.2)
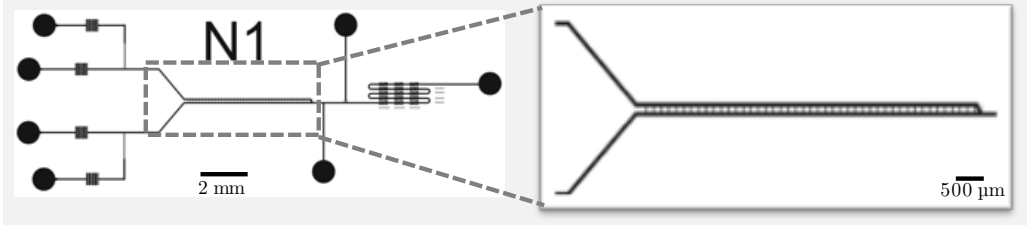
Droplet Alternator (Figure 4.2)
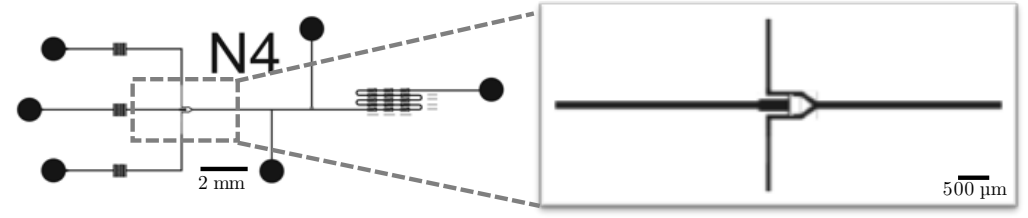
Large Y-Junction (Figure 4.3)
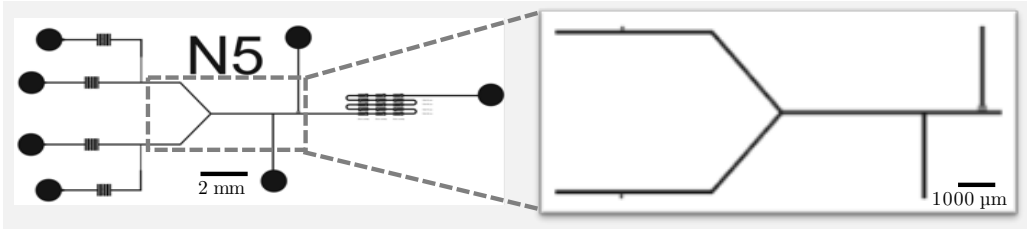
Narrow Y-Junction (Figure 4.12)
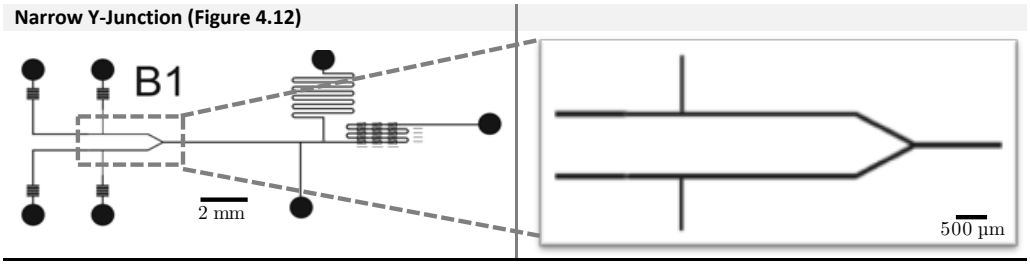

Another alternating method involves a fluidic device (Figure 4.2- Left) consisting of two dispersed phase channels, which are hydrodynamically identical. During the droplet formation, the aqueous stream in one of the two channels blocks the oil coming from the central channel, leading to an increase in oil flow through the

second channel. Once the droplet is released the oil flow switches back to the first channel allowing droplet formation at the second nozzle. This fluctuation of oil flow leads to droplet alternation at high pressures. This device design has been adapted from Frenz *et.al.* 2008[156] by reducing the size of the gaps connecting the continuous phase to the oil phase, with the aim to increase Laplace pressure and prevent flow through the side channel. This change allows the device to be used at lower pressures, which as it is needed the prevent droplet merging.

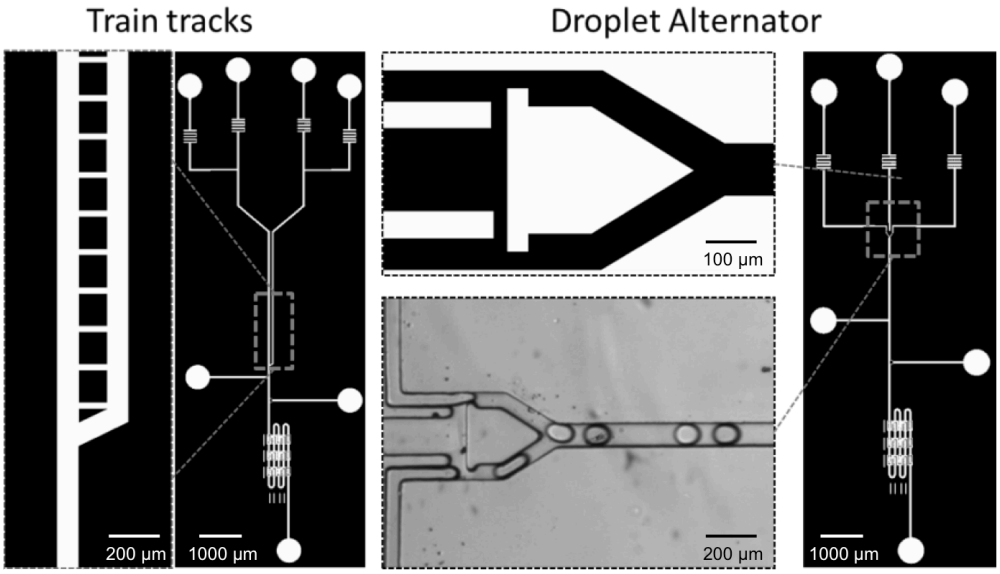

Figure 4.2 Droplet alternating geometries. The train tracks geometry has been adapted from Ahn et. al. 2011[161] as a method of synchronizing droplets. Here we have increased the length of one of the channels to achieve alternation. A different structure was adapted from Frenz et.al. 2008[156] to be used at low pressure flows.

However, at low fluidic pressures (30-200 mbar) none of these geometries demonstrated any advantage over a Y-junction alternation geometry (Figure 4.3). Therefore, the final device produced was based on the hydrodynamic coupling of two spatially separated T-junctions. The T-junctions were connected downstream by a Y-junction where droplets alternated (Figure 4.3). Here, T-junctions automatically synchronized to form alternating droplets pairs at low-pressure values. Using two separate T-junctions was required to avoid coalescence of the aqueous phase with the adjacent stream, leading to contamination. The design was adapted to ensure that

the droplets were fully enveloped in lipids before they met each other at the arraying area.

During droplet formation, the aqueous stream in one of the two T-junctions blocks the oil coming from the central channel, leading to an increase in oil flow through the second channel. Once the droplet is released the oil flow switches back to the first channel allowing droplet formation at the second nozzle. This fluctuation of oil flow is possible because the devices are pressure driven leading to greater stability in the frequency of droplet formation.

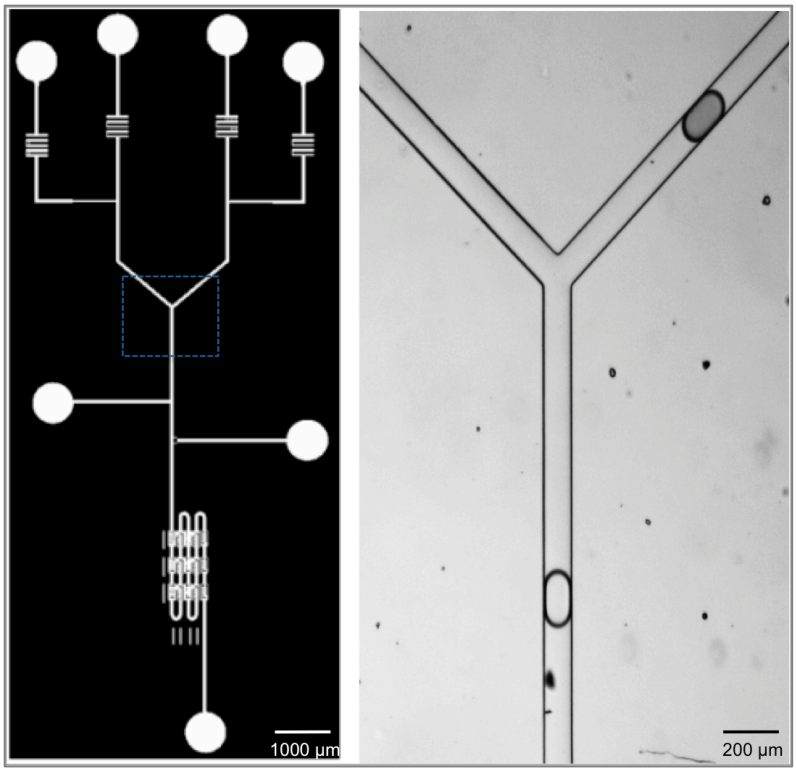

Figure 4.3 Y-Junction geometry. Schematic of device geometry and an image of droplet alternation of the insert on the schematic. The Y-junction was used here as a method for droplet alternation, it allowed specific control of the aqueous and oil phases. This allowed alternation efficiencies between 80% - 90%.

Quantitative analysis was done by producing droplets at flow rates optimal for DIB formation, typically in the rage of 30–150 mbar. One of the aqueous phases was labelled with fluorescein and the other only buffer, droplets were formed and subsequently trapped. Image analysis was used to evaluate the reliability of droplet pairing. A typical snapshot is displayed in figure (Figure 4.4). We have evaluated that

using this alternating geometry 80% - 90% pairing efficiency was achieved. Droplet pairing efficiency was seen to vary depending on the composition of the aqueous phases and whether lipids or surfactants were used. Perfect pairing of droplets is hindered by small variations in the channel depths, flow-rates or the interfacial tensions of the aqueous streams. There have been intensive studies on droplet coordination, but the most promising approach is to use a synchronization mechanism directly at the production nozzle.

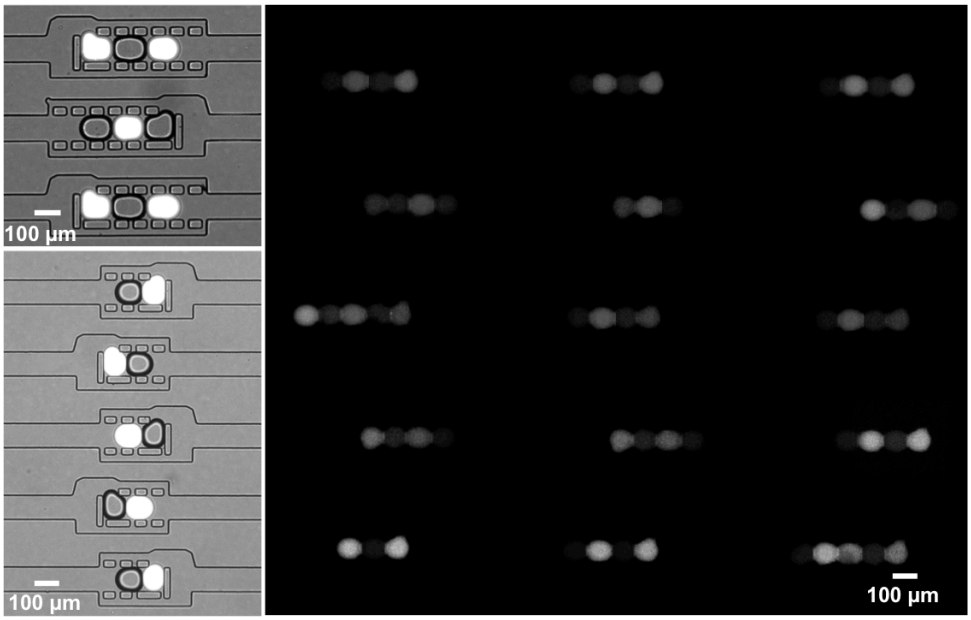

Figure 4.4 Droplet alternation efficiency. Droplet pairs, one containing 10 mM HEPES, 200 mM KCl, pH 7.4 and the other with and 100 µM fluorescein added were produced alternatingly as described on Chapter 3 Section 3.3.1, and trapped to estimate the alternating efficiency of the droplet pairing structures mentioned at Section 4.1.3. In the fluorescence image picture above droplet alternation efficiency is 92%.

Finally, this design allows individual inlet pressures to be independently controlled by a square-wave generator. This increases droplet-pairing efficiency allowing the creation of an automated droplet on demand production system.

4.1.4 Droplet Shift Registers

The formation of DIBs requires two lipids encased droplets to come into contact thus forming a bilayer lipid membrane (Chapter 1.4.4). Here, we introduce droplet shift registers capable of trapping and storing droplets.

Droplet shift registers (Figure 4.5) were wider than the main channel and segmented in three parts. Adding gutters to each side of the main channel acted as a pressure relieve which slowed down droplets and increased trapping efficiency. The gutters and the main channel were separated by pillars that allow the flow of the continuous phase to flow through, the end of the register was blocked, and droplet were forced to squeeze out through the side aperture. The layout was designed to induce droplets to flow through the central channel, while the oil phase also flows in the two side gutters. After a register element was filled with the continuous phase, a droplet arriving at the element was trapped in the central branch if the differential hydrodynamic pressure between the upstream (P1, at the point x) and the downstream side (P2, at the point y) of the droplet was lower than the Laplace pressure generated at the outlet of the register (Figure 4.5 Left). The design was first described by Zagnoni, 2010[179].

When the first droplet entered a register, it followed the least resistive path and if capillarity was small enough, surface tension would hold the droplet in place, whilst the oil continued to flow through the gutters. Droplet trapping relied on the balance between hydrodynamic forces and surface tension forces.

Once a droplet was trapped within a register, the cross-sectional area of the channel decreased, and this change caused the resistance of the channel to increase. For a system driven at a constant pressure, if the overall resistance increases, the difference in pressure across the trapped droplet will also increase. Thus, a higher number of trapped droplets led to a higher differential pressure.

A COMSOL Multiphysics® simulation (simulation parameters can be found in section 3.3.2) was used to optimise experimental conditions and demonstrate the increase in differential pressure across trapped droplets (Figure 4.5 middle). Each droplet present in the register changes the value of the fluidic resistance of the central channel within the pillar area, causing the overall resistance of the channel to increase. V_{in} (V) represents the constant pressure applied to drive the fluidic phases, R_1 (Ω) is the resistance from the inlet to the start of the register, R_2 (Ω) is the resistance in the main channel which varies depending on how many droplets have been trapped, R_3 represents the resistance from the two gutters, R_4 (Ω) denotes the resistance from the end of the register to the outlet and V_2 (V) is the differential pressure across the trapped droplets.

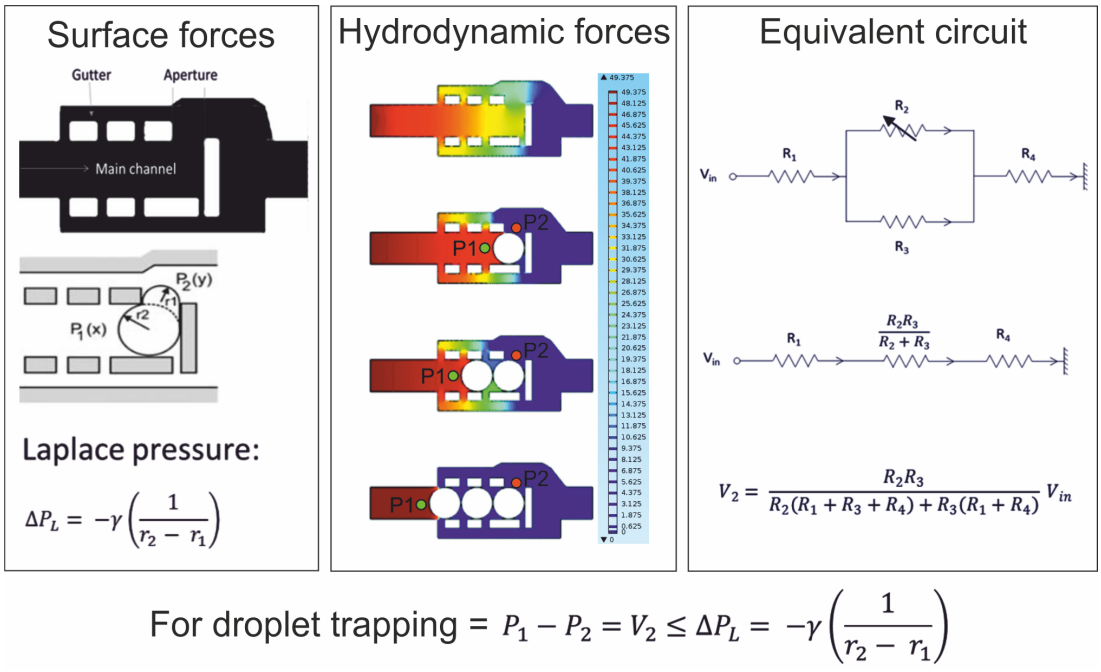

Figure 4.5 Working principle of a microfluidic droplet shift register. (Left) Schematic of a droplet shift register. (Middle) Numerical simulations of the Navier-Stokes equations for a shift register geometry with an increasing number of droplets trapped within the register. Any additional droplet arriving after the first at the upstream side of the element arrayed along its length. The colour scale shows a steady increase in differential pressure (P1-P2) for a higher number of droplets trapped. When the register length is filled with droplets, an additional one forces the drop at the downstream side to exit the register, creating a serial shift of the drops stored within the pillars. (Right) Simplified analytical model of a register element using an equivalent electric circuit.

Therefore, a trend develops between interfacial tension (directly related to lipid concentration) and differential pressure across a register for trapping efficiency, as described by the equation above. A model for the resistances within the register can be simplified using an equivalent electric circuit, shown in Figure 4.5 right, where V_{in} (V) represents the constant pressure applied to drive the fluidic phases, R_1 (Ω) is the resistance from the inlet to the start of the register, R_2 (Ω) is the resistance in the main channel which varies depending on how many droplets have been trapped, R_3 (Ω) represents the resistance from the two gutters, R_4 (Ω) denotes the resistance from the end of the register to the outlet.

The differential pressure attained by droplet trapping within the main channel can be represented by the potential change across R_2. The change in potential can be solved and the following expression obtained:

$$V_2 = \frac{R_2 R_3}{R_2(R_1 + R_3 + R_4) + R_3(R_1 + R_4)} V_{in}$$

Equation 4-2 Differential Pressure

From the expression above it is possible to predict how changes to the main channel will influence the overall system. If a droplet were trapped in the register thus increasing R_2, the differential pressure, V_2, would also increase. The more droplets were trapped, the higher the differential pressure. Eventually, the pressure on the droplet would be high enough to deform the first trapped droplet and overcome the Laplace pressure (P_L) given by Equation 3-1.

Thus, a low differential pressure across V_2, is desired for efficient droplet trapping. According to the equation above, this can be achieved by decreasing R_2, i.e. the resistance inside the register. Many parameters within the register can be changed to decrease R_2, such as the size of the gutter channels and distance between pillars[182]. These direct the oil phase through a different route decreasing the overall resistance, consequently decreasing the pressure pushing on the droplet and the differential

pressure. The size of the aperture can also be reduced to increase Laplace pressure thus decreasing the differential pressure. Therefore, for a given geometry and fluidic condition, droplet trapping should always be achievable, assuming that the flow is controlled at low enough pressure to reduce the hydrodynamic differential pressure. The required condition is summed up below:

$$V_2 \leq \Delta P_L = -\gamma\left(\frac{1}{r_2 - r_1}\right)$$

Equation 4-3 Condition for Droplet Trapping

To increase droplet-trapping efficiency the shape of the pillars in the shift registers were adjusted (Figure 4.6 A & B), allowing each droplet to retain a spherical shape, thus locking them into position once the oil flow was stopped due to an increase in surface tension forces.

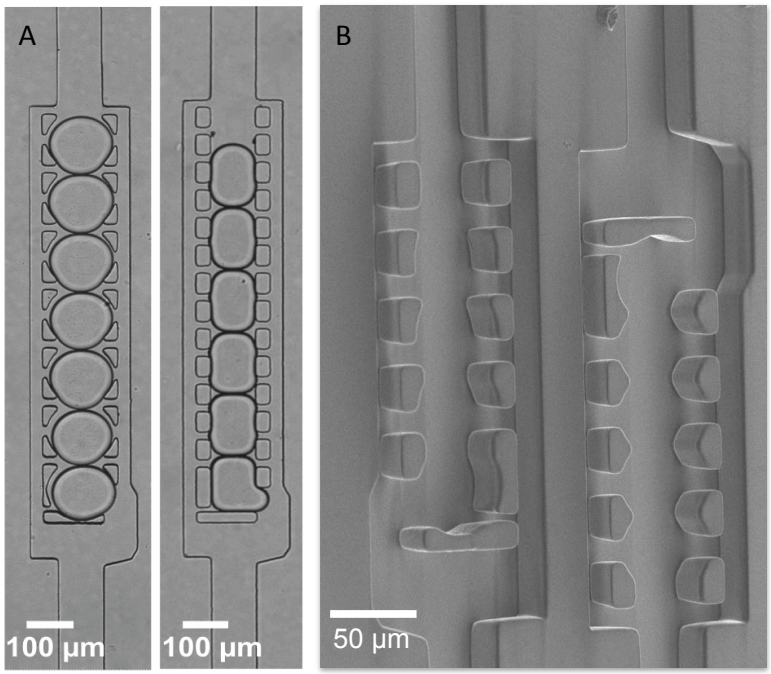

Figure 4.6 Shift registers that allow droplets to lock within the pillars in the absence of oil flow for long-term droplet storage. (A) Experimental images showing the difference between droplet arrangements in long shift registers with different shapes of pillars. The pillar structure on the left allowed droplets to remain trapped within the register when the oil flow was stopped, while droplets on the right-hand image tended to backflow or move outside the registers upon detaching the tubing at the inlets. (B) SEM of shift registers show the rounded pillars designed to accommodate droplets, locking them into place.

4.2 Capillary Number Dependence in Droplet Shift Registers

A droplet flowing through a shift register is either arrested at the constriction or squeezed through it. The dynamics of the trapped and squeezed states are dependent on capillary number, droplet size, viscosity ratio and the channel cross-section. Here, we studied trapping and squeezing of droplets trapped within shift registers using image analysis. Four different droplet shift-register geometries of varying aperture sizes were examined, shown on Table 4.6. In order to understand the dynamics behind these processes, a wide range of capillary numbers, viscosities and interfacial tensions were investigated.

Table 4.6 Design iterations for the droplet shift-register geometries.

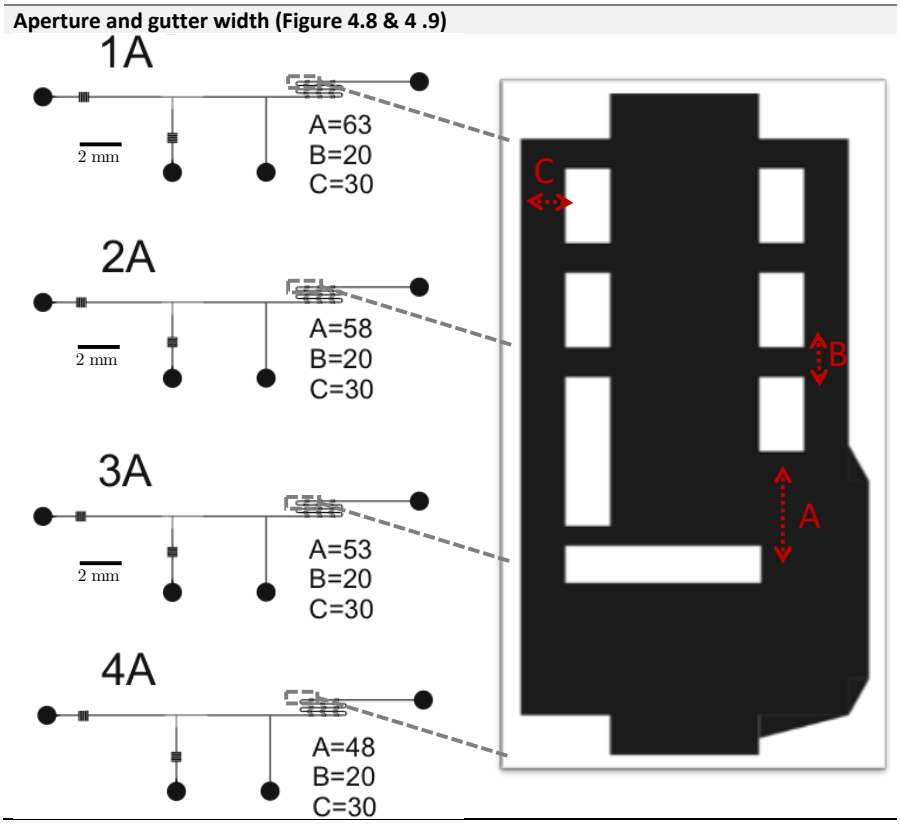

4.2.1 Effect of Capillary Number on Droplet Trapping

Droplet deformation and breakup is governed by the capillary number and the interplay between the viscous and surface forces. A low value of Ca indicates that the stresses due to interfacial tension are stronger compared to viscous stresses. Droplets flowing under such a condition minimise their surface area becoming spherical. In the opposite situation of high Ca, viscous effects dominate and droplet deformations can be observed (Figure 4.7).

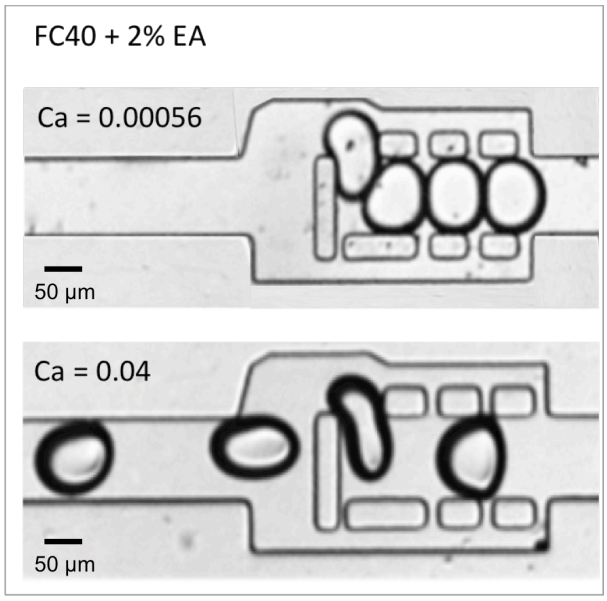

Figure 4.7 Effect of Capillary Number on droplet deformation. As the capillary number increases droplets becomes increasingly elongated and deformed. This prevents droplet trapping within the droplet shift registers. Both images show experiments done at the same conditions, where the oil phase constitutes of FC40 oil with 2% EA surfactant and the aqueous phase is di-water, varying only the capillary number. The image at the top shows that at low capillary numbers (Ca $<10^{-5}$) the droplets tend to adopt a spherical shape aiding droplet trapping. When capillary number is increased, droplets tend to deform aligning with the flow, this deformation prevents droplet trapping and promotes droplet splitting.

Different combinations of oils and surfactants were prepared to obtain a range of interfacial tensions and viscosities. For a device of a given register aperture, droplets were driven at 3 different pressures for each of the oil and surfactant combinations, to obtain different capillary numbers. The capillary number was calculated by video analysis to study how viscous forces influenced droplet trapping. Droplet trapping was assessed physically by having devices with different aperture size (63 µm, 58 µm,

53 µm, 48 µm) and observing whether a droplet was able to get trapped or not. A table of all different conditions is shown on

Table 4.7.

Table 4.7 Viscosity and interfacial tension of different oil and surfactant combinations

Oil	**Surfactant**	**Viscosity, η (mPa*s)**	**Interfacial tension, γ (mN/m)**
FC 40	2% EA	4.1	11
FC 40	2% Krytox (ionic)	4.1	1
Mineral Oil	None	30	49
Mineral Oil	2% Span80	30	4.5
Mineral Oil	2% Tween80	30	9
Mineral Oil	2% Span80, 2% Tween80	30	0.3

Generally, droplets with a capillary number higher than Ca=0.002 did not get trapped even within the smallest aperture, 48 µm, 0.0017 for apertures of 53 µm, 0.0015 for 58 µm and 0.0013 for 63 µm (Figure 4.7). A variation of 0.0002 capillary numbers per 5 µm was obtained. This same trend was seen for every oil and surfactant combination (Figure 4.8) tested. The only combination of oil and surfactant not to follow this trend was FC 40 with 2% Krytox, Ca = 4.1 and Ca = 1. Even at very high capillary numbers, the droplets resisted deformation and were easily trapped in all devices.

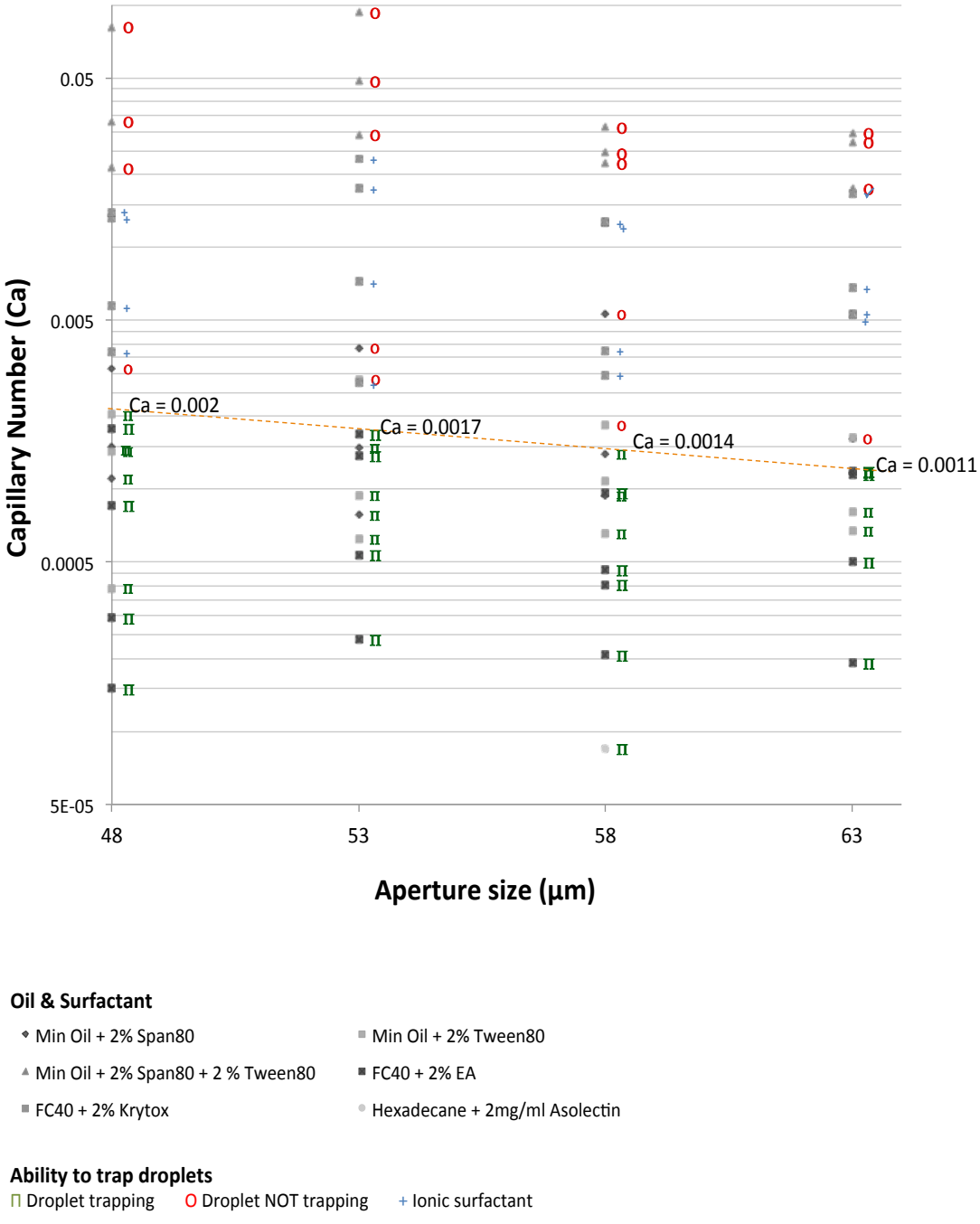

Figure 4.8 Graph showing the ability to trap droplets of different oil and surfactant compositions within registers of varying aperture size. A green symbol indicates success in droplet trapping; a red cross indicates that the droplets were not trapped. The orange dashed line is an arbitrary line between the highest trappable capillary number and the lowest trappable capillary number; it indicates a capillary number threshold above which no droplets are trapped. A pattern is seen for all non-ionic surfactants, droplet trapping is cannot be achieved at high capillary numbers due to high droplet deformation. For ionic surfactants such as Krytox droplet trapping is seen even at very high capillary numbers. Experiments were done with the chip designs shown on Table 4.6.

4.2.2 Effect of Capillary Number on Droplet Coalescence

Another significant phenomenon observed was droplet coalescence, a completely undesirable trait for the formation of DIBs. Both Krytox and Tween 80 induce droplet coalescence. Droplet coalescence appears independent of viscosity or interfacial tension and is mostly related to the surfactant used. Evidence can be seen when the different combinations of oils and surfactants are compared. For instance, the surfactant Span80 was used in many occurrences with different oils yielding a variety of viscosities, interfacial tensions and capillary numbers. However, coalescence was never seen. Yet, when the surfactant Tween80 was used under similar conditions coalescence was almost inevitable. It can be concluded that coalescence is in this case highly dependent on surfactant type and surfactant packing.

4.3 Emulsion Stability

Droplet microfluidics requires droplets to be stable against coalescence, which is achieved by adding surfactants in the solution[122]. These molecules, which are generally made up of a compact polar head and a long hydrophobic tail, are attracted to the interface separating the drop and the carrier fluid where they align perpendicular to the surface. The surfactant layers on two adjacent drops interact together to delay the merging in two ways: first, they can apply electro-static repulsion between the interfaces, in the case of ionic surfactants. Second, they slow down the hydrodynamic flow along the interface through Marangoni effects or through added surface viscosity.

An essential requirement for robust DIB formation is that two phospholipid-enveloped droplets must come into contact without merging. For this to happen, the concentration of phospholipids adsorbed at the oil-water interface must be sufficiently high to prevent coalescence of two aqueous droplets upon contact. Both thermodynamic and fluid-dynamic effects will influence the lipid behaviour at a droplet interface within a microfluidic flow. To investigate this condition, we characterised droplet coalescence within shift register structures as a function of lipid concentration and droplet velocity (where droplet velocity is defined here as the

constant velocity of a droplet flowing in a rectangular microchannel before entering a shift register structure).

For each lipid concentration tested (all above their respective CMC), the droplet diameter was kept constant by adjusting the ratio of aqueous to oil phase pressure at the inlets, thus enabling a range of droplet velocities to be obtained for similarly sized droplets. The frequency of droplet coalescence for a particular lipid concentration decreased with decreasing droplet velocity.

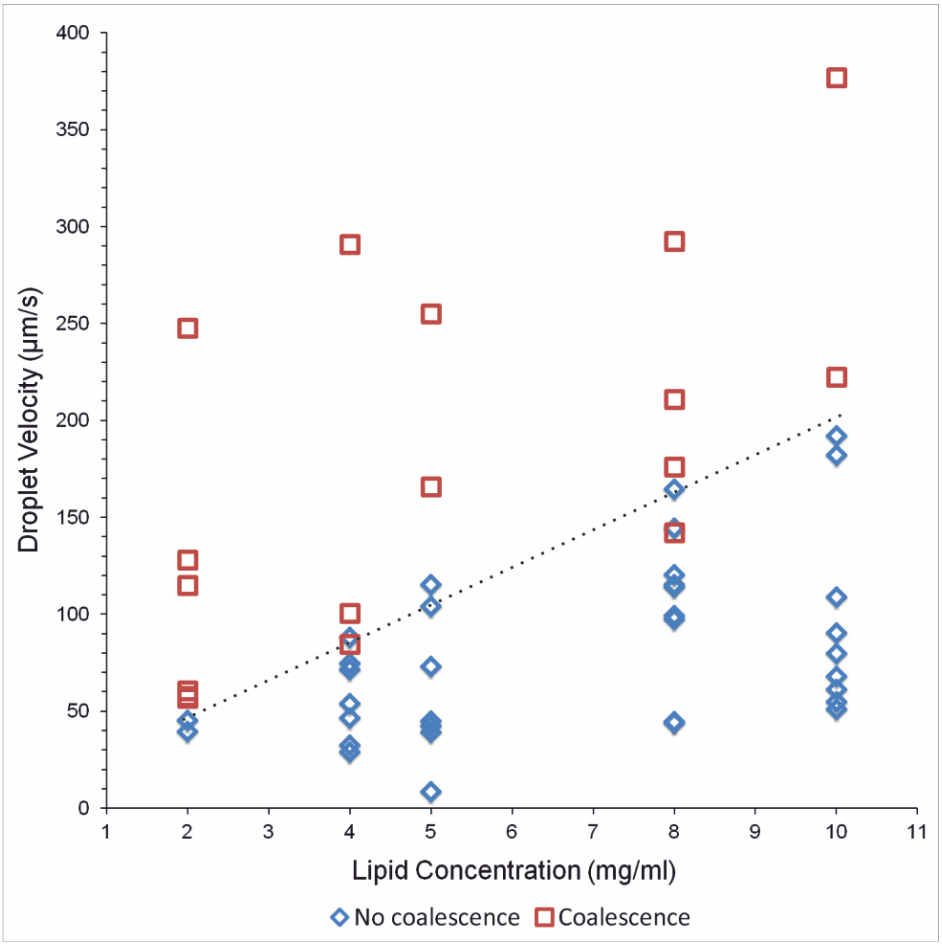

Figure 4.9 Relationship between droplet velocity and lipid concentration. At higher lipid concentrations and lower droplet velocities, droplets became less susceptible to coalescence upon contact within the registers. The dashed line shows an approximately linear dependence between lipid concentrations and droplet velocity. Figure adapted from Schlicht and Zagnoni 2015[183]. Experiments were done with the chip designs shown on Table 4.6.

Overall, a threshold velocity was observed separating coalescing droplets and non-coalescing droplets against increasing lipid concentration, a trend that can be considered linear in first approximation (Figure 4.9). Collisions above the threshold line exhibited a higher likelihood of droplet coalescence, whereas below this line emulsions remained stable and coalescence never occurred. This trend proved valid for different types of phospholipids (asolectin, DPhPC and DOPC).

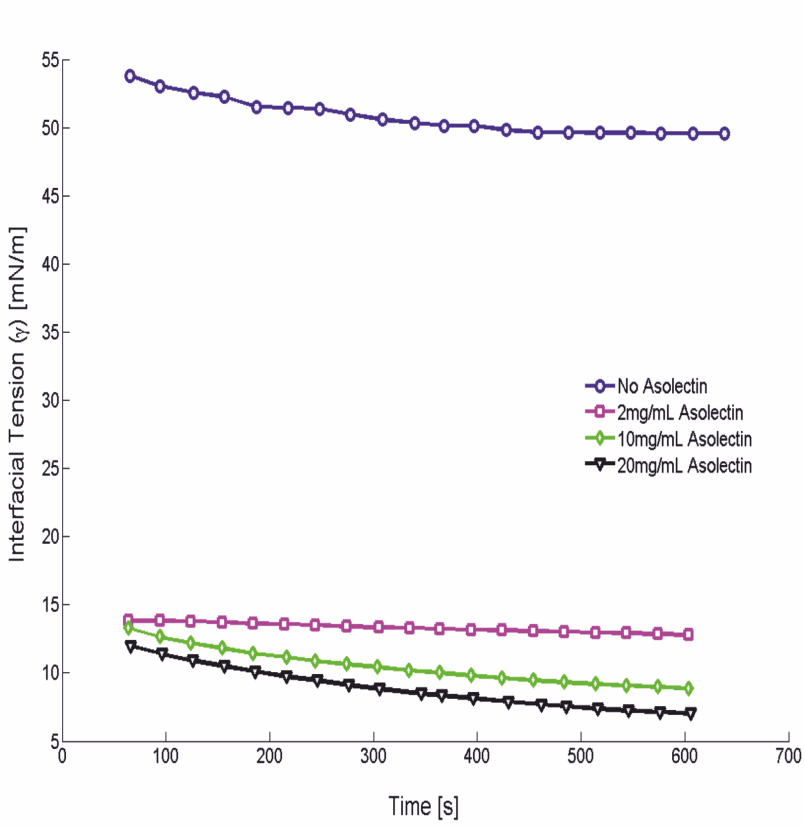

Figure 4.10 Temporal measurements of interfacial tension using the pendant drop method for different concentrations of asolectin in hexadecane. Buffer was 10 mM HEPES, 200 mM KCL and the oil phase was asolectin in hexadecane. The decreasing trend is due to adsorption of lipid molecules (present in micellar form in the hexadecane) to the drop interface by diffusion. The higher the lipid concentration in hexadecane, the lower the interfacial tension.

Additionally, to investigate whether coalescence was dependent on the phase in which lipids were added, for each concentration, tests were carried out where lipids were suspended in the aqueous phase as liposomes, dissolved within the oil phase or added to both phases at the same time. No coalescence trend was identified for these different cases, indicating that coalescence was not dependent on the phase in which the lipids were present.

It is also worth noting that increasing lipid concentration resulted in a decrease of interfacial tension (Figure 4.10). At lower interfacial tensions, droplets were more deformable due to an increase in capillary number thus lowering the trapping efficiency and effecting DIB formation.

The observed decrease in droplet coalescence for increasing lipid concentrations is consistent with previous reports[68] for DPhPC bilayers formed between a resting aqueous droplet in hexadecane and an agarose substrate. In addition, a trend where higher lipid concentrations induced longer- lasting bilayers has also been reported, with the self-assembly process (i.e. from multilamellar to bilayer) of lipids at the droplet interface taking longer to occur for higher lipid concentration[68]. In our system instead, if coalescence did not occur within seconds after contact between droplets, DIB coalescence was never observed.

In static or 'slow' dynamic conditions, droplets coalescence can be avoided by sufficiently increasing the phospholipid concentration thus ensuring phospholipid coverage at a droplet interface. Inversely, for 'fast' dynamic conditions, the lipid coverage at a droplet interface depends also on the hydrodynamic forces and the aqueous solutions used[184,185]. On the one hand, the faster a droplet moves, the greater the lipid adsorption rate at its interface[186]. On the other, lipids at the front of a travelling droplet tend to be displaced to the back of the droplet interface, creating a gradient of interfacial tension and leading to lipid depletion at the front of the droplet[187]. This localised decrease in lipid concentration can induce coalescence upon collision of lipid stabilised W/O droplets.

The dynamics of emulsion stability has been previously investigated in rectangular microchannels[188,189]. Both studies have described the relationship between the rate of droplet coalescence and surfactant concentration depending on the size and dispersion of a group of colliding droplets within a microfluidic chamber. Additionally, previous reports[184,190] have also described coalescence effects in micro droplets when fast fluid dynamics induce a local depletion of the surfactant at the

interface between two contacting droplets. Finally, droplet stabilization in 'very fast' flow rates (i.e. twice the magnitude as in our system) has also been investigated[186]. For the microchannel geometry used and a continuous train of adjacent droplets, a trend was identified where higher droplet velocities increased the coalescence rate of lipid-stabilised droplets. Overall, regardless of the microfluidic geometry, it can be concluded that to avoid droplet coalescence it is necessary to ensure that the lipid adsorption dynamics at a W/O interface are faster than the lipid depletion dynamics caused by interfacial shear before droplet collision.

Specific to this work, Figure 4.11 shows schematically the two possible scenarios that can occur during a droplet arraying process within a shift register. In both cases, we consider the first droplet as static (already trapped in a register), while the second is approaching and eventually contacts the first to form a DIB. Both droplets are exposed to interfacial shear stress caused by the drainage of the interstitial oil (through the gap between pillars in a shift register structure - arrows in Figure 4.11), which occurs as the moving droplet approaches the resting one. If droplet velocity is used as a measure of the shear stress at a droplet interface moving in a rectangular channel, a higher velocity corresponds to greater shear[185], causing a more pronounced change in the phospholipid distribution at the droplet interface. Consistent with what was discussed above, a high shear stress induces a rapid depletion of the phospholipid film, rendering emulsion interfaces prone to coalescence (Figure 4.11 A). Successful formation of DIB occurs when lipid adsorption dynamics are dominant over interfacial phospholipid depletion, thus preventing coalescence. When analysing the magnitudes of the velocities of phospholipid stabilised (ps) W/O droplet trains in rectangular microchannels in the literature[74,145] , similar velocity values to those identified in Figure 4.9 are obtained, suggesting that the considerations outlined above are generally applicable to phospholipid stabilised emulsions at the microscale. In conclusion, the correlation between droplet velocity, lipid concentration and coalescence can be identified for a specific lipid mixture. This information was then used for instructing the design of our channel networks.

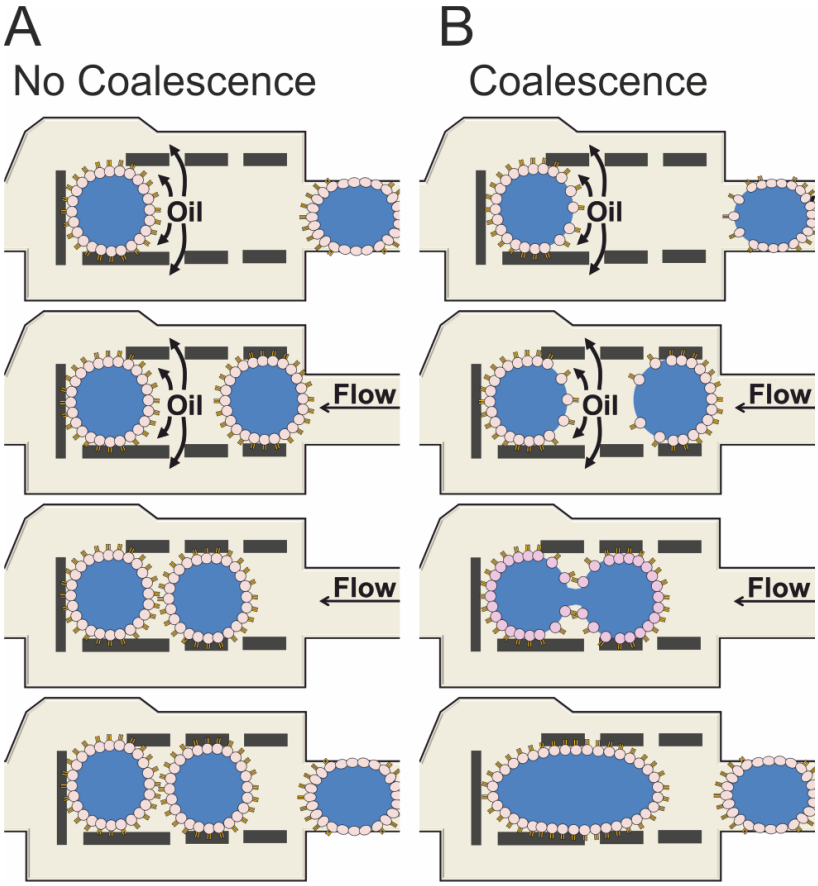

Figure 4.11 Schematic representation of coalescence (A) and non-coalescence (B) mechanisms of psW/O droplets within a shift register due to a difference in droplet velocity. During normal device operation, when a droplet reaches an empty shift register it remains trapped within the pillar structure if the correct balance between the hydrodynamic pressure difference between the inlet and outlet points of the register and the Laplace pressure of the droplet interface is achieved. Because the oil is flowing within the register and exiting through the gaps between the pillars, the interface of a trapped droplet can be depleted of phospholipids proportionally to the magnitude of the shear forces parallel to the oil flow directions. When a second droplet, presenting a phospholipid-depleted front interface, enters the register, the oil layer between the two drops is drained through the pillars and contact between the two psW/O droplets will occur. Depending on the phospholipid adsorption dynamics (i.e. phospholipid concentration and magnitude of hydrodynamic forces), the two droplets will coalesce depending on the degree of phospholipid coverage.

4.4 Microfluidic Device Geometry

Considering the information obtained for each module, a microfluidic platform consisting of a passive microchannel network capable of droplet production, droplet alternation, in-line change of droplet velocity, DIB formation and their storage was designed and characterized (Figure 4.12).

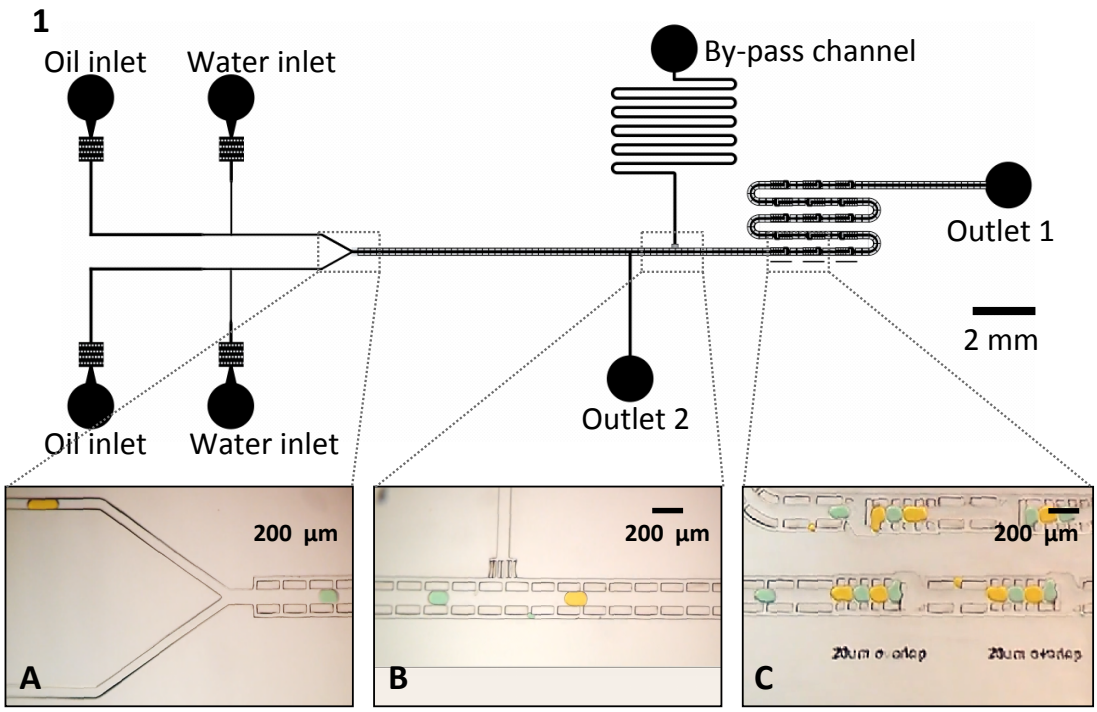

Figure 4.12 Device geometry, adapted from Schlicht and Zagnoni 2015[183]. Schematic drawing of the microfluidic device developed. A double T-Junction was used to produce droplets encapsulating different buffers. (A) a Y-Junction enabled droplet alternation; (B) the channel structure and a by-pass channel were designed to divert the oil phase and reduce droplet velocity after formation and before the register area; (C) a series of droplet traps (shift registers) had an optimised pattern to maintain droplets stored in the absence of flow.

The microfluidic design comprises a double T-junction (for droplet formation), a Y-junction (for droplet alternation, Figure 4.12 A), a bypass channel (to adjust the velocity of the droplets, Figure 4.12 B) and a series of microfluidic shift registers[179] (for droplet trapping, DIB formation and storage, Figure 4.12 C). When a droplet enters a shift register, the balance between hydrodynamic and interfacial tension forces will determine the trapping efficiency. DIB formation is achieved when two lipid covered W/O droplets come into contact and the lipid molecules at each droplet interface interact spontaneously, self-assembling into a lipid bilayer, a condition that is achieved through the use of the shift registers. The register structures can be adjusted to form the desired droplet train lengths (i.e. DIB array) and enable from one to an array of DIBs to be formed in series.

Outlet 2 (Figure 4.12) allowed the extraction of residual air when initially filling the device. This outlet was subsequently blocked and not used during normal

device operation, thus forcing fluids through the passive network of registers. Of particular benefit for reliable DIB formation was the addition of a by-pass channel (Figure 4.12 B). This feature facilitates control over droplet velocity by diverting the continuous phase, consequently allowing a reduction in droplet speed. Reduction in velocity ultimately increased trapping efficiency and prevented droplet coalescence. To control droplet in line velocity various chip design were tested until the final design (Figure 4.12) was chosen. These can be seen on Table 4.8

Table 4.8 Design iterations for the in-line control of droplet velocity

Two small outlets (Figure 4.3)	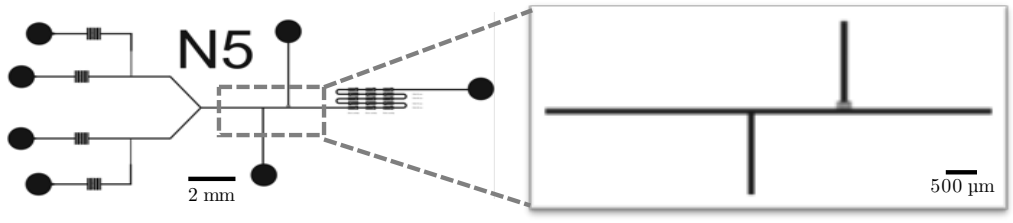
Long middle channel	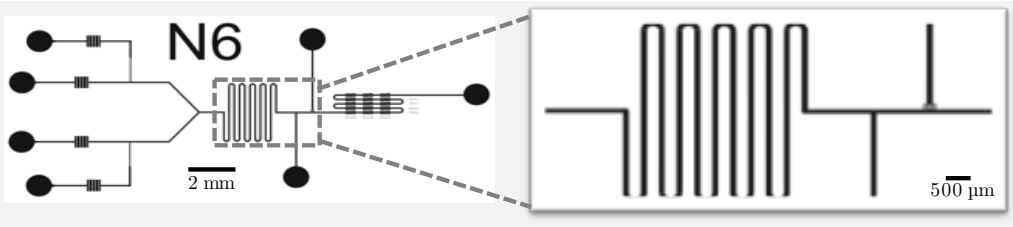
Wider main channel with gutters (Figure 4.12)	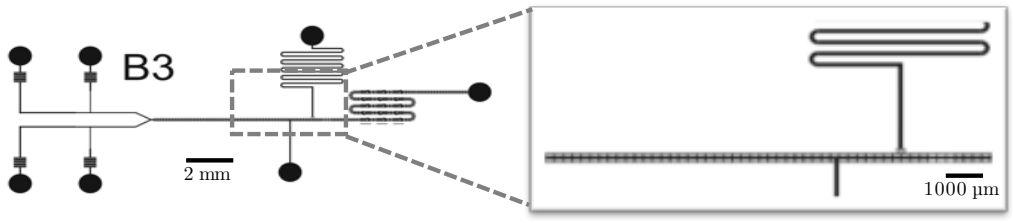

4.5 Summary

A microfluidic system for the controlled production and storage of droplets in DIB format was designed and characterized. The size ratios of the droplets were directly controlled by the pressure rates of the fluidic phases. A well-defined regime of pressures required for droplet trapping was determined, which is achieved when the hydrodynamic pressure and Laplace pressures are balanced. Lipid stabilized droplets

were successfully trapped and stored within register elements. This device is aimed at the creation of DIBs for the study of membrane proteins in the following chapters. For this purpose, the next experiments focussed on DIBs validation and characterization as well as exploring the ability of the bilayers to host a channel peptide

Chapter 5

DIBs for Permeation and Membrane Protein Studies

In this chapter, we present the validation of the DIBs formed within the device described in the previous chapter both in terms of permeability and the ability to host a functional ion channel. A fluorescence -based assay was developed to confirm the formation of lipid bilayers and to quantify the bilayer permeability.

5.1 Applications of Droplet-Interface-Bilayers

Membranes are not closed boundaries but regulate the passage of molecules by different mechanisms. The three main pathways of transmembrane solute permeation are passive diffusion, facilitated diffusion and active transport[191]. Passive diffusion describes the passive movement of solutes through the lipid bilayer following their concentration gradient involving neither carrier nor channel proteins. Facilitated diffusion, instead, describes the facilitated transport of a solute by protein pores following its concentration gradient. Active transport comprises all transport processes that require an active binding of the solute to a transporter protein, which transports the solute either into the cell or effluxes it from the cell, both against a concentration gradient and therefore requires energy.

Basic biophysical studies and pharmacological processes can be investigated *in vitro* by mimicking the intracellular and extracellular environments across an artificial cell membrane construct. The ability to reproduce simplified scenarios found in live cell membranes in an automated manner has great potential for a variety of synthetic biology and compound screening applications. Of particular interest for both drug discovery and biophysical research is the ability to interrogate and characterise the functional behaviour of membrane proteins in a reliable, scalable and miniaturised format.

The experiments described in this chapter centre on lipid bilayers formed between two droplets within the platform described in Chapter 4. In this configuration, the droplets are produced and assayed on-chip. The system allows the precise and positioning of droplets within droplet shift registers, offering new solutions for developing DIB permeation assays in an automated fashion using fluorescence microscopy. By encapsulating the desired cocktail of buffers, molecules and peptides into the phospholipid stabilized W/O droplets, a large number of DIBs were characterized using fluorescence-based assays. The DIBs formed were characterized both as a microfluidic method for passive permeation assays and for the ability of the bilayers to host a channel peptide as a platform for membrane protein studies. In both

studies, we fluorometrically measured permeation of molecules using donor and acceptor droplets, and calculated permeability values at the droplet membranes and at the α-haemolysin pores using a model based on diffusion transport.

Such artificial bilayer platforms can potentially replace conventional screening technologies, which are expensive and highly complex and be up-scaled for high-throughput applications.

Here, we describe a microfluidic method for a diffusion-based permeation assay using droplet lipid membranes. Aqueous droplets were produced in donor and acceptor alternations in hexadecane with solved lipids. Subsequently, at droplet shift registers, droplets come into contact creating arrayed DIBs between donor and acceptor compartments. Figure 5.1 shows the layout of the microfluidic shift registers permitting the formation of droplet arrays of varying droplet numbers.

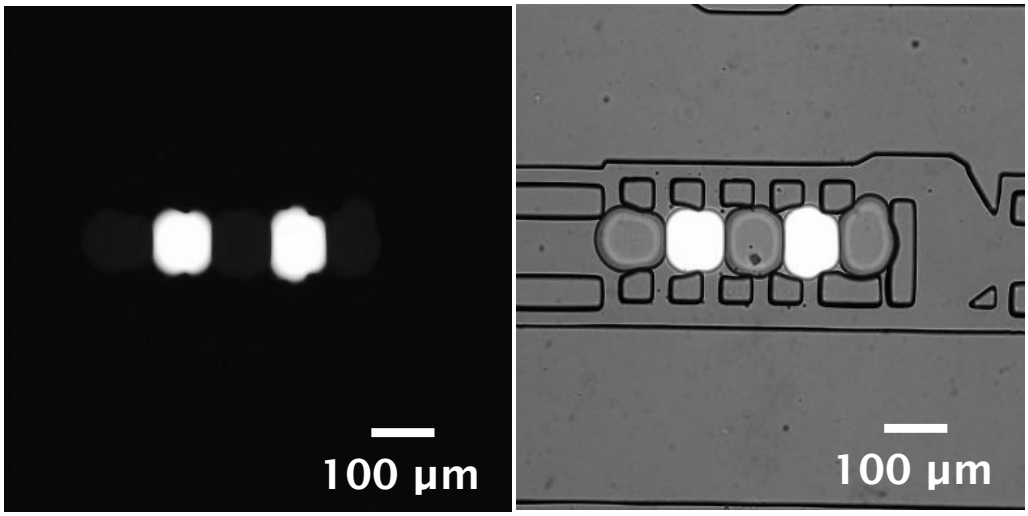

Figure 5.1 Fluorescence (left) and Bright field (right) images showing the formation of donor and acceptor droplets configuration within droplet shift registers. The oil phase is hexadecane with 10 mg/ml asolectin and the aqueous phase was composed of 350 mM KCl, 10 mM HEPES for non-fluorescent aqueous phase and 100 µM calcein was added to the fluorescent phase. Registers capable of holding up to 5 droplets were used to observe permeation of fluorescent particle from the donor droplets (fluorescent) to the acceptor droplets (non-fluorescent). Droplets were produced in alternating fashion as described on Chapter 3, section 3.3.1. Droplet production was halted by decreasing the pressure driving the phases and droplets were monitored periodically.

DIB formation was validated by employing a membrane permeability assay[192] to characterise the leakage of fluorescent molecules through the lipid bilayer. This assay was performed by comparing the passive diffusion of fluorescein and its derivative, calcein (bis[N,N0-di(carboxy- methyl)-aminoethyl] fluorescein). Molecules with a lower charge are more permeable through a lipid layer than those with a higher charge[193,194]. At neutral pH, the fluorescein and calcein moiety is mainly found as monoanios and dianions, with fluorescein yielding mainly monoanions and calcein yielding mainly dianions. Since monoanions are the only form that permeates the lipid bilayer, droplets containing fluorescein are expected to permeate a lipid bilayer faster than those containing calcein due to the lower charges of these species in solution.

For the organic phase, asolectin phospholipids were dissolved in hexadecane to make a 10 mg/mL solution. The lipids were dissolved in chloroform, and dried to a thin film under a continuous stream of nitrogen gas, before being resuspended in the hexadecane solution. For the measurement of fluorescein permeation, we trapped 5 droplets per register, 2 donor droplets containing fluorescein (100 μM fluorescein, 350 mM KCl, 10 mM HEPES) and 3 acceptor droplets (350 mM KCl, 10 mM HEPES). Fluorescence and bright field images were observed and recorded and the captured fluorescence images were processed using ImageJ (NIH).

After DIB formation, transport through a lipid bilayer of fluorescent dye molecules due to passive diffusion was tested, demonstrating proof-of-concept and the suitability of the proposed microfluidic system for automated and scalable DIB-based permeation assays based on fluorescence. Furthermore, dye permeation (Figure 5.2) demonstrated that DIB formation occurred, if not instantaneously, within a few minutes from droplet contact.

Low pressures were used for droplet production to ensure the formation of lipid monolayers at the interface of the droplets to prevent coalescence upon contact. We confirmed the formation of lipid layers in the microfluidic channels by observing the passive permeation of fluorescein through droplet membranes.

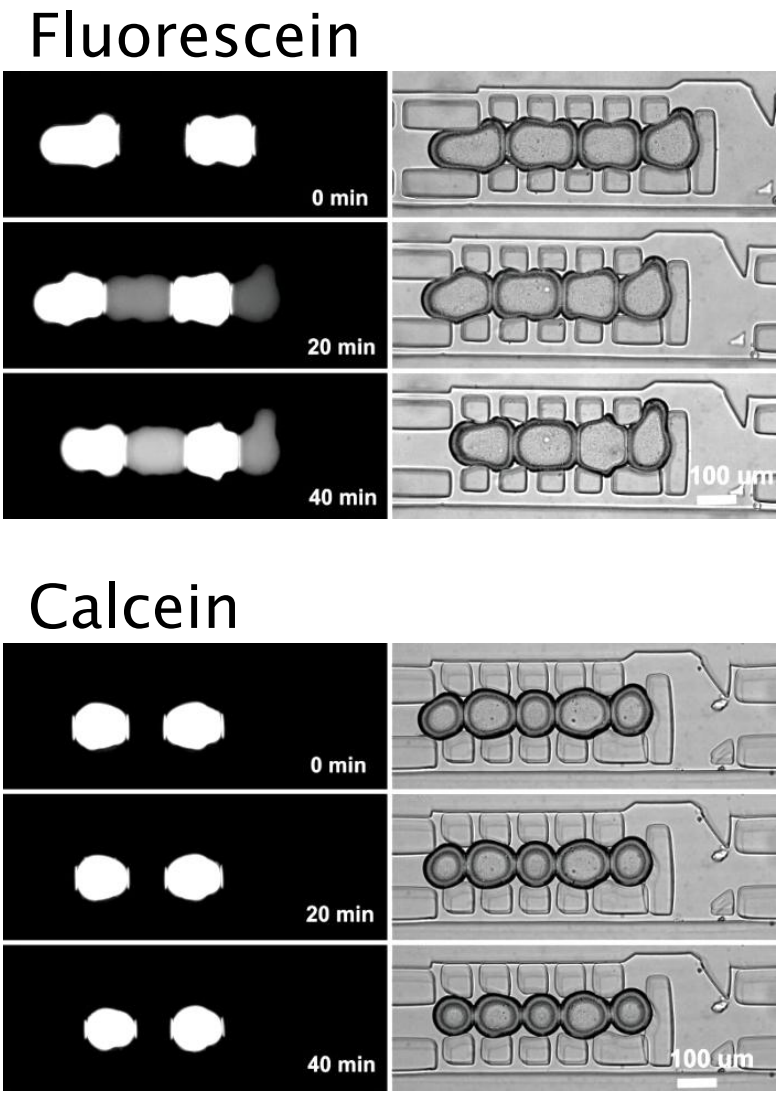

Figure 5.2 Passive molecular transport across microfluidic DIBs. Fluorescent (donor) and non-fluorescent (acceptor) droplets were trapped within registers and images where acquired every 5 minutes for 1 hour. The left-hand column shows fluorescence microscopy images taken using a FITC filter. The corresponding bright field can be seen in the right-hand column. 10 mg/ml asolectin dissolved in hexadecane was used as the oil phase and fluorescent droplets contained either 100 µM fluorescein or 100 µM calcein. From these images, it can be calculated that fluorescein leaks through the lipid layer, increasing the fluorescence of adjacent droplets at a much faster rate than calcein. Over the same time period, calcein was not seen to permeate through to the neighbouring droplets. The experiment was operated according to the description in Chapter 3, section 3.3.1.

As shown in Figure 5.2, we imaged the permeation of fluorescein across the lipid membrane separating the fluorescent donor droplet and the non-fluorescent acceptor droplet. In similar experiments conducted using the same conditions but using calcein instead, we did not observe any evidence of calcein permeation (Figure 5.2). We employed calcein in experiments specifically designed as a control to confirm

if lipid membranes separating aqueous droplets in the microfluidic chamber were indeed selectively permeable. The ability of fluorescein, but not calcein, to permeate the DIB confirmed the formation of a selectively permeable lipid interface.

It is important to note that dye leakage experiments alone do not prove the existence of a single lipid bilayer (whilst the flow of ions through α-haemolysin pores does). Previous reports have in fact shown that the interactions between lipid molecules and dyes are dependent on the number of lipid layers (or lipid multilayer), with leakage time being directly proportional to the number of lipid bilayers[195].

5.2 Alpha-Haemolysin

Alpha-haemolysin (αHL) is a heptameric, 14-strand β-barrel, transmembrane pore from *Staphylococcus aureus*[196]. These bacterial toxins function by assembling identical subunits into a membrane-spanning pore. Cell lysis (and death) is caused by the leakage of small molecules and ions through the large water-filled central channel. Alpha-haemolysin consists of seven identical subunits arranged around a central axis (Figure 5.3). Seven hairpins associate to form a transmembrane β-barrel of 52 Å length and 26 Å diameter.

The transmembrane part of the lumen is a β-sheet with two antiparallel strands. The extra membrane domain contains a large cavity that houses the transmembrane domain during the assembly process, which is available for developing an assembled pore[197]. Alpha-haemolysin is secreted as a monomer, but links into a heptamer at the surface of the target cells. The water-soluble monomers bind to the lipid bilayer before associating to form a heptameric prepore[198–200]. Subsequently, the heptameric membrane-associated species inserts through the bilayer, forming a channel. The channel formed by α-haemolysin allows any kind of ions to penetrate through the membrane.

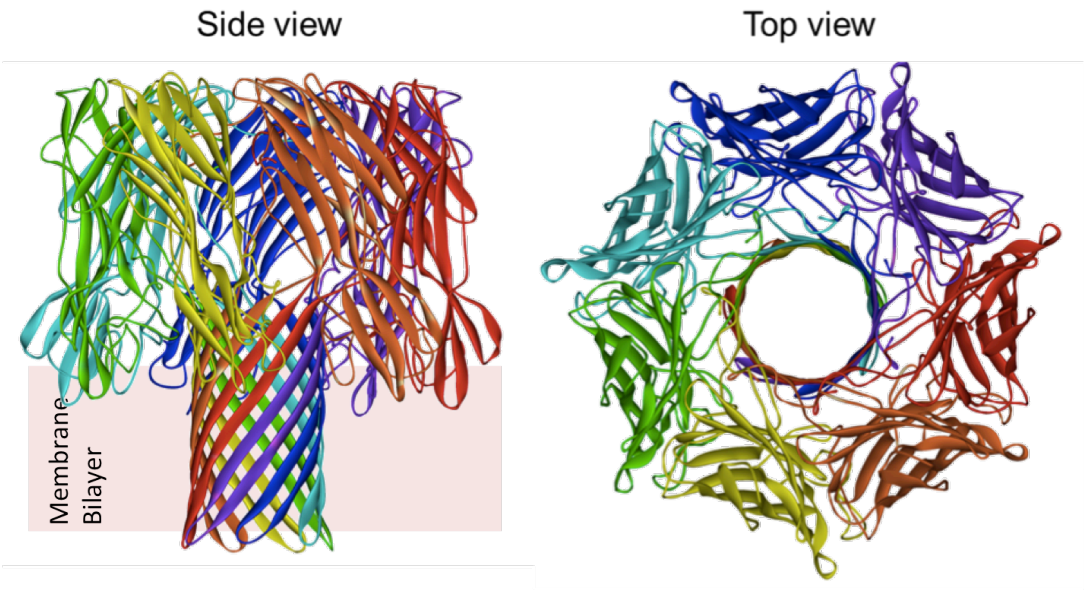

Figure 5.3 α-Haemolysin from Staphylococcus aureus with each monomer segment in a different colour. Taken from L. Song et al. 1996[201], PDB reference 7AHL.

5.2.1 Incorporation of α-Haemolysin in DIBs

Incorporation of α-haemolysin pores into DIBs was monitored by detecting the permeation of Ca^{2+} ions across the bilayers using the fluorescent calcium marker Fluo-8, a bilayer impermeable dye that increases in fluorescence when bound to calcium (Figure 5.4).

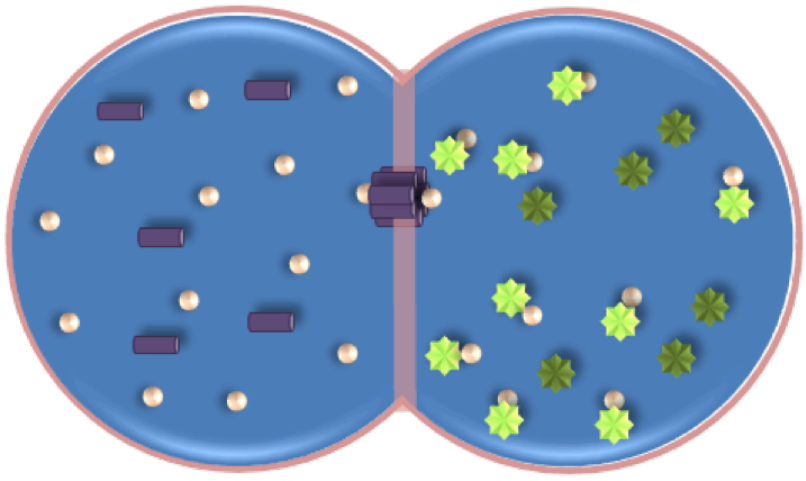

Figure 5.4 Schematic of Ca^{2+} permeation across α-haemolysin channels. The purple barrels represent the α-haemolysin subunits, the white spheres represent the calcium ions. The stars represent Fluo-8 molecules in two different states, dark green for the non-fluorescent form and light green when it is calcium bound and fluorescent.

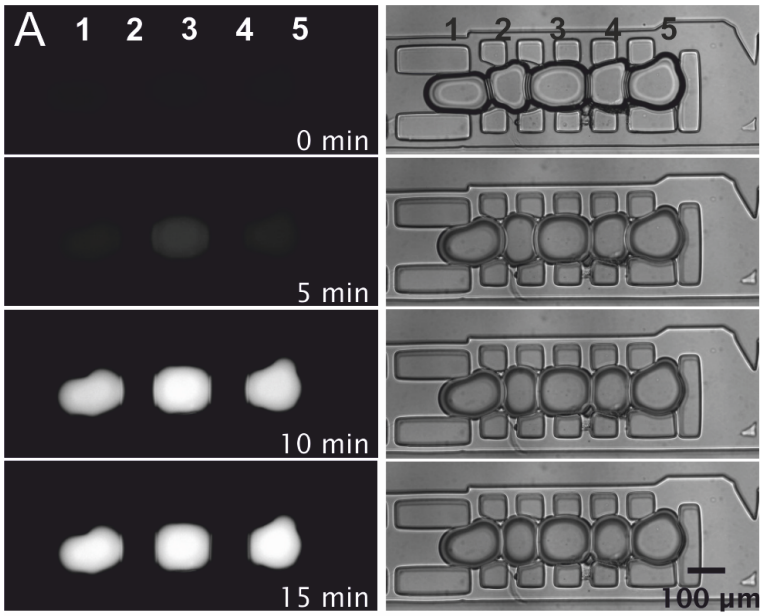

Figure 5.5 α-haemolysin pore formation in microfluidic DIBs. Acceptor droplets (1, 3 and 5) containing 250 mM Fluo-8, 10 mM HEPES, 333 mM EDTA, 2 M KCl and donor droplets (2 and 4) containing, 2 mg/ml α-haemolysin, 10 mM HEPES, 20 mM EDTA, 1 M $CaCl_2$ pH 7.4 were trapped in ABABA configuration. Incorporation of the α-haemolysin pore into the DIB produced a diffusive calcium flux into the neighbouring droplets. The left-hand column shows fluorescence microscopy images taken using a FITC filter. The corresponding bright field can be seen in the right-hand column. 5 mg/ml DPhPC in hexadecane was used as the oil phase. The experiment was operated according to the description in Chapter 3, section 3.3.1.

Arrays of droplets in ABAB configuration were produced, with one droplet encapsulating α-haemolysin monomers in a Ca^{2+} buffer (donor droplets) and its neighbour containing a Fluo-8 in an isosmotic K^+ buffer (acceptor droplets). The permeation of Ca^{2+} ions through the channel peptide was monitored immediately after droplet arraying and DIB formation for a period of one hour. As α-haemolysin monomers spontaneously inserted into the bilayer, ion channel pores were formed allowing the permeation of Ca^{2+}, but not Fluo-8 molecules. Consequently, a pronounced increase in fluorescence could be observed over time as a result of the facilitated diffusion of Ca^{2+} through the α-haemolysin pores and subsequent binding to Fluo-8.

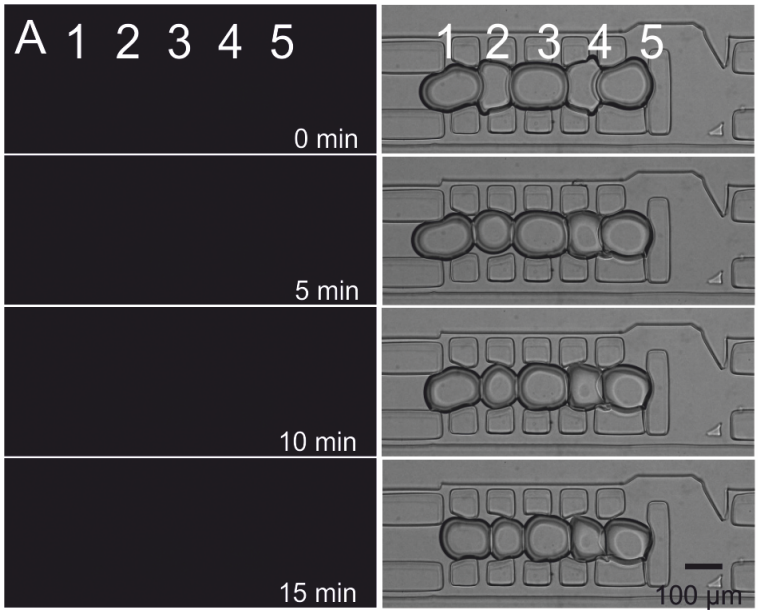

Figure 5.6 Control experiment for Figure 5.5 in the manuscript. Droplets in ABABA configuration contained 10mM HEPES, 20 µM EDTA, 1M $CaCl_2$, at pH 7.4 (donor droplet) and 10mM HEPES, 333 µM EDTA, 2M KCl, 250 µM Fluo-8, at pH 7.4 (acceptor droplet). (A) The left-hand column shows fluorescence microscopy images taken using a fluorescein isothiocyanate (FITC) filter; the corresponding bright field images can be seen in the right-hand column. (B) When no α-haemolysin monomers were encapsulated in the droplets, no diffusion of calcium ions occurred across the DIBs. Experiments were carried out for 45 minutes with no detectable increase in fluorescence signal. 5 mg/ml DPhPC in hexadecane was used as the oil phase. The experiment was operated according to the description in Chapter 3, section 3.3.1.

From Figure 5.5, it can be observed that the middle droplet becomes fluorescent at a faster rate than the side droplets, due to the fact that two DIBs were interfaced to the Fluo-8 containing droplet. After 15 min, all three acceptor droplets were seen to reach a similar level of fluorescence as Fluo-8 molecules were saturated. As a control, the same experiment was carried out with droplets lacking in α-haemolysin monomers. The process was monitored over the same time period and no detectable increase in fluorescence was observed (Figure 5.6). Ion flux through DIBs varied among experiments due to the stochastic nature of monomer insertion and pore formation in a lipid bilayer.

5.3 Quantification of Diffusion

The importance of carrying out permeation assays in vitro and both the qualitative and quantitative estimation of ion-channel mediated molecular transport is well documented[175,194,202]. A system that can allow such assays to be performed in an automated and customisable manner can find applications in the pharmacokinetic screening of compounds during the drug development process. Here, proof-of-concept data is shown estimating the permeability of fluorescein through microfluidic DIBs and ion transport across α-haemolysin bearing DIBs.

To evaluate the permeation of substances from a donor droplet to an acceptor droplet, we used the apparent permeability index P_{app} (cm/s) [175], which was calculated using the adapted Equation 5-1:

$$P_{app} = \frac{V_R(t)}{A(t) * C_{D0}} \frac{dC_R(t)}{dt}$$

Equation 5-1 Apparent Permeability

where C_{D0} (mol) is the initial concentration of the compound in the donor droplet, $C_R(t)$ (mol/s) is the concentration of the compound in the acceptor droplet over time, A(t) (μm^2) is the estimated total surface area of the DIB (i.e. taking into account that some droplets had two DIBs) and $V_R(t)$ (pL) is the estimated volume of the acceptor droplet over time.

The droplet volumes and DIB surface areas at each time point were estimated from the respective microscopy images (approximating droplets to ellipsoids and DIB areas to ellipses). The calculation takes into account variability in droplet size and bilayer area for all measurements therefore temporal changes do not affect the estimate of the permeability coefficient. As the fluorescence intensity is proportional to molecular concentration, the intensity values were used as a proxy for compound concentration. The estimated P_{app} value for fluorescein at pH 7.4 was $2.5 \times 10^{-6} \pm 1.463 \times 10^{-6}$ cm/s (calculated from 5 different experiments Table 9) which falls within

the range reported in the literature between 1.6 x 10^{-6} cm/s and 21.23 x 10^{-6} cm/s[194,202,203] according to the pH used.

Table 9 Permeation values for the flux of fluorescein through DIBs

	$A(t)$	$V_R(t)$	C_{D0}	$\frac{dC_R(t)}{dt}$	P_{app}
EXP 1	2.5 x10^{-5}	2.94 x10^{-7}	795.49	0.126	2.14 x10^{-7}
EXP 2	2.5 x10^{-5}	2.94 x10^{-7}	1268.36	0.511	1.83 x10^{-7}
EXP 3	2.5 x10^{-5}	2.94 x10^{-7}	1172.42	0.120	1.43 x10^{-7}
EXP 4	5.0 x10^{-5}	2.94 x10^{-7}	16383	0.962	3.44 x10^{-7}
EXP 5	5.0 x10^{-5}	2.94 x10^{-7}	3445.3	0.107	3.65 x10^{-7}

The estimated P_{app} value for Ca^{2+} ion across α-haemolysin pores was 7.08 x 10^{-6} ± 1.76 x 10^{-6} cm/s (calculated from 3 different experiments Table 10) for the concentration of monomers used. This approach can provide an insight into the transport dynamics through ion channels when, for instance, determining the effects on ion flux through proteins caused by blocking agents[171]. To calculate the concentration of calcium ions in the microfluidic droplets from fluorescence images, we conducted a series of calibration experiments designed to report the fluorescence intensity of Fluo-8 at various known concentrations in aqueous solutions. Care was taken so that spatial intensity differences arising from varying excitation or emission sensing properties of the fluorescence microscope was minimized. Fluorescence images were acquired using a fluorescein isothiocyanate filter (FITC) with 200 ms exposure time. Fluorescence intensity from the droplets was obtained by averaging the intensity values of a squared region of interest (ROI) of 50 x 50 pixels. The corners of squared ROI touched the internal edges of the droplet thus covering most of the droplet. With a set of discrete data points, an estimation of calcium concentration from the fluorescence intensity can be attained. An example of a calibration curve is given in Figure 5.7 for various Fluo-8 and Ca^{2+} concentrations.

Table 10 Permeation values for the flux of ca^{2+} through α-HL channels in dibs

	$A(t)$	$V_R(t)$	C_{D0}	$\frac{dC_R(t)}{dt}$	P_{app}
EXP 1	2.512 x10^{-5}	2.94 x10^{-7}	563	3.7058	7.71 x10^{-5}
EXP 2	2.512 x10^{-5}	2.94 x10^{-7}	562	3.825	7.96 x10^{-5}
EXP 3	2.512 x10^{-5}	2.94 x10^{-7}	562	3.1775	6.62 x10^{-5}

Fluo-8 and calcium ion droplets were produced in a co-flow T-junction shown in Figure 5.7 A, to ensure that the reaction started in the droplets. Due to laminar flow property, only a thin fluorescent interface is instantaneously formed before droplet production (Figure 5.7 B). Fluo-8 and Ca^{2+} solutions (in a range 100 µM to 1 M $CaCl_2$) where mixed in a 50:50 ratio to produce fluorescent droplets which were subsequently stored downstream from droplet production. Once enough droplets were collected fluorescence images were taken for each different calcium concentration and a calibration curve was drawn (Figure 5.7 C).

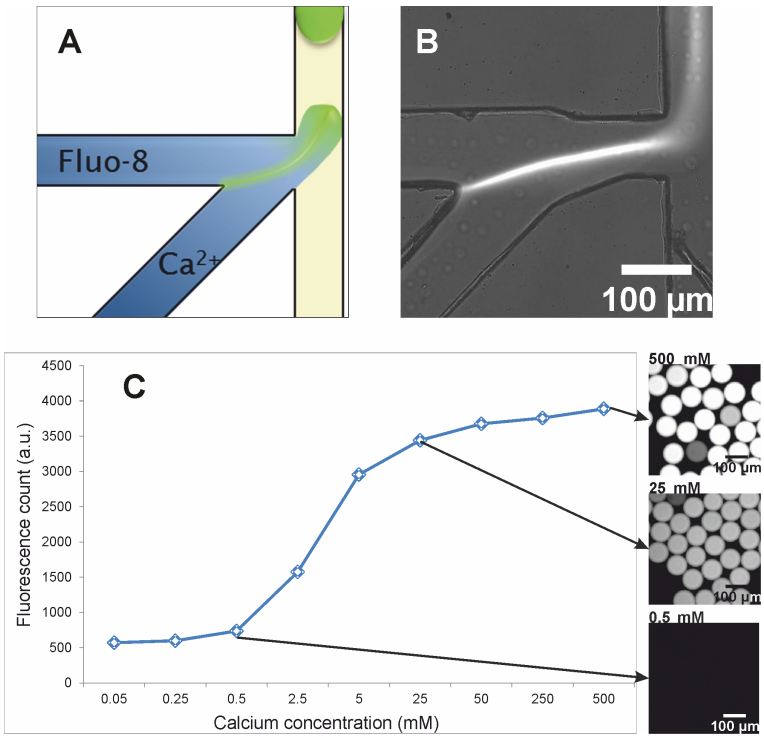

Figure 5.7 Calibration curve for quantitative analysis of calcium transport across DIBs. Schematic representation (A) and fluorescence microscope image (B) of a co-flow T-junction where two streams containing Fluo-8 dye solution (250 µM Fluo-8, 10 mM HEPES, 333 µM

EDTA, 2M KCl at pH 7.4) and calcium buffer (10 mM HEPES, 20 µM EDTA, 100 µM - 1M $CaCl_2$ at pH 7.4) were mixed and emulsified. (C) The fluorescence intensity of 10 droplets was measured for each concentration tested and the average value was used to produce a calibration curve, which can be used to estimate the concentration of calcium within droplets during α-haemolysin experiments. 5 mg/ml DPhPC in hexadecane was used as the oil phase. The experiment was operated according to the description in Chapter 3, section 3.3.1.

5.4 Summary

The ability to qualitatively and quantitatively identify DIB permeation values demonstrates the suitability of our system for investigating processes occurring across an artificial lipid bilayer in a miniaturised and scalable format.

Using the platform described in Chapter 4 arrays of alternating donor and acceptor aqueous droplets were brought into contact in droplet shift registers, forming parallel planar droplet-interface-bilayers between donor and acceptor compartments. This recreates intra/extracellular mimics. Here, we have demonstrated passive molecular permeation and ion-channel mediated permeation of molecules and ions through DIBs using fluorescence assays.

We employed a simple diffusion model to calculate permeability from experimental data, and the calculated permeability values, which fell in the range previously reported in the literature. This study suggests our platform has the potential to analyse the permeability of numerous pharmaceutical compounds. Finally, this system benefits from the potential to use different lipid types that can aid the modelling of permeation through different tissue and channel types.

Passive diffusion through cell membranes is the most common method of transport for drugs to enter cells therefore, permeation assays play an important role in intracellular drug delivery, toxicity screening and drug discovery[41]. Many drugs are developed to target intracellular biomolecules located in the cytoplasm or nucleus. Drug permeation assays determines their pharmacokinetic behaviour, which can be critical for the failure or success of a drug. Despite its significance as most important transport mechanism for drugs, lipid bilayer diffusion is poorly understood[204,205].

Summary

The need of exploring a solute's ability to pass membrane barriers has led to the development of a variety of permeation assays. For the valuation of intestinal drug administration permeability, epithelial cell culture models such as Caco-2 cells (described in Chapter 1) are regularly used and deliver good estimations about the fraction of drug absorbed in humans after oral administration[206]. Depending on the specific characteristics of the cell line, their use allows not only the investigation of passive diffusion but also of active transport processes. This versatility is, however, of disadvantage for the exclusive investigation of simple diffusion across the lipid bilayer. To gain insight into the process of passive diffusion across lipid bilayers the use of artificial lipid membranes is considered to be more instructive than cell culture models since any other permeation process can be excluded.

Permeability assays that are tissue specific are commercially available. PAMPA assays that model gastrointestinal epithelium, blood brain barrier, and skin tissue have been developed[41,191,207]. Using this technology similar assays can be employed, for example instead of using asolectin phospholipids into the hexadecane organic solution, brain lipid extract can be used as a way to simulate permeability of drugs in tissue that closely resembles the blood brain barrier.

Chapter 6

CLIC1 ion channel in DIBs

This chapter describes studies on the structure and insertion conditions, according to pH and oxidative state, of the Chloride Intracellular Channel 1 into a lipid vesicle and a DIB. A number of biophysical studies have also been done to determine the orientation of the transmembrane region, giving clues to the structure of membrane bound CLIC1. Finally, we have used the microfluidic device described in Chapter 4 to study CLIC1 function and to consider if the DIBs we have formed are able to host self-inserting eukaryotic channels.

6.1 Introduction

Ion channels embedded within the plasma membrane of a cell have been widely studied and characterized, nonetheless relatively little is known about ion channels residing in the membranes of intracellular organelles, such as the mitochondria and nucleus. Electrophysiological characterization of plasma membrane ion channels is usually done using patch clamps and despite recent technological developments, there remain severe technical restraints, which make it very problematic to patch onto intracellular cell membranes when they are present in their native form and physiological environment.

Usually, intracellular channels can be directed to the plasma membrane by overexpressing them in cells, but due to the presence of specific cellular localization signals, they are often transported back to the intracellular membranes[55]. Engineered protein sequences can also be used to assist the targeting of these ion channels to the plasma membrane, but this approach has its own physiological limitations[55]. Hence, advantages can be gained by studying intracellular channels when reconstituted in artificial lipid bilayers.

6.1.1 *Chloride Ion Channels*

Chloride ions are the most physiologically abundant and predominantly conducted ion species. Chloride channels are a diverse group of channel proteins that regulate essential cellular processes[208]. They transport chloride ions, though occasionally they have been seen to be less specific and conduct other anions. Chloride channels typically contain between 1 and 12 transmembrane segments[209].

They can be classified into four types: ligand-gated chloride channels such as the gamma-aminobutyric acid receptors (GABAs) and the glycine receptors which are triggered by the binding of a ligand to the extracellular domain of the channel, the cystic fibrosis transmembrane conductance regulators (CFTRs), the voltage-dependent chloride ion channels (CLCs) and the chloride intracellular channels (CLICs)[208,210]. A unique feature of the CLIC proteins is their ability to exist in a

soluble globular form as well as a membrane-bound form. They are thus termed metamorphic proteins.

6.1.2 *Chloride Intracellular Channels (CLICs)*

Chloride intracellular channel proteins (CLICs) are a relatively new class of putative anion channels. The first CLIC protein was isolated in 1987[211], when found bound to indanyloxyacetic acid 94 (IAA 94)- a known chloride blocker. The CLIC family has 6 members in vertebrates (CLIC 1-6), 3 in invertebrates (DmCLIC in *Drosophila melanogaster*, EXC4 and EXL1 in *Caenorhabditis Elegans*) and at least 4 genes in Arabidopsis thaliana[55]. These channels possess distinct properties such as a single transmembrane domain and a metamorphic character as they are found in either a water-soluble globular form or as an integral membrane protein. Almost all the members of the CLIC family share substantial similarity in their sequence (60-75%) varying mainly in their cellular and subcellular allocation[210]. Among all the CLIC channels, CLIC1 channels are the most widely studied due to their ability to form functional ion channels in the absence of any auxiliary protein[212,213], thus making them a good target for synthetic biology studies.

Immunofluorescence investigations of CLIC1 transfected Chinese Hamster Ovary (CHO) cells demonstrated that these proteins mostly localize in the nuclear membrane, lysosomes, endosomes, secretory vesicles as well as the cytoplasm and nucleoplasm[214]. CLIC1 has been associated with Alzheimer's disease (AD), which is characterized by the accumulation of plaques containing β-amyloid (Aβ) protein. It has been shown that Aβ stimulates the translocation of CLIC1 from cytoplasm to the plasma membrane consequently increasing CLIC1 mediated chloride flux[215]. Activation of microglial cells by Aβ has been shown to generate reactive oxygen species (ROS)[216]. Both the increased chloride conductance of the microglial cells and the overproduction of ROS are believed to aid neurodegeneration in AD[217–219]. Inhibition of CLIC1 channels has been demonstrated to decrease chloride flux and decrease the production of ROS[215]. These findings make CLIC1 a prospective novel therapeutic target for AD.

Endogenous CLIC1 channels have also been seen to displace to the plasma membranes during the G2/M phase of cellular mitosis and assisting towards an increased in anion conductivity of cells, thus implying a role of CLIC1 channels in cell cycle regulation[220]. This vast and diverse distribution of CLIC1 in cells suggests roles in a wide range of physiological processes.

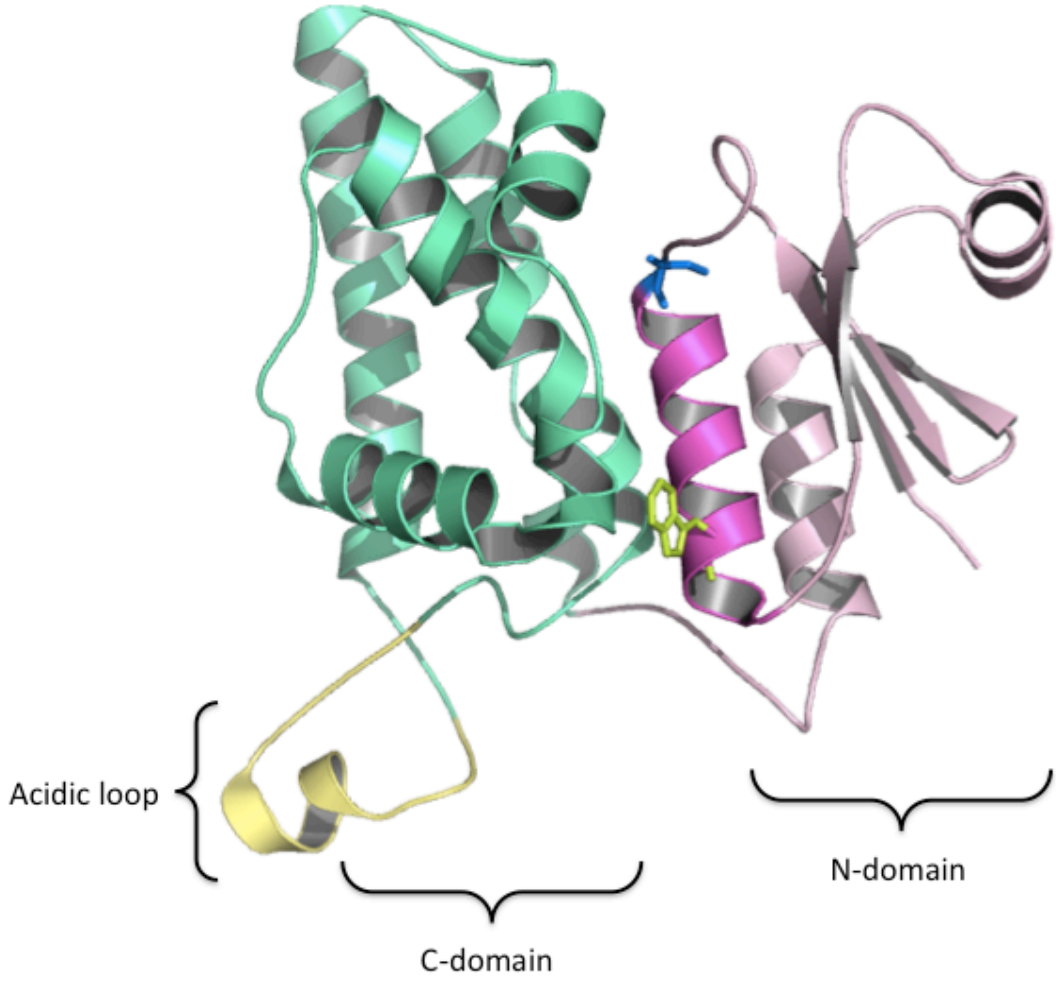

Figure 6.1 CLIC1 crystal structure. Ribbon diagram of the crystal structure of reduced, soluble CLIC1. The N-domain is shown in pink and magenta, and the C-domain in green and yellow. The putative transmembrane region is coloured magenta and the acidic loop is shown in yellow. Selected residues are shown in a line models. The single Trp residue (Trp35) is shown in green and the redox- active CYS (Cys24) in yellow. PDB code 1K0M[221]). Image rendered using PyMOL™ v. 0.99 (DeLano Scientific, 2006).

CLIC1 is a reasonably small protein with a sequence of 241 amino acids (Figure 6.5) and a molecular weight of 27 kDa[222]. The crystal structure of soluble, monomeric CLIC1 was solved at 1.4 Å resolution at pH 5.0[221] (Figure 6.1). The sequence contains one tryptophan residue, Trp35, in the N-terminal domain near the domain boundary,

and eight tyrosine residues, two in the N-domain and six in the C-domain. There are 35 acidic and 27 basic residues in the CLIC1 sequence, giving the protein a net negative charge of -7 at physiological pH. CLIC1 has six cysteine residues, three in each domain. One of these, Cys24, is redox-active, and forms a glutaredoxin-like active site, although CLIC1 has not been shown to exhibit any catalytic activity[221].

To form a functional ion channel, CLIC1 undergoes a conformational transition from its soluble globular state to an integral membrane form that auto-fuses into a phospholipid bilayer[223]. CLIC1 structure comprises of two domains, a mixed α-helix/β-sheet N-terminal domain and a majority α-helix C-terminal domain Figure 6.1.

CLIC1 channels share substantial structural homology with the members of the glutathione S-transferase (GST) superfamily (Figure 6.2). The CLIC family diverges from the conventional GSTs in that they have an active cysteine residue (Cys24 in human CLIC1), which is rendered reactive by the protein itself. The GSTs, instead, activate the thiol group of the glutathione (GSH), which binds non-covalently within their active sites with very high affinity[224]. The location of the GSH thiol in classic GSTs corresponds approximately to the location of the active site cysteine in CLIC proteins. All CLICs have two additional conserved cysteine residues (Cys178 and Cys223 in CLIC1).

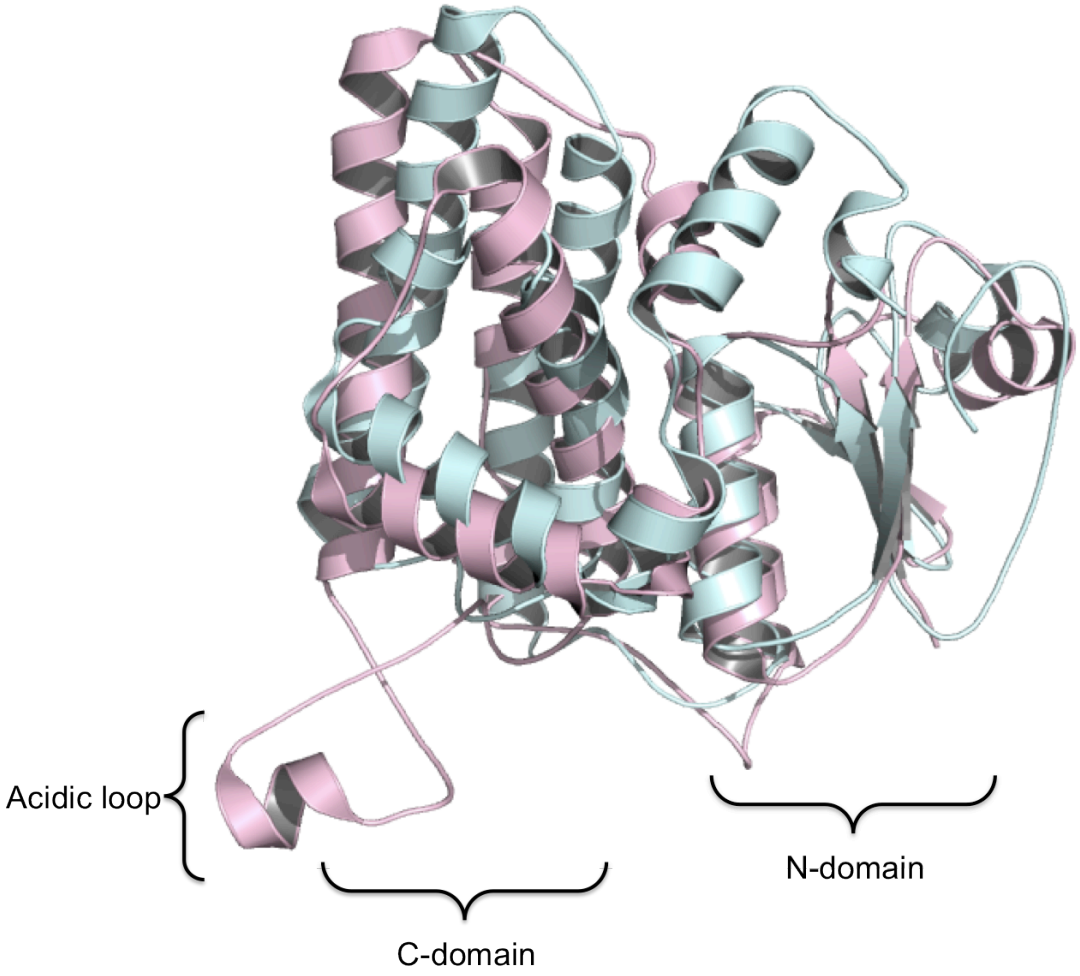

Figure 6.2 Structural alignment of CLIC1 with GST O1-1. CLIC1. CLIC1 (pink) alignment with a monomer of GST O1-1 (blue), with RMSD = 1.65 Å. The structure is remarkably conserved, with the N-domains aligning only slightly less than the C-domains. The major differences are in helix (top right) and in the acidic loop region of CLIC1, which is absent in GST O1-1. The alignment was performed using the MultiProt server (Shatsky et al., 2004) and PDB codes 1K0M[221] and 1EEM[225]. Image rendered using PyMOL™ v. 0.99 (DeLano Scientific, 2006).

Upon oxidation, CLIC1 is able to transform reversibly to an all α-helical non-covalent dimeric conformation during which an intramolecular disulphide bond forms between Cys24 and Cys59, which are usually distant from each other[226] (Figure 6.3.). The C-domain undergoes little change, but the N-domain displays a major structural transition. The four-stranded mixed β-sheet that is a distinguishing feature of the thioredoxin fold is absolutely transformed into helices and loops upon oxidation. The dimer interface is mainly hydrophobic, and could form part of a membrane-docking interface if exposed in vivo. The dimer does not resemble those of the GSTs.

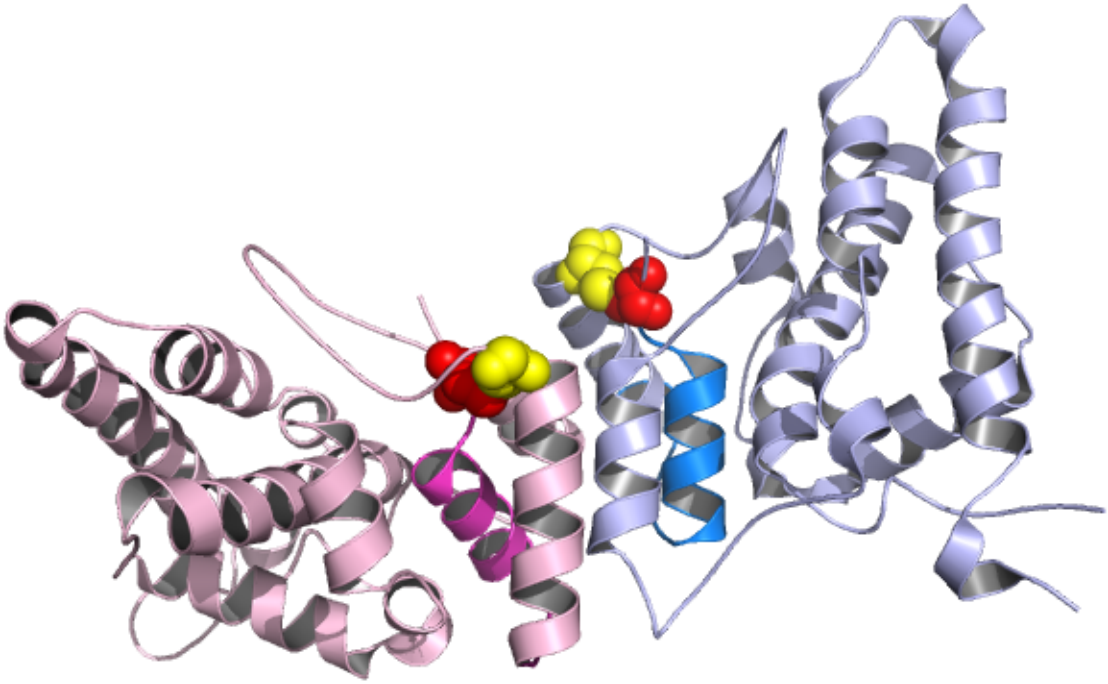

Figure 6.3 Crystal structure of oxidised CLIC1. Oxidised CLIC1 undergoes a major structural transition to form a dimer with intramolecular disulphide bonds between Cys24 (red) and Cys59 (yellow). The transmembrane domains are indicated in magenta and dark blue. The C-domain structure changes very little, while the N-domain transforms completely from a mixed α-helical/β-sheet conformation to an all α-helical conformation. PDB code 1RK4[226] was used. Image was rendered using PyMOL™ v. 0.99 (DeLano Scientific, 2006).

CLIC1 is shown to maintain its functionality as a chloride channel when expressed and purified from *E. coli* bacteria and reconstituted in artificial lipid bilayers[227]. However, the study of biophysical properties of CLIC1 is still in its early years. CLIC1 conducts chloride ions and other halides, pseudohalides and bicarbonates. CLIC1 is reported to be anion-selective though electrophysiology studies have shown fluoride and pseudohalides to be more permeable than chloride ions[228].

CLIC1 has also been described to be a poorly selective or non-selective ion channel in artificial lipid bilayers[212,229]. Figure 6.4 compares the electrical traces of CLIC1 and α-HL, highlighting the poor conductivity of CLIC1 channels to Cl^- ions. In some of these cases, the channel was seen to be permeable to both cations and anions at very similar rates. The ionic permeability can be biased in the presence of a large cation like Tris, where the CLIC channels were found to become more anion-selective[212]. From these observations, it can be theorized that upon incorporation into

artificial bilayers, CLIC channels may have lost an important element necessary for ionic selectivity.

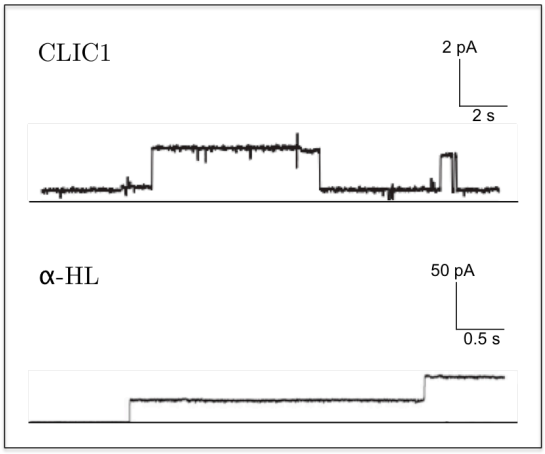

Figure 6.4 Examples of single-channel current recordings for CLIC1 and α-HL. CLIC1 holding potential of + 100 mV under asymmetric ionic conditions (500 mM KCl in the *cis* chamber, 50 mM KCl in the *trans* chamber) and α-haemolysin holding potential + 150 mV, under asymmetric ionic conditions (0.1 mM $CaCl_2$ in the *cis* chamber and no $CaCl_2$ in the *trans* chamber). Figure adapted from Kawano *et al.* 2013 and Singh *et al.* 2007

The exact mechanism of how CLIC1 unfolds, targets and auto-inserts into the bilayer from a soluble cytosolic protein to an integral membrane channel is still unknown. All hypothetical models agree that a dramatic structural rearrangement of the N-domain would be required for the transformation to occur.

6.1.3 *CLIC1 Transmembrane Domain*

It has been proposed that CLIC proteins may use a similar mechanism for membrane insertion to alpha pore forming toxins such as α-haemolysin[213]. These fusogenic toxins unfold to reveal a long hydrophobic helical loop that directs the proteins into the membrane forming the transmembrane helix due to a change in pH[210]. The CLIC proteins host a similar helical structure (highlighted in magenta Figure 6.1 and Figure 6.3) in their N-domain. This region has significant hydrophobicity having the potential to insert itself into the membrane.

Analysis of the CLIC1 amino acid sequence (Figure 6.5) indicates that residues 21 to 46 in the N-domain of CLIC1 are most likely to form the transmembrane domain (TMD), with the rest of the N-terminal locating to the exterior of the membrane.

This includes residues Cys24-Val46 in CLIC1[230], a region that is highly conserved in the CLIC proteins, is long enough to span the membrane (31 Å) and does not contain acidic residues, an essential feature for an anion channel.

Studies on the transmembrane domain (TMD) show that this region is essential for both membrane localisation and ion channel function. By deleting the first 66 amino acids of the N-terminal sequence in the TMD of the *Caernorhabditis elegans*, CLIC protein, EXC-4 Berry *et al.*, 2003[230] demonstrated that this sequence is essential for protein localization at the membrane. The deletion of the second beta-strand resulted in incomplete membrane insertion and a strong cytosolic partition. Likewise, disruption of the transmembrane helix by substituting one of the conserved amino acids to proline interrupted membrane localisation completely. Conversely, the addition of extra helical structures to the N-terminal of the protein did not disrupt membrane localization or insertion. It is evident that the N-terminal sequence is fundamental to membrane insertion and function and that its conserved secondary structure is necessary and sufficient for membrane insertion.

MAEEQPQVELFVKAGSDGAKIGNCPFSQRLFMVLWLKGVTFNVTTVDTKRRTE
TVQKLCPGGQLPFLLYGTEVHTDTNKIEEFLEAVLCPPRYPKLAALNPESNTAGLD
IFAKFSAYIKNSNPALNDNLEKGLLKALKVLDNYLTSPLPEEVDETSAEDEGVSQR
KFLDGNELTLADCNLLPKLHIVQVVCKKYRGFTIPEAFRGVHRYLSNAYAREEFAS
TCPDDEEIELAYEQVAKALK

XX – Required for membrane protein integration
XX – Potential Helical transmembrane domain
XX – Disulfide bond formation (Cys24 and Cys59)
XX – GST C-terminal domain
XX – Glutathione binding sites
XX – Cysteine Sites
XX – Tryptophan Residue

Figure 6.5 Human CLIC1 amino acid sequence. The putative transmembrane region is shown in yellow. The sequence within this 23-residue region is practically invariant within the CLIC family.

Duncan *et al.,* 1997 demonstrated that to form the transmembrane structure, the N-domain must separate from the C-domain of soluble CLIC1, extend and refold to reveal the hydrophobic residues and allow protein-lipid interactions as it enters the lipid bilayer. pH is thought to be a vital part in this conformational change, due to evidence that channel formation and activity increased with a change from neutral to a more acidic pH[176,213,214]. At low pH values the N-domain become less stable and more flexible, allowing the structural changes necessary for membrane insertion[231]. The TMD is thought to be destabilised as it enters a lower pH environment nearing the membrane, subsequently extending and refolding into a helical structure that can insert into the membrane[231]. Dimer formation is thought to be a necessary membrane intermediate where the N-domain undergoes a transition into an all-helical structure (Figure 6.3) upon disulphide bond formation. A low pH is thought to have a similar effect to the overall structure of the protein and both elements have been postulated as a vital aspect of the transition from soluble into membrane-bound CLIC1[55].

A fundamental step to understanding CLIC1's metamorphic existence is to have a greater understanding of its membrane-bound state. Here we propose the use of an artificial membrane system with multiplexing potential where CLIC1 insertion and function can be studied. In addition to conventional *in vitro* studies to characterize CLIC1 insertion, this project aimed to illustrate the insertion of CLIC1 into DIBs using the platform described in Chapter 4. Moreover, a fluorescence-based functional assay similar to that described in Chapter 5 is suggested, which could permit a quick quantitation of the relative levels of activity of CLIC1 under different conditions.

In this chapter, we aim to identify the best conditions to promote CLIC1 insertion into a lipid bilayer membrane and to characterize the channel in terms of its secondary and tertiary structure. We studied CLIC1 at redox conditions and various pH values in order to identify if these environments had an effect on the structure and stability of CLIC1. Moreover, experiments were conducted to determine TMD amino acids environment, in order the elucidate CLIC1's membrane bound

structure. Finally, we aim to study the ability of DIBs to host CLIC1, a pharmacologically relevant protein, thus demonstrating proof of concept for a novel platform to study membrane insertion, function and potential drug targets.

6.2 Overexpression and Purification of Chloride Intracellular Ion channel-1 (CLIC1)

To study CLIC1 it is first necessary to obtain milligram quantities of pure, monodisperse and stable protein. Mild non-ionic detergents (e.g. DDM) are often used to remove proteins from biological membranes as they are not sufficiently harsh to strip away all of the native-lipids (some of which are essential for protein function)[232]. pET28a–hCLIC1 plasmid, containing an N-terminus hexa-HIS tag, was transformed into C41 (DE3) cells and selected for kanamycin resistance as described in Chapter 3. Overexpression of CLIC1 was induced by the addition of IPTG followed by 2 hours incubation. Cells were lysed and fractions were separated by centrifugation. Figure 6.6 shows the centrifugal fractionation of the lysed cells on a 4-12 % acrylamide SDS-PAGE both as a coomasie stain and as a western blot. A band corresponding to CLIC1, a 27 kDa protein, is indicated by the arrow. It can be noticed that CLIC1 was mostly located in the cytosolic fraction instead of the membrane fraction.

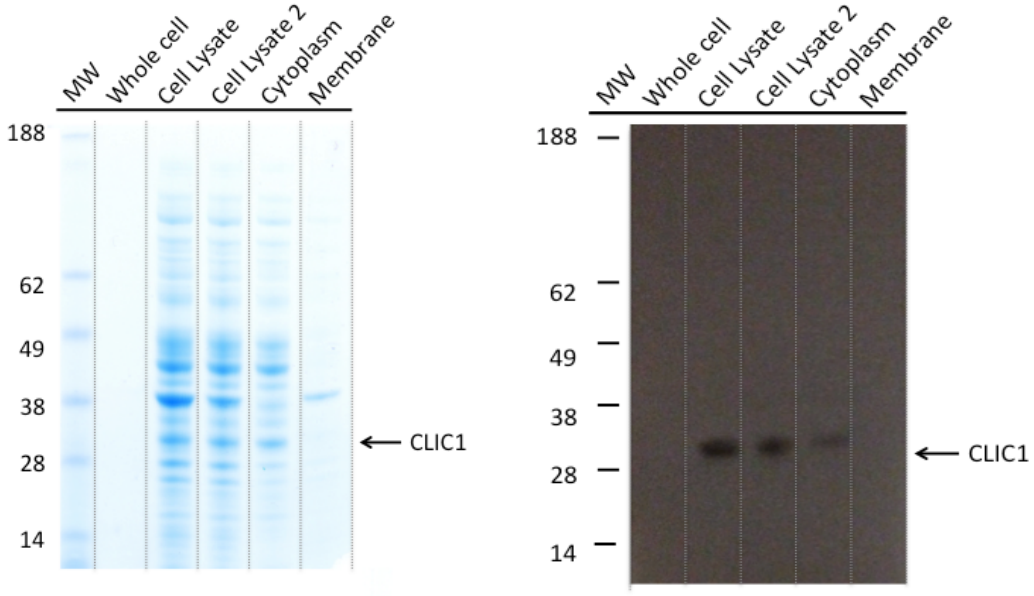

Figure 6.6 SDS-PAGE analysis of CLIC1 overexpression. Bacterial extracts of IPTG induced cultures were run on 4-12% SDS-PAGE and stained with Coomassie blue (left). Arrows indicate the induced CLIC1. Immunoblot analysis of induced bacterial lysates expressing CLIC1 (right). The gel was transferred to a membrane, and probed with an anti-CLIC1 antibody. The molecular weight (MW) of standard proteins is indicated on the left in kilodaltons (kDa).

Although CLIC1 is a 27 kDA protein it shows up as a 30 kDa band because it travels anomalously slowly. This appears to be a general characteristic of CLIC family proteins, and others have found the same to be true[213,227,233]. It is most likely that the acidic nature of CLIC1 interferes with SDS binding, lowering the mass:charge ratio thus leading to lower than expected mobility[234,235]. CLIC1 has 35 negatively charged residues, an overall charge of -7.5 at pH 7.0 and a pI near 5.17, so this is the most likely explanation.

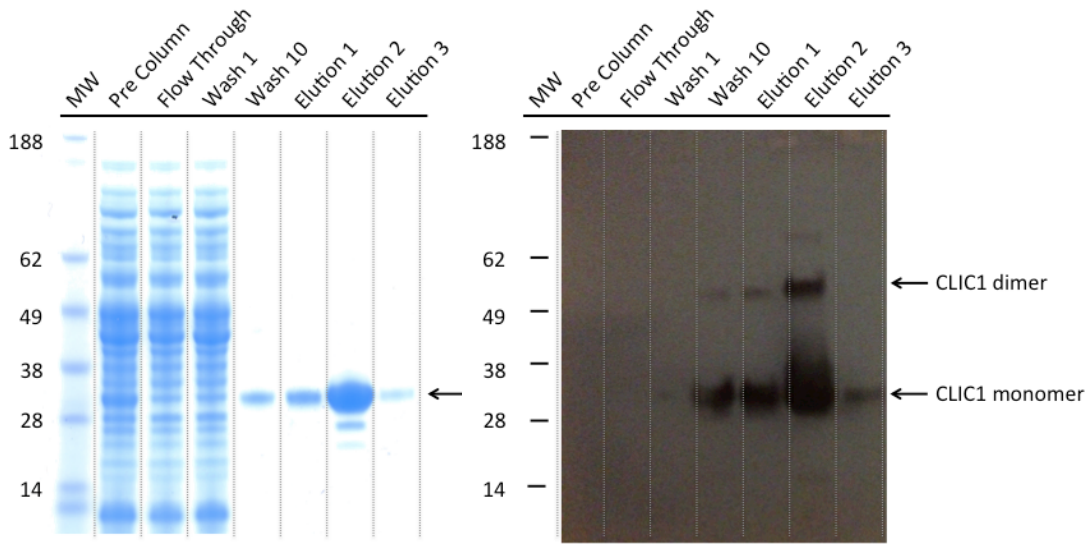

Figure 6.7 SDS-PAGE analysis of CLIC1 purification. CLIC1 extracts were purified using a Nickel affinity column. The recombinant CLIC1 contains a N-terminus 6xHis tag, which binds to Ni^{2+}. Following 10 washes with a 40 mM Tris, 300 mM NaCl, 1mM DTT, 20 mM imidazole buffer at pH 8.0, the protein was released from the column by increasing the concentration of imidazole in the buffer to 400 mM. The second eluted fraction (Elution 2) was collected, dialyzed against 150 mM NaCl buffer and used in the subsequent assays. The purification steps were run on 4-12% SDS-PAGE and stained with Coomassie blue (left). Arrows indicate CLIC1. The band that migrates faster than CLIC1 in the Coomassie stain presumably represents a bacterially derived degradation product of CLIC1. (Right) Immunoblot analysis of the purification procedure: samples were resolved by 4-12% SDS-PAGE, transferred to nitrocellulose membranes, and probed with an anti-CLIC1 antibody. Note that there are additional bands that migrate slower than the CLIC1 monomer these are assigned to CLIC1 oligomers, i.e. dimers and tetramers indicated by the arrow. The molecular weight (MW) of standard proteins is indicated on the left in kilodaltons (kDa). This procedure was done several times, as more protein was required.

The cytosolic fraction containing the soluble protein was removed and purified through a Nickel affinity column. After the protein bound to the column, it was washed with buffer containing 40 mM immidazole (to remove contaminant His-rich proteins) and 500 mM NaCl (to remove those proteins that had bound to the column by ionic interactions). The protein was eluted from the column using a 400 mM imidazole buffer and the fractions analysed by SDS-PAGE both in a coomasie stain and a western blot (Figure 6.7). The elution fractions were very pure following the Ni^{2+} column, and elution 2 was collected, dialyzed against a 150 mM NaCl buffer and used in further assays as it contained a higher concentration of the protein. Concentrations of the protein ranged from 2-3 mg/ml. From the western blot, it can

be seen that CLIC1 can form higher order oligomers. Monomers, dimers and tetramers are clearly visible from Figure 6.7.

All procedures were optimized to allow the highest protein yield and highest protein purity. Key parameters were optimized in small-scale trials. For example, the protein was allowed extra binding time (10 min) to bind to the Ni^{2+} column by reducing the flow rate during the loading. Optimal concentration of imidazole during binding, washing and elution steps were also determined during pre-trial experiments with a fixed aliquot of resin.

6.3 Fluorescence Size Exclusion Chromatography

Fluorescence size exclusion chromatography (FSEC) was used in order to further investigate the molecular weight of CLIC1 and its oligomers. This method should be a more accurate way to determine a protein's molecular weight as it is not influenced by charge.

The soluble monomeric GST-like CLIC fold consists of two domains: a thioredoxin-like N-domain containing a glutathione binding site and an all-α-helical C-domain (Figure 6.1). The presence of the conserved glutathione binding site in the CLIC soluble monomer form led to the suggestion that chloride ion channel activity of the CLICs may be under the control of redox-active signalling molecules in vivo[221].

Under reducing conditions i.e. in the presence of DTT, CLIC1 is forced into its monomeric state, while it oxidizes to form a dimer in presence of an oxidizing agent like H_2O_2[226]. We verified that fact by running the oxidized and reduced protein on a size exclusion chromatography column. 100 µl of elution 2 was analysed at a minimum concentration of 1 mg/ml and peaks analysed at A280 nm via the AKTA Prime Plus System.

In Figure 6.8, it can be seen that under reducing conditions, the protein sample is predominantly in its monomeric form (molecular weight ~27 kDa). Adding an

oxidizing agent to the solution induces the formation of higher order oligomers, dimers and tetramers.

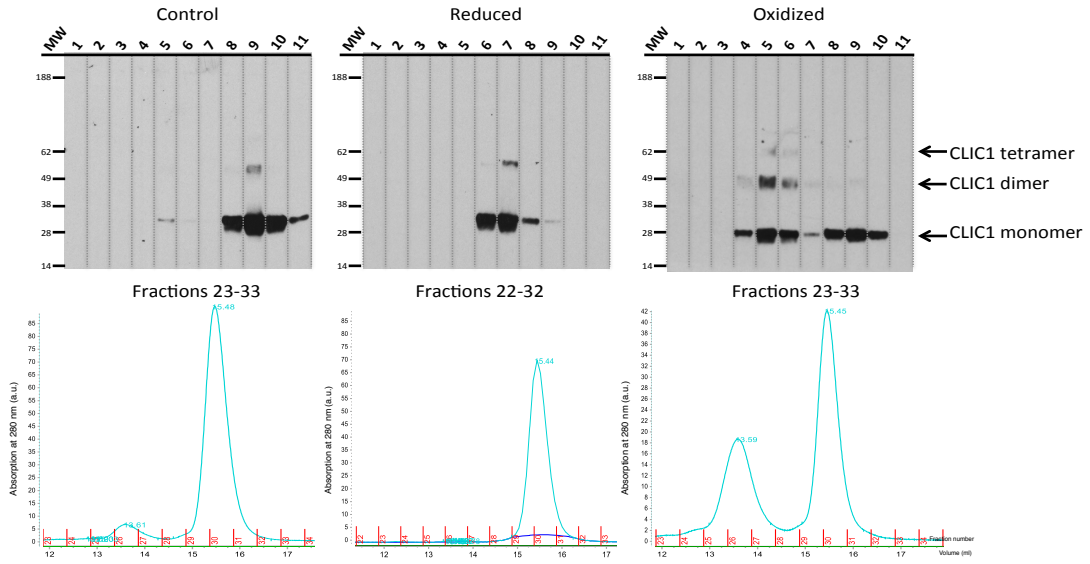

Figure 6.8 FSEC analysis of CLIC1 under reducing and oxidizing conditions. The molecular weight values are pre-calibrated using standard protein samples. (Control) CLIC1 is stored in buffer containing 150 mM NaCl, 40 mM Tris-base (pH 8.0). Two peaks are observed a large peak corresponding to a molecular mass of ~27 kDa, and a smaller peak corresponding to ~54 kDa. Under neutral conditions CLIC exists in both its monomeric and its dimeric forms, however the monomeric form is more abundant. (Reduced) CLIC1 is stored in reducing buffer conditions containing 150 mM NaCl, 40 mM Tris-base and 2 mM DTT (pH 8.0). The FSEC peak corresponds to a molecular mass of ~27 kDa. CLIC1 exists primarily in its monomeric form under reducing conditions. (Oxidized) CLIC1 is stored in an oxidizing buffer containing 150 mM NaCl, 40 mM Tris-base and 2 mM H_2O_2 (pH 8.0). Two peaks are seen at ~27 kDa and ~54 kDa. The peaks correspond to monomeric and dimeric CLIC1. Oxidizing conditions seem to increase dimer formation.

6.4 Channel Incorporation in Liposomes

It has been hypothesized that oxidation is essential for the transition of CLIC1 from the monomer to the integral membrane chloride channel form[226]. The physiological relevance of the oxidized dimeric state of CLIC1 is unclear, particularly since this state has only been observed for CLIC1. The non-covalent dimer interface is formed by residues from the N-domain and it comprises a flat, hydrophobic surface. It has been proposed that in vivo, such a surface would insert into a lipid bilayer rather than form a protein dimer, thus, the half dimer structure may represent the membrane docking form of CLIC1[226]. If the half-dimer structure represents the membrane

docking form, an additional structural change is required to integrate the transmembrane domain into the membrane. This is likely to be followed by oligomerisation to form the active ion channel.

To study which conditions promote CLIC1 insertion into the membrane bilayer, liposomes were formed with in a 10:1 phosphatidylcholine to cholesterol (w/w) ratio and extruded through a 100 nm membrane to ensure uniformity (Figure 6.9). The liposomes were then incubated with CLIC1 at a ratio of 200:1, protein to liposome (v/v) and incubated at 4 ^{o}C overnight. CLIC1 is unusual in its ability to auto-insert into lipid bilayers, but how precisely the soluble conformation transits into the membranous form is not known. A phase change from soluble structure to unfolding, insertion, and refolding is a complex process.

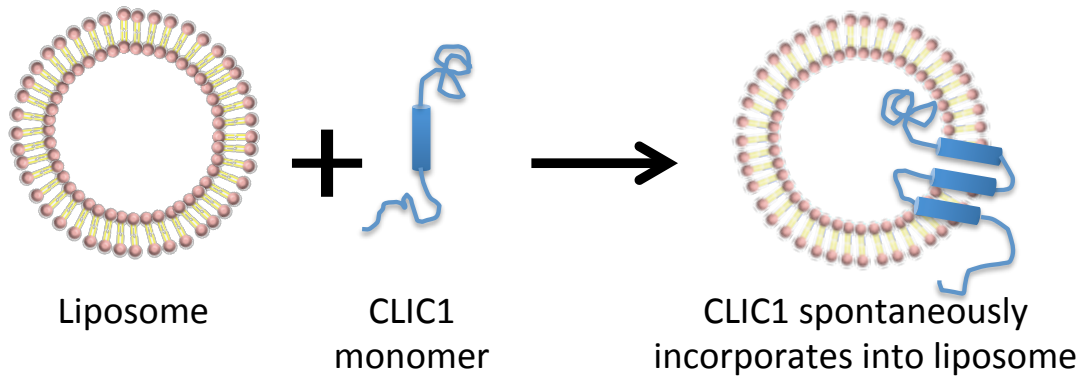

Figure 6.9 Schematic representation of CLIC1 insertion into liposomes. CLIC1 was incubated overnight with liposomes. Due to its self-inserting properties CLIC1 is seen to incorporate into liposomes upon incubation or associate to the surface.

6.4.1 *Effect of redox reactions on membrane insertion*

A feature of CLIC1 is that it possesses a glutaredoxin-like active site, suggesting that its conformational transitions (from soluble to integral membrane protein) and function may be under redox control[221]. The propensity for CLIC1 to undergo this structural rearrangement in the absence of the lipid bilayer suggests that oxidation, disulphide bond formation and formation of the non-covalent dimer may play a role

in membrane insertion and formation of the CLIC ion channel. To investigate this, we have examined the role of oxidation of the CLIC1 monomer in the presence of membranes to determine if oxidation plays a significant role in the process of membrane insertion. This was compared to results for the protein under reducing conditions and in a control buffer in the presence of the membranes.

Purified CLIC1 was incubated overnight at 4 ºC in the presence of either 2 mM hydrogen peroxide (H_2O_2), 2 mM dithiothreitol (DTT) or neither, as a control, then analysed by SDS-PAGE and western blotting. To verify that soluble CLIC1 did not migrate alongside the liposomes, the liposomes were purified by centrifugation at 18,000 x g for 10 min at 4 ºC, the supernatant was separated and pelleted liposomes were resuspended in the appropriate buffer. Three fractions were collected, a mixed fraction pre-centrifugation, a supernatant fraction, which did not contain liposomes, and a pelleted liposome fraction. Figure 6.10 shows that under oxidizing conditions CLIC1 inserts into liposomes more readily and forms larger concentrations of dimers (seen in the oxidised, mixed and supernatant fractions). The liposome fraction shows very few dimers, and a higher concentration of higher order oligomers. The reduced samples show very few proteins in the liposome fraction. This suggests that dimerization aids CLIC1 insertion into lipid bilayers and oxidation promotes multimer formation in the membrane.

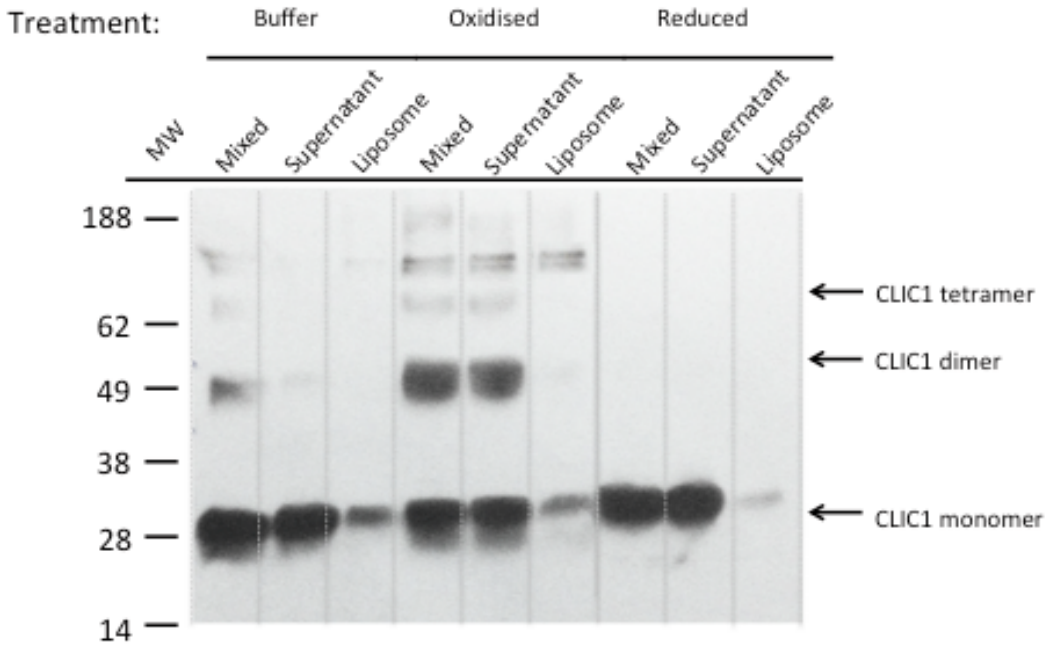

Figure 6.10 Study on the effect of oxidisation on CLIC1 membrane insertion efficiency. CLIC1 was incubated overnight with liposomes in 3 different conditions: lane 1-3 shows untreated CLIC1 in a 40 mM TRIS, 150 mM NaCl buffer, lanes 4-6 shows CLIC1 treated with added 2 mM H_2O_2 and lanes 7-9 shows reduced CLIC1, treated with added 2 mM DTT. It can be seen (on lane 6) that under oxidising conditions higher order oligomers are associated with the liposomal fraction or associated to the surface.

6.4.2 *Effect of pH on membrane insertion*

To determine the effect of low pH on CLIC1 association with lipid bilayers, CLIC1 was combined with liposomes, and the pH of the mixture was adjusted to pH 8.0, pH 7.0 or pH 6.0. The mixture was incubated overnight at 4 ^{o}C in an oxidising buffer, containing 2 mM H_2O_2. To verify that soluble CLIC1 did not migrate alongside the liposomes, the liposomes were purified by centrifugation at 18,000 x g for 10 min at 4 ^{o}C, the supernatant was separated, and pelleted liposomes were resuspended in the appropriate buffer. Three fractions were collected, a mixed fraction pre-centrifugation, a supernatant fraction, which did not contain liposomes, and a purified liposome fraction, all three were analysed by SDS-PAGE and Western blotting shown in Figure 6.11.

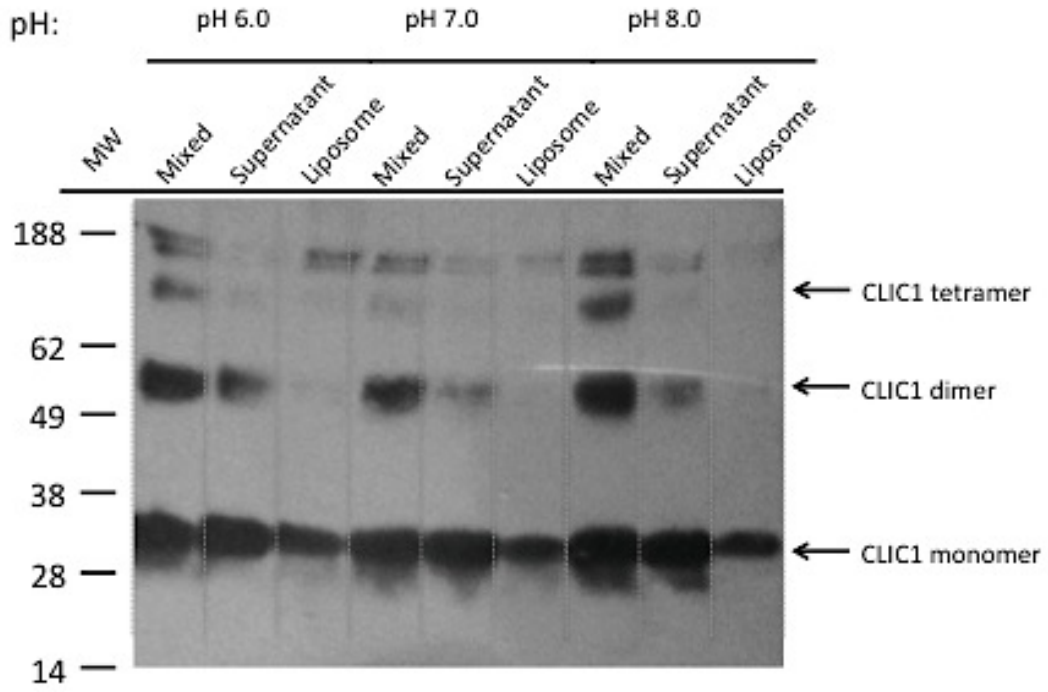

Figure 6.11 Effect of pH on CLIC1 insertion efficiency under oxidizing conditions. CLIC1 was incubated overnight with liposomes in a buffer containing a 40 mM TRIS, 150 mM NaCl and 2 mM H_2O_2 at 3 different pHs 6.0, 7.0, 8.0. Lane 1-3 shows CLIC1 at pH6.0, lanes 4-6 show CLIC1 at pH 7.0 and lanes 7-9 shows CLIC1 at pH 8.0. It can be seen (on lane 6) that at pH 6.0 CLIC1 forms higher order oligomers within the liposomal fractions.

For every pH tested, the liposome fractions show a high concentration of CLIC1 monomer, indicating that the soluble protein does associate with artificial lipid bilayers as determined biochemically. The supernatant fraction contains CLIC1, which had not associated with the liposomes and remained in a soluble state. At pH 6.0 the liposome associated CLIC1 tends to form higher order oligomers, which indicates the formation of a functional channel. A high concentration of CLIC1 monomers is seen in all the fractions, this is due to the denaturing nature of SDS, which dissociates multimers.

6.4.3 *Fluorometric studies to determine the environment of residue TRP35*

The tertiary structure of a protein can be characterised by fluorescence spectroscopy because of the presence of the intrinsic aromatic fluorophores, such as Tyr and Trp in just about every protein molecule. Fluorescence spectroscopy gives information

about the packing and local environment of aromatic residues[178], although protein fluorescence spectra are generally dominated by tryptophan emission.

Fluorescence emission intensity and wavelength for tryptophan changes according to the polarity of the environment within which the residue is found, and the degree of quenching experienced by the fluorophore as a result of that environment[178]. Tryptophan can be selectively excited at 295 nm and the greater the exposure of Trp to the polar aqueous environment, the longer its wavelength of maximum emission will be, since the polar solvent molecules lower the energy of the excited state. CLIC1 has only one Trp residue, Trp35, which is present in the putative transmembrane region in the N-terminal domain, acting as a local reporter for that region (Figure 6.1).

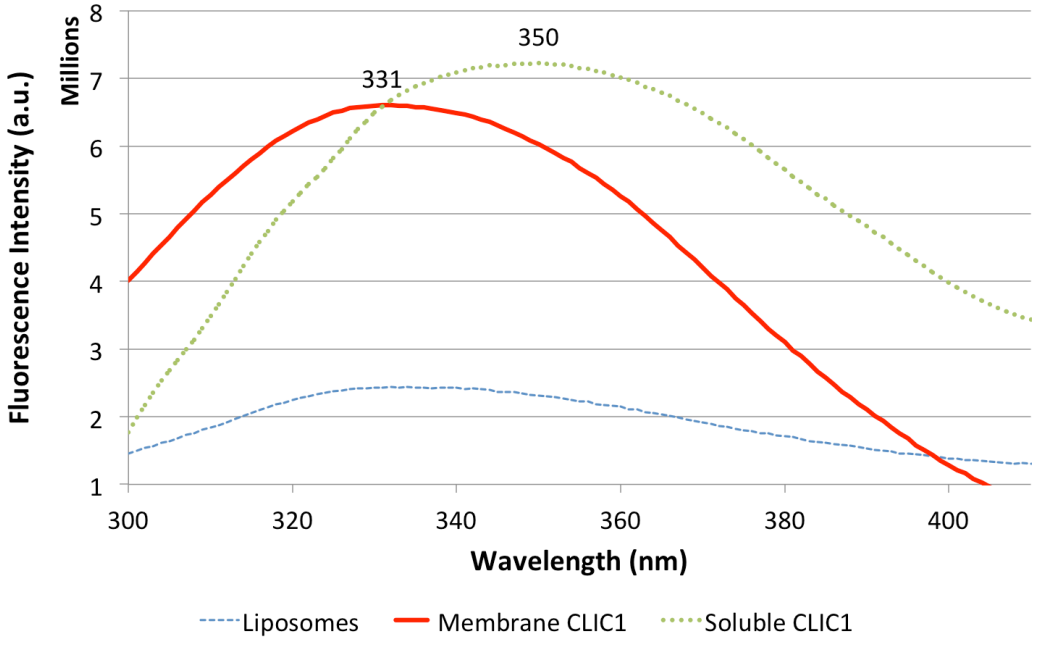

Figure 6.12 Fluorescence emission spectra of soluble and membrane bound CLIC1. Fluorescence emission spectra of 2 µM CLIC1 in 40 mM TRIS, 150 mM NaCl, 2 mM H_2O_2 at pH 6.0 at 20 °C. Membrane bound (solid red) and soluble CLIC1 (green dots) were excited at 295 nm to investigate the environment of Trp35. As a control, the same was done to liposomes only, in the same buffer (blue dashes). Peak values are shown above the curves. A shift, from 331 nm to 350 nm, is observed when CLIC1 is in its soluble state, which is indicative that Trp35 is more exposed to the aqueous environment. Trp35 seem to be less exposed when CLIC1 is incorporated into liposomes.

Figure 6.12 shows the emission spectra of soluble CLIC1 and compared to its membrane bound form. The wavelength of maximum emission (λ_{max}) for excitation at 295 nm is red-shifted when CLIC1 is in its soluble state ($\lambda_{max} = 350$ nm) compared to membrane bound CLIC1 ($\lambda_{max} = 331$ nm), this is a large change and consistent across multiple data sets. The maximum emission wavelength of 331 nm is indicative of a buried Trp. The red shift to 350 nm indicates increased exposure of Trp35 to the polar solvent. Although, the presence of Trp (and often Tyr) residues at the interfacial region, is frequently observed for of transmembrane helices, where they act as protein 'stabilizers'[236], evidence from the literature[176,223] also suggests that Trp35 might be buried within the bilayer, a somewhat unexpected location. These studies were performed using a quencher, acrylamide, which diminished Trp fluorescence at different rates depending on the level of exposure of the residue. When CLIC1 is incorporated into the bilayer quenching of Trp fluorescence was seen to be slower than that of soluble CLIC1. The decrease on the quenching rate is believed to be due to the shielding of the Trp residue into the lipid bilayer, however, a quenching delay would also be observed if Trp residue was exposed to the aqueous environment in a trans position across the lipid bilayer due to the delay in the permeation of acrylamide across the membrane, though that is unlikely due the large conformational change required as the transmembrane helix would have to bend to solely expose the Trp residue.

6.4.4 *Pegylation studies to determine the environment of cysteine residues*

To further study the membrane bound CLIC1 into the bilayer and gain knowledge of how it inserts into the membrane a pegylation assay was devised.

This assay employs methoxy-polyethylene glycol maleimide (PEG-MAL), which has a molecular weight of 5 kDa and binds covalently to the thiol groups of cysteine residues, resulting in an increase in the apparent molecular weight of the protein when resolved on an SDS gel. When the protein is incorporated within liposomes, the exposed cysteine residues on the extramembrane region of the protein

are mass-tagged with PEG-MAL and detected by gel electrophoresis. PEG-mal is too large a molecule to permeate the lipid bilayer therefore, unless the liposomes are disrupted with a detergent such as Triton, only cysteine residues on the outside of the liposomes will be pegylated.

Thiol-reactive reagents such as the membrane permeable N-ethylmaleimide (NEM) and the membrane impermeable 4-acetamido-4'-maleimidylstilbene-2,2'-disulfonic acid (AMS) were systematically used as blockers, preventing the binding of PEG-MAL to cysteine residues. CLIC1 only contains 6 cysteine residues, 3 of which are within the TMD region, therefore this assay helps in ascertaining the orientation of the protein by showing where the cysteine residues are located. If the TMD region is fully extended, thus hosting Trp35 within the bilayer, it is likely that Cys24 could be exposed on the inside of the bilayer.

No shift is seen when samples were treated with NEM as it is membrane permeable, and consequently prevents the binding of PAG-MAL by blocking every cysteine residue within the protein, whether on inside or outside the liposome (Figure 6.13 lanes 2,6,7). AMS is a 0.5 kDa molecule, therefore when bound to cysteine residues a minimal shift is evident. This has been observed on the monomer's apparent mass where a small shift is seen in every lane in which AMS has been used (Figure 6.13 lanes 3,5,8). On lane 3 a significant 5 kDa shift is seen when the liposomes are disrupted, since AMS blocked all the external cysteines, this suggests that once CLIC1 inserts, one cysteine residue protrudes across the bilayer to be exposed on the interior of the liposomes. This finding confirms the suggestion from the tryptophan fluorescence experiments in Figure 6.12, where Trp35 was seen to be less exposed when inserted into the bilayer. It is likely that the cysteine causing the shift is Cys24, which is found at the beginning of the TMD. If this is the case, the C-domain locates to the exterior of the liposomes while the N-terminal is inserted into the membrane with Cys-24 piercing through and being fully exposed on the interior of the liposomes. Cys24 is thought to have a function in the redox regulation of dimer formation and if

found outside the bilayer once inserted it could play a role in redox regulation of channel function.

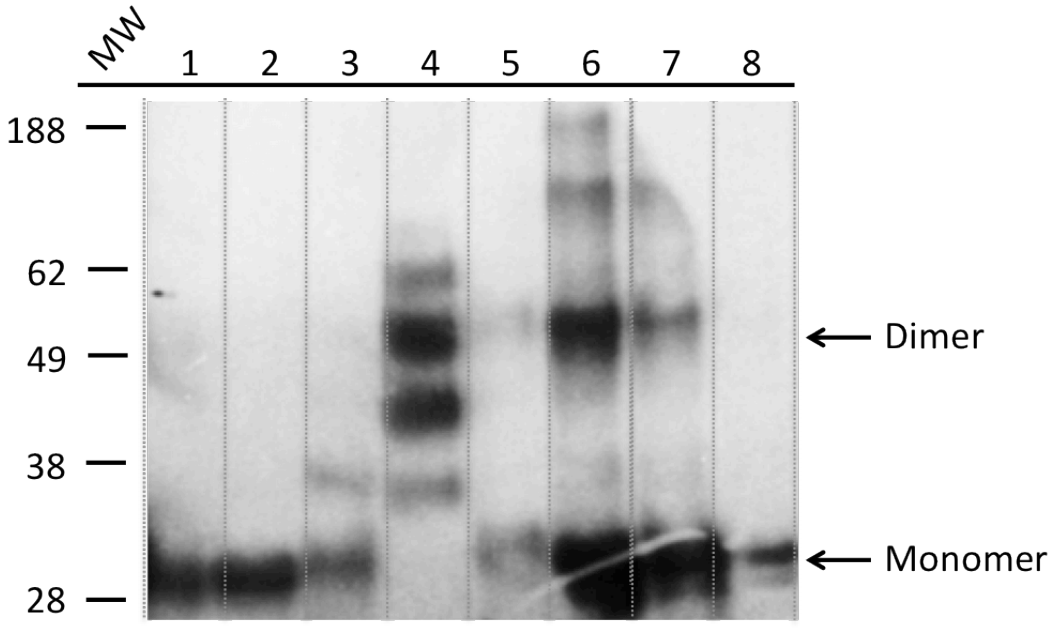

	1	2	3	4	5	6	7	8
NEM	–	+	–	–	–	+	+	–
AMS	–	–	+	–	+	–	–	+
PEG	–	+	+	+	–	–	+	+
Triton	–	+	+	+	–	–	–	–

Figure 6.13 Pegylation of cysteine residues in CLIC1 when incorporated into liposomes. After incorporation into liposomes CLIC1 was treated either with 1 mM NEM (membrane permeable) or 1 mM AMS (membrane impermeable) for 30 min at room temperature. Following incubation, liposomes were pelleted and washed to remove the cysteine blockers. Liposomes were either left intact or disrupted by adding 10% Triton and incubated for 1 hour with 1 mM PEG-MAL. The table below shows how each of the lanes were treated. Binding of PEG-MAL to a free cysteine residue is indicated by a mass shift of 5 kDa compared to unpegylated product. A single shift is observed on lane 3 when CLIC1 is treated with AMS and the liposomes are disrupted. This indicated the presence of a single cysteine residue inside the liposome.

An additional control was performed to determine the degree of cysteine pegylation achieved in the absence of blockers (Figure 6.13 lane 4). A total of 6 cysteine residues seem to have been bound by PEG-MAL, the highest shifted band was just below 60 kDa which constitutes a shift of ~ 30 kDa. This shows that all cysteine residues within CLIC1 should be reachable following liposome disruption with Triton.

6.5 CLIC1 Functional Studies

The final aim of this chapter is to study CLIC1 incorporation within DIBS and protein function. All functional work on CLIC1 to date has been done using electrophysiology[221,222,226,228]. This type of electrophysiology requires much investment in highly specialised equipment and some technical skill. The droplet microfluidics device described in Chapter 4 allows the development of a fluorescence-based functional assay that could be performed relatively easily and could be used to compare CLIC1 and CLIC1 mutant-mediated chloride flux into liposomes. The aim of the assay would be simply to indicate that CLIC1 was actually inserted into the membrane and was functioning also allowing the quantification of chloride conductance across the membrane.

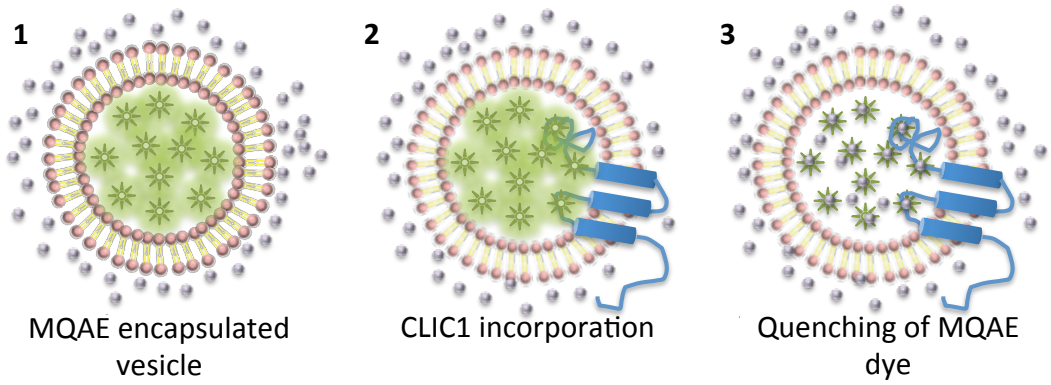

Figure 6.14 Schematic representation of MQAE quenching due to chloride ion transport through CLIC1 channels in liposomes. 1. MQAE dye (green stars) was encapsulated into vesicles and incubated in a solution containing chloride ions (white spheres) and CLIC1 monomers. 2 & 3 CLIC1 incorporation validated by the quenching of MQAE fluorescence due to binding of chloride ions transported through CLIC1 channels.

The work described in Chapter 5 lays the foundation for such an assay. For the functional study of CLIC1 a halide-sensitive fluorescent dye, N-(ethoxycarbonylmethyl)-6-methoxyquinolinium bromide (MQAE), was encapsulated inside PC:chol droplets and lipid vesicles. The fluorescent dye, MQAE, (λ_{ex} 350 nm; λ_{em} 460-470 nm) is quenched upon binding of chloride ions as the quenching rate is a reference to ion permeation rate, the efficiency of the channel can be established. If the channel protein is inserted into the membrane and transports chloride ions across

the bilayer, the MQAE signal should be quenched. If not, the signal will remain the same and it can be assumed that the protein is not operational (Figure 6.14).

6.5.1 Functional studies within liposomes

MQAE was encapsulated into liposomes by resuspending the vacuum-dried lipid mixture in buffer containing 250 µM MQAE and extruded to produce uniform liposomes as described in Chapter 3. Extra vesicular MQAE was removed by size-exclusion chromatography as described in Chapter 3.3.5. Each elution fraction was then tested for the presence of liposomes by exciting fractions at 350 nm. Fractions containing MQAE encapsulated liposomes where resuspended in a NaOH buffer pH 6.0 and incubated with CLIC1 at a 1 mg/ml concentration. Following the incubation, the samples were analysed by fluorescence spectroscopy to study the channel's activity as a function of the rate of MQAE fluorescence quenching.

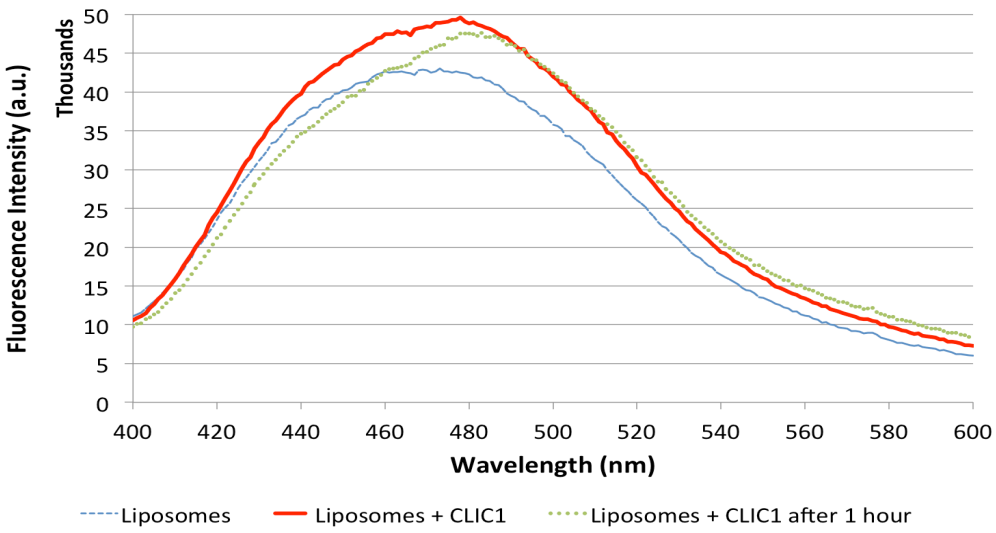

Figure 6.15 Fluorescence emission spectra showing decrease in MQAE fluorescence due to CLIC1 ion conductance. Liposomes containing 250 µM MQAE, 40 mM TRIS and 500 mM NaOH at pH 6 in 40 mM TRIS, 150 mM NaCl, 2 mM H_2O_2 buffer, pH 6.0 at 20 °C were excited at 350 nm, 1 mg/ml CLIC1 was added to the liposomes and the fluorescence recorded at 0 min (solid red) and 60 min (dotted green) to show that CLIC1 can insert into the bilayers and mediate the transport of chloride ions indicted by fluorescence quenching over time. As a control, the same was done to liposomes containing MQAE only, in the same buffer (blue dashes). A decrease in fluorescence is seen after the protein is incubated with liposomes for 1 hour, showing that CLIC1 is able to form functional channels within model membranes.

The fluorescence spectroscopy data (Figure 6.15) shows a slight decrease in fluorescence intensity after liposomes were incubated with CLIC1 for one hour. This suggests that the protein is able to insert into the bilayer and function. Although the decrease in fluorescence is small, previous studies have also shown that experiments involving Cl^- permeation through CLIC1 incorporated into small unilamellar liposomes[213,226] have been difficult to construe where ion permeation was exceptionally prolonged, suggesting that very few liposomes contained functional channels.

CLIC1 Functional studies within DIBs

Finally, we have studied the ability of DIBs to host CLIC1 within the droplet microfluidic platform described on Chapter 4. The *in vitro* experiments described in this chapter aided the characterization of the conditions necessary to obtain insertion of a functional channel protein into DIBs.

Phospholipid stabilised W/O droplets were arrayed in an alternating configuration as shown in Chapter 5 for the α-haemolysin experiments, with one droplet encapsulating CLIC1 in a 40 mM TRIS, 150 mM NaCl, 2 mM H_2O_2 buffer at pH 6.0 and its neighbouring droplet containing a 250 µM MQAE, 40 mM TRIS and 500 mM NaOH at pH 6 buffer. The buffers used were osmotically balanced to prevent droplet shrinking. The permeation of chloride ions was monitored immediately after droplet arraying and DIB formation. CLIC1 should spontaneously insert into the bilayer, forming a functional ion channel thus allowing the permeation of chloride ions, detected by quenching of MQAE fluorescence.

A slight decrease in MQAE fluorescence can be seen in Figure 6.16 after 30 min. The first 15 min shows a steady decrease in fluorescence intensity, however due to droplet shrinking, MQAE fluorescence seems to increase again. This assay could only be done once and droplet monitoring could not be longer than 30 min as the droplets coalesced. The coalescence could be due to too high concentrations of CLIC1, where the large pores sizes disrupts the lipid bilayer allowing the droplets to merge.

More studies have to be done to assess the optimal concentration of CLIC1 channels for which chloride ion flux is detected and bilayer disruption is prevented.

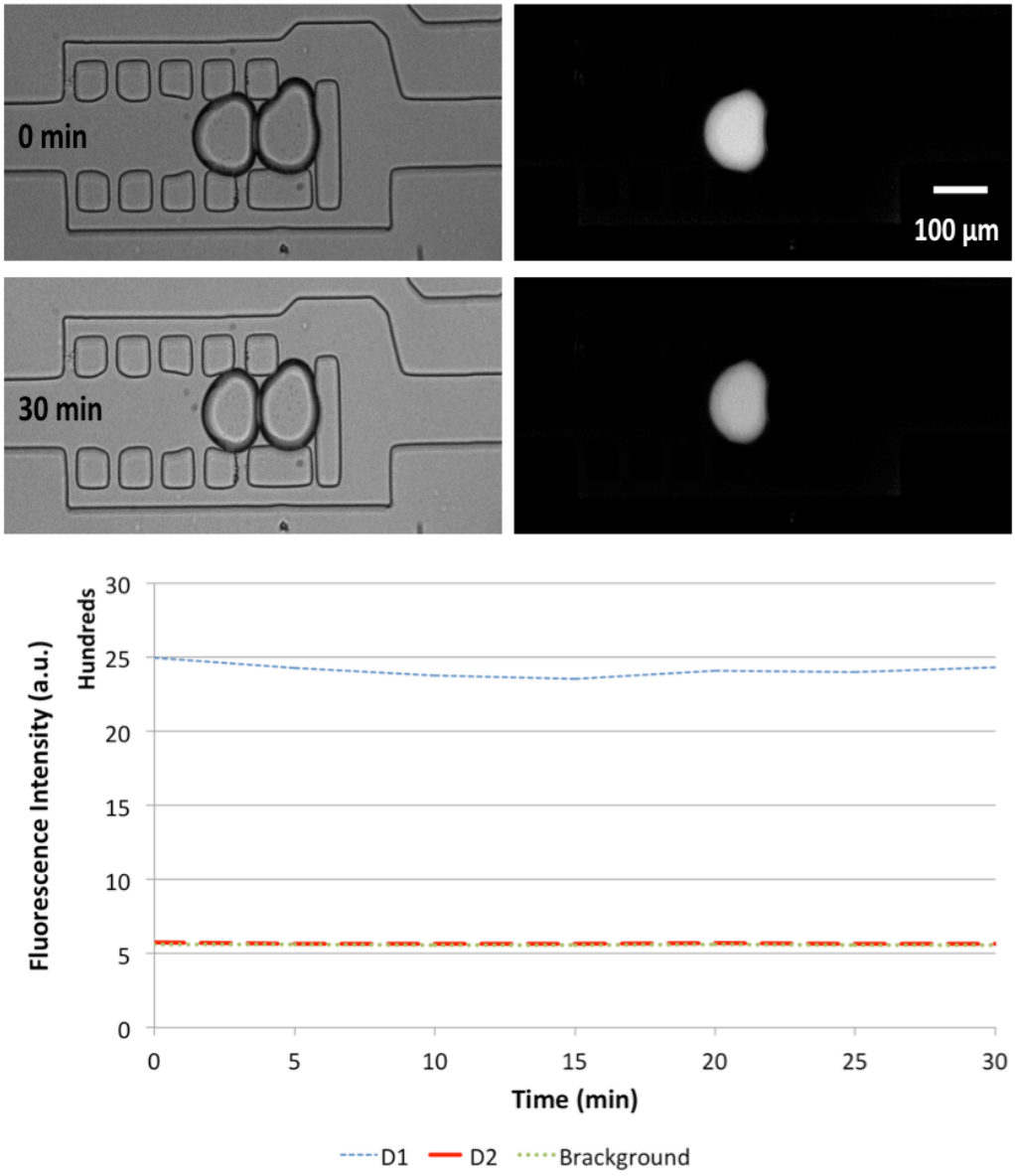

Figure 6.16 Functional studies of CLIC1 within DIBs. The dark droplet contained CLIC1 in a 40 mM TRIS, 150 mM NaCl, 2 mM H_2O_2 buffer at pH 6.0 and the fluorescent droplet contained a 250 µM MQAE, 40 mM TRIS and 500 mM NaOH at pH 6 buffer. Incorporation of the CLIC1 channel into the DIB is expected to produce a diffusive chloride flux into the neighbouring droplets. The right hand column shows fluorescence microscopy images taken using a DAPI filter. The corresponding bright field images can be seen in the left hand column. . 5 mg/ml DPhPC in hexadecane was used as the oil phase. The experiment was operated according to the description in Chapter 3, section 3.3.1. The graph shows a steady decrease in fluorescence intensity after for 15 min after this droplet fluorescence seems to increase.

6.6 Summary

The experiments presented in this chapter were all performed in the presence of artificial membrane constructs to mimic some of the factors that would be present at the surface of a biological membrane in vivo. The lower pH at the surface of a biological membrane has been shown to aid the insertion of the dimeric CLIC1 intermediate. The physiological role of this intermediate state would be to lower the energy barrier for insertion into the membrane. CLIC1 channel activity has been observed to increase at lower pH values[213,214], this is likely due to the destabilisation of the dimer, which favours the ability of the protein to interact with the membrane.

During CLIC1 transition from the soluble, cytosolic conformation to an integral membrane-bound conformation, pronounced structural changes are believed to happen. The transmembrane region is fully helical and has a distinct amphipathic character with a hydrophobic dipole moment. The fluorometric experiments suggested that Trp35 has to be positioned right in the centre of the hydrophobic portion of the membrane, an unexpected location, given that Trp residues of membrane proteins are generally found just inside the interfacial region of the membrane surface. The pegylation experiments were done to investigate the steric position of the cysteine residues. The experiments suggest that the Cys24 residue protrudes through the bilayer into the interfacial region on the outer leaflet of the membrane where it could play a role in redox regulation of channel function for this to happen the transmembrane helix must bend pushing the cysteine out of the bilayer.

CLIC1's most interesting feature is its metamorphic nature, existing both in soluble and membrane-bound states. While the soluble structure and the functioning of the membrane-bound form have been extensively characterized, little is known about the structure of the membrane-integrated form. One of the primary aims of this chapter, in addition to a structural and stability characterization of CLIC1, was to characterise a model membrane system that can be used in future studies to develop a deeper understanding of the functional and structural properties of eukaryotic membrane proteins. A basic requirement for any future study undertaken to

investigate the structure and function of membrane protein is confirmation that the protein is actually inserted into the membrane.

From the liposomes experiment, we were able to detect CLIC1 insertion and function into the lipid bilayer by observing a significant decrease in MQAE fluorescence. The gradual quenching of MQAE fluorescence in Figure 6.15, indicates a concentration-dependent influx of Cl^- ions in the liposomes facilitated by CLIC1 channels. This assay shows that the lipid composition of the liposomes and the assay conditions are enough to promote the insertion of a functional CLIC1 channel into a model bilayer. Further confirmation of CLIC1 association with the liposome bilayer is shown by a red shift (Figure 6.12) in the fluorescence spectrum of the Trp residue when soluble CLIC1 is compared to the membrane bound form, indicative of a conformational change.

Experiments on DIBs were less successful. Although, the same assay conditions were used, MQAE quenching was only detected on one occasion for a short time. Typically, DIB rupture occurred spontaneously after 15-30 minutes of DIB formation. It can be hypothesized that the bilayer instability was mainly due to channel insertion. Initial experiments were attempted with higher concentrations of the purified channels and droplets coalesced within only a few minutes of bilayer formation. CLIC1 concentration was then decreased and DIBs were monitored for 30 min until droplets coalesced. More work is needed to increase DIB stability in order to record channel activity. CLIC1 activity has been monitored in model bilayers composed of a variety of lipids[212,214], thus changing lipid composition might increase DIB stability and prevent droplet coalescence.

Chapter 7

Discussion and Outlook

In this final chapter, a brief summary on the content of each chapter is given, together with a discussion about the main results and conclusions. Subsequently, potential improvements are suggested that are required to adapt the developed microfluidic system into a high-throughput drug-screening platform.

7.1 Summary

This thesis describes the development of a microfluidic device for lipid bilayer experimentation. The potential applications and its employment for drug screening on ion channels were explored and discussed. In the last decade, miniaturization technologies and microfluidics have received increasing attention in the field of artificial cell membranes. A number of systems have been reported, using various types of membrane models, including suspended bilayer lipid membranes (BLMs) and droplet interface bilayers (DIBs). These systems have shown potential for automation and multiplexing, as well as for commercial purposes. One particular promising application and one of the driving forces for the development of these miniaturized bilayer platforms, is drug permeability screening both through ion channels and membranes alone, as discussed in detail in Chapter 1. Ion channels are involved in a number of diseases, making them attractive targets for the pharmaceutical industry.

Microfluidic bilayer platforms have emerged as an attractive alternative, since they allow studying ion channels in a highly controlled environment, while reducing the volumes of the reagents and the overall cost of the assay. So far, first attempts for automation, multiplexing and parallel electrophysiological measurements have been described using this microfluidic approach, and platforms have been validated through preliminary drug screening experiments on ion channels[59,237,238], clearly revealing the potential of microfluidics in the field of drug screening.

The primary focus of the work presented here is to develop a fully integrated droplet microfluidic platform based on fluorescence measurements for the high throughput study of cellular membranes and membrane proteins. The goals of this work were to understand the trade-offs between capillary number and droplet trapping, droplet velocity and coalescence in order to understand how changes in the system parameters will affect droplet-interface-bilayers (DIBs) formation. Such knowledge is vital for designing a robust device that can target high throughput screening and automation. The device can form multiple DIBs capable of incorporating functional channel membrane proteins such as α-haemolysin, thus

making the platform potentially suited for the study of membrane and channel permeability.

Considerable effort was put into a systematic study of the parameters influencing droplet trapping and droplet coalescence. Through video analysis and simulations, significant findings on the effects of capillary number and droplet velocity on droplet deformation and trapping within the register elements were identified, including the capillary number threshold for droplet trapping at different size apertures. It was shown that the ability to trap a droplet within shift registers is related to the extent of droplet deformation and can be overcome by regulating the velocity of the carrier. Droplet velocity also proved to be an important factor in order to prevent droplet coalescence. Threshold velocities for a given lipid concentration were identified that prevented phospholipid coated droplet from coalescing. These findings helped the development of devices capable of in-line droplet velocity regulation and with a specific register aperture size based of the interfacial tension and viscosity of the phases.

The complete device characterization captured all dependencies observed in experiments including the influences of the Y-junction geometry, shape of shift registers, capillary number and droplet velocity.

The use of DIBs for membrane studies has many significant advantages over other artificial bilayer methods. Amongst these is their longevity, the absence of a solid support, the ability to form asymmetric conditions and the possibility of integrating electrodes for electrophysiological studies. Additionally, this system allows the alteration of the lipid content in the organic solution so that membranes that more closely mimic those of a particular tissue could be used to develop tissue specific permeability calculations.

Using fluorescence microscopy to assess the leakage of fluorescein through the membrane, the suitability of this device was assessed as a platform for drug permeation studies similar to PAMPA. Currently, the membrane transport can be

studied with in vitro assays such as PAMPA or Caco-2 cell monolayers. The Caco-2 assay consists of a cell monolayer, grown on a porous and thin substrate separating two stacked microwell plates, and the transport of the substance or drug from one to the other compartment is analysed. This technique is used to study passive and active transport across the cell membranes. However, it lacks in reproducibility and the assay is rather time intensive[41]. In the PAMPA, a similar approach is used, but instead of cells a lipid bilayer is formed from phospholipid solution in solvent on the filter between two compartments. This assay is much quicker compared to the Caco-2 assay, but only measures passive transport. In both cases, the transport is analysed with UV spectroscopy[41]. Here, our bilayer platform could have advantages compared to PAMPA, as our BLMs are formed across an aperture without any additional filter substrate present that could influence the measurements. Furthermore, optical or electrical measurements can be performed giving the opportunity to measure *in situ* the transport across the membrane by using fluorescent labels and monitoring the fluorescence intensity in one compartment over time. Furthermore, the DIBs formed in our devices have been characterized in terms of ability to host fully functional α-HL pores. This demonstrates potential for this platform to be used for ion channel studies.

Following the DIB validation, the ability to use this system to study a pharmacologically relevant ion channel was examined. Attempts were made to incorporate a eukaryotic membrane protein - chloride-intracellular-channel 1 (CLIC1) into the DIBs. However, no successful recording of channel activity was obtained due to droplet coalescence. Whilst droplet coalescence has been analysed as dependent on droplet velocity, in the experiments with CLIC1, droplets only coalesced after 30 min of being in contact, suggesting that perhaps channel incorporation could be a factor in droplet coalescence.

Although we have not successfully demonstrated the incorporation of a eukaryotic ion channel within our microfluidic platform, the system shows potential to be used for drug permeability assays.

However, optimisation is needed to allow this platform to be used as a tool for membrane protein studies. For instance, a longer delay line could be introduced between droplet production and bilayer formation to allow better droplet stabilization and further prevent droplet coalescence. Another possible improvement on the device is to have the registers connected in parallel instead of in series in order to prevent potential cross-contamination between assays. A potential new device could look like the figure below:

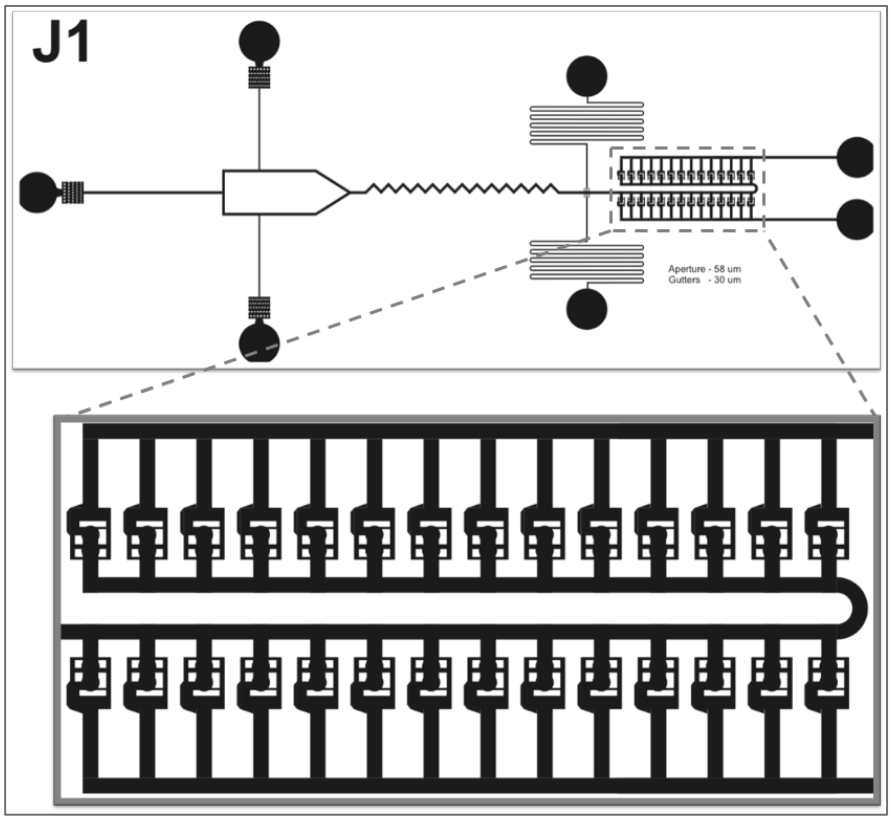

Figure 7.1 Potential next design iteration for the droplet-interface-bilayer device. The shift registers have been parallelised to decrease so that once a bilayer is formed it is not interrupted by another incoming droplet.

7.2 General Considerations

The experiments described in this thesis primarily highlight the versatility of the developed microfluidic bilayer platform. However, the successful insertion of pharmacologically relevant ion channels in the bilayer must still be demonstrated.

7.2.1 A Platform for Large Scale Membrane Protein Studies

Two important features of droplet microfluidics are the throughput of experiments and the potential for automation that can be achieved with the technology. The exploitation of these properties is therefore very attractive for scaling up biomembrane studies and developing synthetic biology-based procedures related to artificial lipid bilayers and ion channels.

The need for fast high-throughput permeation measurements resulted in the development of PAMPA (Parallel Artificial Membrane Permeability Assay)[39]. PAMPA, which uses two-layered multi-well plates to measure permeation between top and bottom wells, has been widely used to assess passive permeability of many drug candidates simultaneously[40]. A filter membrane is saturated with an organic lipid solution. The filter membrane is used to separate an aqueous solution containing a test compound from an aqueous buffer initially free of the molecule[239] (described in Chapter 1). The test compound is quantified in the acceptor compartment by spectroscopic methods. Every step is automatable, which is the enormous advantage of PAMPA. The system is commercially available and usually run in a 96-well plate format. Nonetheless, the lipid and oil mixture forms membranes of 10-100 μm in thickness, which is much thicker than biological membranes, leading to longer assay times and limiting measurement throughput. Moreover, the permeation data have to be corrected for the membrane thickness and the phenomenon of the unstirred water layer, which limits the uptake of highly permeable drugs[240]. PAMPA has been used and modified many times, aiming to create a lipid barrier close to physiological membranes, e.g. of the gastrointestinal barrier or the blood-brain barrier.

Surprisingly, although microfluidics offers a great potential for parallelization and reduction of sample consumption, only a few examples have been reported where passive permeation was studied. Kuyper *et al.* 2006[241] used tethered large unilamellar vesicles (LUVs) inside a microfluidic channel to study proton permeation across lipid bilayers. A pH sensitive dye, carboxyfluorescein, was encapsulated in the liposomes and enabled the observation of the intravesicular pH. By using surface sensitive total-

internal fluorescence microscopy and fast buffer exchange with microfluidics, pH changes in individual vesicles was observed. Proton permeation occurred in two steps, first directed by a transient pore and then by the solubility-diffusion mechanism.

In a similar approach to what was done here, Nisisako *et al.* 2013[242] used droplet microfluidics to quantify the permeation of fluorescein through DIBs in a droplet microfluidics format. Droplets were produced on chip and alternated to form a droplet array. The hexadecane oil was subsequently drained from the chip to allow the droplets to come into contact. Using fluorescence microscopy fluorescein permeation was measured at DIBs between arrayed donor and acceptor droplets. Soon after DIB formation the fluorescence intensity in donor droplets gradually decreased over time, suggesting that the donor droplets were losing fluorescein molecules. While the fluorescence intensity in acceptor droplets increased over time, meaning the acceptor droplets were gaining fluorescein molecules. In this system only a few droplets could be studied at a time and the system had to be reinitiated in order to take the second measurement.

Increasing the throughput by scaling up the register network can be particularly useful for either acquiring statistical information from a single device using one compound or when testing a variety of compounds at the same time. However, reflecting on the compromise identified in Chapter 4, for lipid concentration and droplet velocity to avoid droplet coalescence and the serial link between registers, the throughput of experiments that can be carried out in parallel is related to the time required to fill the register network. Therefore, within our device geometry, the throughput of significant experiments that can be carried out in parallel with the proposed system is directly related to the time taken for the permeation to start (T_P). This is important because if the permeation of a compound through a lipid bilayer (or ion channels) occurs on a faster timescale than that required for a droplet to shift along a register, a droplet's content would permeate across a DIB during the filling procedure of the register network.

Therefore, in a system containing N shift registers where only two droplets can be stored in each register (Figure 7.) the total time required to fill the registers is as follows:

$$T_{Tot} = (2 * N * T_D) + (N - 1) * T_T$$

Equation 7-1 Total time required to fill registers

where T_D (s) is the interval of time at which a droplet reaches any register in a steady state condition and T_T (s) is the droplet travelling time between equidistant registers. Consequently, by the time all N registers are full, due to the serial connection between the registers, a droplet would have been in touch with any adjacent droplet for some time (Figure 7. D1). Therefore, when all the registers are full and no more droplets are being produced, the permeation process taking place across the final DIB had already been occurring in previous registers during the filling procedure. This identifies a compromise between the total time taken to fill the all registers, T_{TOT} (s), the time each droplet stays in contact with each other and the time taken by molecules to permeate the DIB, T_P (s).

This effect can be compared when using calcein and fluorescein (Figure 7. B & C), as the molecules permeate across a DIB at different rates. Calcein permeates across DIBs at a very slow rate therefore all the registers can be filled before any permeation is seen. On the other hand, fluorescein permeates across DIBs at a very fast rate, thus a gradient of transport is seen by the time the last register is filled and only the first two registers can be simultaneously monitored for fluorescein-filled droplets.

Considering the scalability of operation and throughput, a different approach should be taken where only one or a small number of registers should be used in the network if molecular permeation is faster than register filling time, and experiments can be repeated periodically. Although it is important to discuss, for the purposes of drug discovery and permeation assays a situation where $T_P < T_{Tot}$ does not occur very often, and only some drugs have been reported in this range[243].

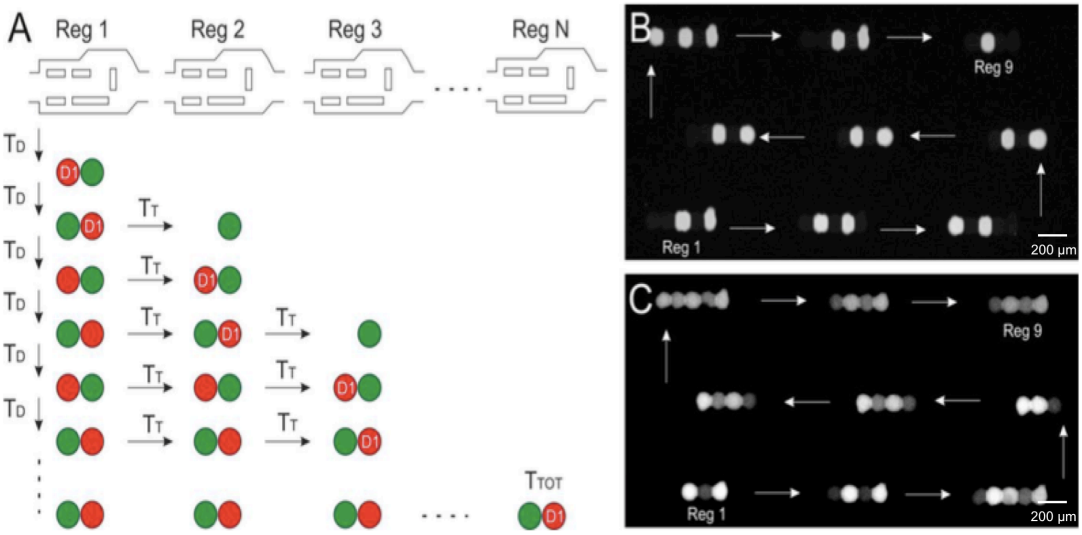

Figure 7.2 Dynamics of mass transport across a DIB and the device operation. Adapted from Schlicht and Zagnoni 2015[183] (A) Schematic shows N droplet shift registers in series. (B) Fluorescence microscopy image showing full registers with alternating droplets containing buffer and calcein. (C) Fluorescence microscopy image showing the same 9 full registers with alternating droplets containing buffer and fluorescein.

Another way to address this problem would involve changing the overall geometry of the device and instead of having the registers in series they could be in parallel. A similar design similar to the trap-and-release mechanism by Tan *et al.* 2007[164] (Figure 2.10) and discussed in Chapter 2 has been attempted and might also be suitable for this application. The idea is that each trap is linked to a bypass channel so when the trap is empty, the resistance of the trap is lower than that of the bypass channel, allowing one droplet go into the trap. Once a droplet gets trapped, resistance in the trap increases becoming higher than that of the bypass channel, the following droplets will choose the less resistive path and go in the bypass channel.

7.2.2 Delivery of Non-Fusogenic Membrane Proteins

A first and essential step is to insert biologically relevant ion channels in the bilayer. So far, only α-haemolysin have been successfully utilized in our experiments, and these porins were added to the buffer solution, from which they spontaneously self-insert. Biologically relevant ion channels, on which drugs are eventually tested, must be

either kept in a hydrophobic and functional environment, such as proteoliposomes, which are subsequently fused with the bilayer, or solubilized with detergents.

Proteoliposome fusion is highly challenging. Typically, the proteoliposomes are delivered manually close to the bilayer in order to initiate fusion, followed by stirring of the solution. In our closed microfluidic device, the proteoliposomes would have to be added to the aqueous phase and transported to droplet shift registers where the droplet remains static. In the microchannels however, no mixing or active transport takes place, which might make it more difficult for the proteoliposomes to actually reach the bilayer. Furthermore, proteoliposome fusion is usually promoted in the presence of an osmotic gradient across the membrane; this gradient induces swelling of the droplets, which might influence bilayer stability.

7.2.3 Buffer Exchange for Drug Screening Assays

Another highly important aspect for ion channel experimentation and drug screening is the fast and reliable exchange of buffer solution in the microfluidic channels without membrane rupture. Ideally, only one ion channel is reconstituted in the BLM, which means fusion of only one liposome containing one protein. To favour this situation, directly after fusion is detected, the osmotic gradient must be changed to prevent further fusion.

To study the effect of drugs on ion channels, perfusion is also required to introduce the drugs on one side of the bilayer. In our system, the proteoliposomes and drugs to be tested would have to be delivered within the aqueous phases from the start, as it was done for the α-haemolysin studies on Chapter 5. A change in osmotic gradient is not possible after bilayer formation. To allow the measurement of single channels within the device presented here, proteoliposomes have to be diluted within the aqueous phase enough in order to favour the encapsulation of only one proteoliposome per droplet. This way a change in osmotic gradient after fusion is not required.

7.2.4 Optical Assessment of Ion Transport

In our devices ion transport across the bilayer can only be assessed optically by utilizing ion sensitive dyes. In the case of CLIC1, ion transport can be conventionally measured by visualizing the Cl^- flux across the membrane using ion sensitive dyes and fluorescence microscopy. Since we cannot control the number of channels that gets inserted into the bilayer, neighbouring CLIC1 channels might influence each other. As a result, electrophysiological information on the single channel level in a controlled environment is desirable to get closer insight into the channel behaviour.

In that context, the availability of a platform combining both measurement approaches - electrophysiology and microscopy - would provide a unique opportunity to correlate optical and electrophysiological recordings, and would bring a better insight into understanding membrane protein channels. The integration of microelectrodes into our devices is also possible which will allow for large scale electrophysiology readouts[244,245], allowing more sensitive assays to be performed than those obtained with fluorescent dye reporters. However, this approach increases the complexity associated with system microfabrication and costs.

7.3 Conclusion

Overall, a microfluidic network based on pressure driven flows, capable of stable and robust droplet generation, alternation and trapping within register elements for the formation of a series of DIB arrays and their storage was developed and validated. Important relationships between capillary number and droplet trapping, as well as droplet velocity and lipid concentration, were identified and characterized. These identified the conditions to prevent droplet coalescence without hindering the microfluidic functionalities of the system. The successful formation of lipid bilayers was demonstrated, providing proof-of-concept results of passive molecular permeation and ion-channel mediated permeation of molecules and ions through DIBs using fluorescence assays. This platform can lead to new systems for

higher-throughput and miniaturised versions of parallel artificial membrane permeability assays. Furthermore, the system can be utilised in large-scale studies of other processes occurring across artificial lipid bilayers, such as molecular transport[73], fusogenic properties of peptides[246] and virus transport and fusion[247]. Although a number of developments, both procedural and technological are still required, the device developed here shows potential to be utilised for drug discovery assays using eukaryotic transmembrane proteins.

Furthermore, our platform possesses the benefit of forming droplets in linear sequences of alternating configuration in a simple and reliable manner. A large range of lipids can be used to create DIBs and this versatility is beneficial to model the natural asymmetry in biological membranes.

The developed device has potential to develop highly sensitive tools for artificial cells mimicry, leading to new approaches for personalized healthcare, drug delivery systems and cell-free protein expression kits.

References

1. Huang, C.-J. *et al.* Characterization of voltage-gated sodium-channel blockers by electrical stimulation and fluorescence detection of membrane potential. *Nat. Biotechnol.* **24**, 439–446 (2006).
2. Brown, R. E. Sphingolipid organization in biomembranes: what physical studies of model membranes reveal. *J. Cell Sci.* **111 (Pt 1)**, 1–9 (1998).
3. Singer, S. J. & Nicolson, G. L. The fluid mosaic model of the structure of cell membranes. *Science* **175**, 720–31 (1972).
4. Rietveld, A. & Simons, K. The differential miscibility of lipids as the basis for the formation of functional membrane rafts. *Biochim. Biophys. Acta* **1376**, 467–79 (1998).
5. Becher, A. & McIlhinney, R. Consequences of lipid raft association on G-protein-coupled receptor function. *Biochem. Soc. Symp.* **164**, 151–64 (2005).
6. Chini, B. & Parenti, M. G-protein-coupled receptors, cholesterol and palmitoylation: facts about fats. *J. Mol. Endocrinol.* **42**, 371–9 (2009).
7. Engelman, D. M. Membranes are more mosaic than fluid. *Nature* **438**, 578–580 (2005).
8. Karnovsky, M. J., Kleinfeld, a M., Hoover, R. L. & Klausner, R. D. The concept of lipid domains in membranes. *J. Cell Biol.* **94**, 1–6 (1982).
9. Munro, S. Lipid Rafts: Elusive or Illusive? *Cell* **115**, 377–388 (2003).
10. Brown, D. Structure and function of membrane rafts. *Int. J. Med. Microbiol.* **291**, 433–7 (2002).
11. Pike, L. J. The challenge of lipid rafts. *J. Lipid Res.* **50 Suppl**, S323–S328 (2009).
12. Simons, K. & Ikonen, E. How cells handle cholesterol. *Science* **290**, 1721–1726 (2000).
13. Zaccai, G. How soft is a protein? A protein dynamics force constant measured by neutron scattering. *Science* **288**, 1604–1607 (2000).
14. Lundbaek, J. a & Andersen, O. S. Spring constants for channel-induced lipid bilayer deformations. Estimates using gramicidin channels. *Biophys. J.* **76**, 889–895 (1999).
15. Mitra, K., Ubarretxena-Belandia, I., Taguchi, T., Warren, G. & Engelman, D. M. Modulation of the bilayer thickness of exocytic pathway membranes by membrane proteins rather than cholesterol. *Proc. Natl. Acad. Sci. U. S. A.* **101**, 4083–4088 (2004).
16. Petrache, H. I. *et al.* Hydrophobic matching mechanism investigated by molecular dynamics simulations. *Langmuir* **18**, 1340–1351 (2002).

17. Dowhan, W. & Bogdanov, M. Lipid-Dependent Membrane Protein Topogenesis. *Annu. Rev. Biochem.* **78**, 515–540 (2011).

18. Stahlberg, H. *et al.* Two-dimensional crystals: A powerful approach to assess structure, function and dynamics of membrane proteins. *FEBS Lett.* **504**, 166–172 (2001).

19. Seddon, A. M., Curnow, P. & Booth, P. J. Membrane proteins, lipids and detergents: not just a soap opera. *Biochim. Biophys. Acta* **1666**, 105–17 (2004).

20. Plewczynski, D. & Rychlewski, L. Meta-basic estimates the size of druggable human genome. *J. Mol. Model.* **15**, 695–9 (2009).

21. Kennedy, S. J. Structures of membrane proteins. *J. Membr. Biol.* **42**, 265–279 (1978).

22. Ashcroft, F. M. From molecule to malady. *Nature* **440**, 440–447 (2006).

23. Nyholm, T. K. M., Özdirekcan, S. & Antoinette Killian, J. How protein transmembrane segments sense the lipid environment. *Biochemistry* **46**, 1457–1465 (2007).

24. Palczewski, K. G Protein-Coupled Receptor Rhodopsin. *Annu. Rev. Biochem.* **75**, 743–767 (2006).

25. Pauling, L. & Corey, R. B. Configurations of Polypeptide Chains With Favored Orientations Around Single Bonds: Two New Pleated Sheets. *Proc. Natl. Acad. Sci. U. S. A.* **37**, 729–740 (1951).

26. Schulz, G. E. beta-Barrel membrane proteins. *Curr. Opin. Struct. Biol.* **10**, 443–447 (2000).

27. Dang, T. X., Hotze, E. M., Rouiller, I., Tweten, R. K. & Wilson-Kubalek, E. M. Prepore to pore transition of a cholesterol-dependent cytolysin visualized by electron microscopy. *J. Struct. Biol.* **150**, 100–108 (2005).

28. Heuck, a P., Hotze, E. M., Tweten, R. K. & Johnson, a E. Mechanism of membrane insertion of a multimeric beta-barrel protein: perfringolysin O creates a pore using ordered and coupled conformational changes. *Mol. Cell* **6**, 1233–1242 (2000).

29. Drews, J. Drug Discovery: A Historical Perspective. *Science (80-.).* **287**, 1960–1964 (2000).

30. Yildirim, M. a, Goh, K.-I., Cusick, M. E., Barabási, A.-L. & Vidal, M. Drug-target network. *Nat. Biotechnol.* **25**, 1119–26 (2007).

31. Arora, A. & Tamm, L. K. Biophysical approaches to membrane protein structure determination. *Curr. Opin. Struct. Biol.* **11**, 540–547 (2001).

32. Wallin, E. & von Heijne, G. Genome-wide analysis of integral membrane proteins from eubacterial, archaean, and eukaryotic organisms. *Protein Sci.* **7**, 1029–38 (1998).

33. White, S. H. Biophysical dissection of membrane proteins. *Nature* **459**, 344–6 (2009).

34. Sachs, J. N. & Engelman, D. M. Introduction to the membrane protein reviews: the interplay of structure, dynamics, and environment in membrane protein function. *Annu. Rev. Biochem.* **75**, 707–712 (2006).

35. Dowhan, W. & Bogdanov, M. Lipid-protein interactions as determinants of membrane protein structure and function. *Biochem. Soc. Trans.* **39**, 767–774 (2011).

36. Ionescu-Zanetti, C. *et al.* Mammalian electrophysiology on a microfluidic platform. *Proc. Natl. Acad. Sci. U. S. A.* **102**, 9112–7 (2005).

37. Zagnoni, M., Sandison, M. E., Marius, P., Lee, A. G. & Morgan, H. Controlled delivery of proteins into bilayer lipid membranes on chip. *Lab Chip* **7**, 1176–1183 (2007).

38. Avdeef, A. *et al.* Drug absorption in vitro model: filter-immobilized artificial membranes. *Eur. J. Pharm. Sci.* **14**, 271–280 (2001).

39. Kansy, M., Senner, F. & Gubernator, K. Physicochemical High Throughput Screening: Parallel Artificial Membrane Permeation Assay in the Description of Passive Absorption Processes. *J. Med. Chem.* **41**, 1007–1010 (1998).

40. Li, C., Wainhaus, S., Uss, A. S. & Cheng, K.-C. High-Throughput Screening Using Caco-2 Cell and PAMPA Systems. in *Drug Absorption Studies* **7**, 418–429 (Springer US, 2008).

41. Orsi, M. & Essex, J. W. Chapter 4. Passive Permeation Across Lipid Bilayers: a Literature Review. in *Molecular Simulations and Biomembranes: From Biophysics to Function* 76–90 (2010). doi:10.1039/9781849732154-00076

42. Goodenough, D. A. & Paul, D. L. Gap Junctions. *Cold Spring Harb. Perspect. Biol.* **1**, a002576–a002576 (2009).

43. Nikaido, H. Porins and specific channels of bacterial outer membranes. *Mol. Microbiol.* **6**, 435–442 (1992).

44. Hucho, F. & Weise, C. Ligand-Gated Ion Channels. *Angew. Chemie Int. Ed.* **40**, 3100–3116 (2001).

45. Gouaux, E. & Mackinnon, R. Principles of selective ion transport in channels and pumps. *Science* **310**, 1461–5 (2005).

46. Schatz, G. The doors to organelles. *Nature* **395**, 439–440 (1998).

47. Studer, A., Demarche, S., Langenegger, D. & Tiefenauer, L. Integration and recording of a reconstituted voltage-gated sodium channel in planar lipid bilayers. *Biosens. Bioelectron.* **26**, 1924–1928 (2011).

48. Hirano-Iwata, A., Niwano, M. & Sugawara, M. The design of molecular sensing interfaces with lipid-bilayer assemblies. *TrAC Trends Anal. Chem.* **27**, 512–520 (2008).

49. Numann, R. & Negulescu, P. A. High-throughput screening strategies for cardiac ion channels. *Trends Cardiovasc. Med.* **11**, 54–9 (2001).

50. MacKinnon, R. Potassium channels. *FEBS Lett.* **555**, 62–65 (2003).

51. Jiang, Q. X. & Gonen, T. The influence of lipids on voltage-gated ion channels. *Curr. Opin. Struct. Biol.* **22**, 529–536 (2012).

52. Tombola, F., Pathak, M. M., Gorostiza, P. & Isacoff, E. Y. The twisted ion-permeation

pathway of a resting voltage-sensing domain. *Nature* **445**, 546–9 (2007).

53. Wood, C., Williams, C. & Waldron, G. J. Patch clamping by numbers. *Drug Discov. Today* **9**, 434–41 (2004).

54. Kirichok, Y., Navarro, B. & Clapham, D. E. Whole-cell patch-clamp measurements of spermatozoa reveal an alkaline-activated Ca2+ channel. *Nature* **439**, 737–740 (2006).

55. Singh, H. Two decades with dimorphic Chloride Intracellular Channels (CLICs). *FEBS Lett.* **584**, 2112–2121 (2010).

56. Montal, M. & Mueller, P. Formation of bimolecular membranes from lipid monolayers and a study of their electrical properties. *Proc. Natl. Acad. Sci. U. S. A.* **69**, 3561–6 (1972).

57. Funakoshi, K., Suzuki, H. & Takeuchi, S. Lipid bilayer formation by contacting monolayers in a microfluidic device for membrane protein analysis. *Anal. Chem.* **78**, 8169–74 (2006).

58. Malmstadt, N., Nash, M. a, Purnell, R. F. & Schmidt, J. J. Automated formation of lipid-bilayer membranes in a microfluidic device. *Nano Lett.* **6**, 1961–5 (2006).

59. Zagnoni, M. Miniaturised technologies for the development of artificial lipid bilayer systems. *Lab Chip* **12**, 1026–39 (2012).

60. Gorter, E. & Grendel, F. ON BIMOLECULAR LAYERS OF LIPOIDS ON THE CHROMOCYTES OF THE BLOOD. *J. Exp. Med.* **41**, 439–443 (1925).

61. Richter, R. P., Him, J. L. K. & Brisson, A. Supported lipid membranes. *Materials Today* **6**, 32–37 (2003).

62. Holden, M. a, Needham, D. & Bayley, H. Functional bionetworks from nanoliter water droplets. *J. Am. Chem. Soc.* **129**, 8650–5 (2007).

63. Hardy, G. J., Nayak, R. & Zauscher, S. Model cell membranes: Techniques to form complex biomimetic supported lipid bilayers via vesicle fusion. *Curr. Opin. Colloid Interface Sci.* **18**, 448–458 (2013).

64. Rajapaksha, S. P., Wang, X. & Lu, H. P. Suspended lipid bilayer for optical and electrical measurements of single ion channel proteins. *Anal. Chem.* **85**, 8951–8955 (2013).

65. White, R. J. *et al.* Single ion-channel recordings using glass nanopore membranes. *J. Am. Chem. Soc.* **129**, 11766–11775 (2007).

66. Kresák, S., Hianik, T. & Naumann, R. L. C. Giga-seal solvent-free bilayer lipid membranes: from single nanopores to nanopore arrays. *Soft Matter* **5**, 4021 (2009).

67. Bayley, H. Understanding and manipulating channels and pores. *Mol. Biosyst.* **3**, 645–647 (2007).

68. Leptihn, S. *et al.* Constructing droplet interface bilayers from the contact of aqueous droplets in oil. *Nat. Protoc.* **8**, 1048–57 (2013).

69. Thompson, J. R., Heron, A. J., Santoso, Y. & Wallace, M. I. Enhanced stability and

fluidity in droplet on hydrogel bilayers for measuring membrane protein diffusion. *Nano Lett.* **7**, 3875–3878 (2007).

70. Heron, A. J., Thompson, J. R., Cronin, B., Bayley, H. & Wallace, M. I. Simultaneous measurement of ionic current and fluorescence from single protein pores. *J. Am. Chem. Soc.* **131**, 1652–3 (2009).

71. Gross, L., Castell, O. & Wallace, M. Dynamic and Reversible Control of 2D Membrane Protein Concentration in a Droplet Interface Bilayer. *Nano Lett.* **11**, 3324–3328 (2011).

72. Hwang, W. L., Chen, M., Cronin, B., Holden, M. a & Bayley, H. Asymmetric droplet interface bilayers. *J. Am. Chem. Soc.* **130**, 5878–9 (2008).

73. Bayley, H. *et al.* Droplet interface bilayers. *Mol. Biosyst.* **4**, 1191–208 (2008).

74. Elani, Y., deMello, A. J., Niu, X. & Ces, O. Novel technologies for the formation of 2-D and 3-D droplet interface bilayer networks. *Lab Chip* **12**, 3514–20 (2012).

75. Thiam, A. R., Bremond, N. & Bibette, J. From stability to permeability of adhesive emulsion bilayers. *Langmuir* **28**, 6291–8 (2012).

76. Sonnleitner, a, Schütz, G. J. & Schmidt, T. Free Brownian motion of individual lipid molecules in biomembranes. *Biophys. J.* **77**, 2638–2642 (1999).

77. Kühner, M., Tampé, R. & Sackmann, E. Lipid mono- and bilayer supported on polymer films: composite polymer-lipid films on solid substrates. *Biophys. J.* **67**, 217–226 (1994).

78. Grime, J. M. a, Edwards, M. a, Rudd, N. C. & Unwin, P. R. Quantitative visualization of passive transport across bilayer lipid membranes. *Proc. Natl. Acad. Sci. U. S. A.* **105**, 14277–82 (2008).

79. Kristl, A. Membrane permeability in the gastrointestinal tract: The interplay between microclimate pH and transporters. in *Chemistry and Biodiversity* **6**, 1923–1932 (2009).

80. Abraham, T. *et al.* Structure-activity relationships of the antimicrobial peptide gramicidin S and its analogs: Aqueous solubility, self-association, conformation, antimicrobial activity and interaction with model lipid membranes. *Biochim. Biophys. Acta - Biomembr.* **1838**, 1420–1429 (2014).

81. Zasloff, M. Antimicrobial peptides of multicellular organisms. *Nature* **415**, 389–395 (2002).

82. Chalmeau, J., Monina, N., Shin, J., Vieu, C. & Noireaux, V. α-Hemolysin pore formation into a supported phospholipid bilayer using cell-free expression. *Biochim. Biophys. Acta* **1808**, 271–8 (2011).

83. Benz, R., Schmid, a & Nakae, T. Pore Formation by LamB of Escherichia coli in Lipid Bilayer Membranes. **165**, 978–986 (1986).

84. Schindler, H. Formation of planar bilayers from artificial or native membrane vesicles. *FEBS Lett.* **122**, 77–79 (1980).

85. Heginbotham, L., LeMasurier, M., Kolmakova-Partensky, L. & Miller, C. Single streptomyces lividans K(+) channels: functional asymmetries and sidedness of proton activation. *J. Gen. Physiol.* **114**, 551–560 (1999).

86. Geibel, S., Kaplan, J. H., Bamberg, E. & Friedrich, T. Conformational dynamics of the Na ⁺K ⁺-ATPase probed by voltage clamp fluorometry. *Pulse* **38**, 31–38 (2002).

87. Yanagisawa, M., Iwamoto, M., Kato, A., Yoshikawa, K. & Oiki, S. Oriented reconstitution of a membrane protein in a giant unilamellar vesicle: Experimental verification with the potassium channel KcsA. *J. Am. Chem. Soc.* **133**, 11774–11779 (2011).

88. Woodbury, D. J. & Miller, C. Nystatin-induced liposome fusion. A versatile approach to ion channel reconstitution into planar bilayers. *Biophys. J.* **58**, 833–839 (1990).

89. Planque, M. De & Mendes, G. Controlled delivery of membrane proteins to artificial lipid bilayers by nystatin–ergosterol modulated vesicle fusion. *IEE Proceedings- ...* **153**, 21–30 (2006).

90. Bear, C. E. *et al.* Purification and functional reconstitution of the cystic fibrosis transmembrane conductance regulator (CFTR). *Cell* **68**, 809–818 (1992).

91. Holden, M. A. & Bayley, H. Direct introduction of single protein channels and pores into lipid bilayers. *J. Am. Chem. Soc.* **127**, 6502–6503 (2005).

92. Thakkar, N., Lockhart, A. C. & Lee, W. Role of Organic Anion-Transporting Polypeptides (OATPs) in Cancer Therapy. *AAPS J.* **17**, 535–45 (2015).

93. Fernandes, T. G., Diogo, M. M., Clark, D. S., Dordick, J. S. & Cabral, J. M. S. High-throughput cellular microarray platforms: applications in drug discovery, toxicology and stem cell research. *Trends Biotechnol.* **27**, 342–349 (2009).

94. Hann, M. M. & Oprea, T. I. Pursuing the leadlikeness concept in pharmaceutical research. *Curr. Opin. Chem. Biol.* **8**, 255–263 (2004).

95. Clark, R. L. *et al.* The Drug Discovery Portal: a resource to enhance drug discovery from academia. *Drug Discov. Today* **15**, 679–683 (2010).

96. JASON W. ARMSTRONG. A review of high-throughput screening approaches for drug discovery. *Am. Biotechnol. Lab.* **17**, 26–28 (1999).

97. An, W. F. & Tolliday, N. Cell-based assays for high-throughput screening. *Molecular Biotechnology* **45**, 180–186 (2010).

98. Boisclair, M. D., Egan, D. A., Huberman, K. & Infantino, R. High-Throughput Screening in Industry. in *Anticancer Drug Development Guide* (ed. Andrews, B. A. T. and P. A.) 23–39 (Humana Press Inc., Totowa, NJ, 2004). doi:10.1007/978-1-59259-739-0_2

99. Szymański, P., Markowicz, M. & Mikiciuk-Olasik, E. Adaptation of High-Throughput Screening in Drug Discovery—Toxicological Screening Tests. *Int. J. Mol. Sci.* **13**, 427–452 (2011).

100. Baret, J.-C. *et al.* Fluorescence-activated droplet sorting (FADS): efficient

microfluidic cell sorting based on enzymatic activity. *Lab Chip* **9**, 1850 (2009).

101. Agresti, J. J. *et al.* Correction for Agresti et al., Ultrahigh-throughput screening in drop-based microfluidics for directed evolution. *Proc. Natl. Acad. Sci.* **107**, 6550–6550 (2010).

102. Kerns, E. H. *et al.* Combined Application of Parallel Artificial Membrane Permeability Assay and Caco-2 Permeability Assays in Drug Discovery. *J. Pharm. Sci.* **93**, 1440–1453 (2004).

103. Brouwers, J., Ingels, F., Tack, J. & Augustijns, P. Determination of intraluminal theophylline concentrations after oral intake of an immediate-and a slow-release dosage form. *J. Pharm. Pharmacol.* **57**, 987–995 (2005).

104. Terry, S. C., Jerman, J. H. & Angell, J. B. A gas chromatographic air analyzer fabricated on a silicon wafer. *IEEE Trans. Electron Devices* **26**, 1880–1886 (1979).

105. Manz, A., Graber, N. & Widmer, H. M. Miniaturized total chemical analysis systems: A novel concept for chemical sensing. *Sensors Actuators B Chem.* **1**, 244–248 (1990).

106. Duffy, D. C., McDonald, J. C., Schueller, O. J. & Whitesides, G. M. Rapid Prototyping of Microfluidic Systems in Poly(dimethylsiloxane). *Anal. Chem.* **70**, 4974–84 (1998).

107. Harrison, D. J. *et al.* Micromachining a miniaturized capillary electrophoresis-based chemical analysis system on a chip. *Science* **261**, 895–7 (1993).

108. Fang, W. F. & Yang, J. T. High performance microreactor for rapid fluid mixing and redox reaction of ascorbic acid. in *DTIP of MEMS and MOEMS - Symposium on Design, Test, Integration and Packaging of MEMS/MOEMS* 285–288 (2008). doi:10.1109/DTIP.2008.4753002

109. Andersson, H. & Berg, A. van den. Microfabrication and microfluidics for tissue engineering: state of the art and future opportunities. *Lab Chip* **4**, 98 (2004).

110. Bhatia, S. N. & Ingber, D. E. Microfluidic organs-on-chips. *Nat. Biotechnol.* **32**, 760–772 (2014).

111. Chin, C. D. *et al.* Microfluidics-based diagnostics of infectious diseases in the developing world. *Nat. Med.* **17**, 1015–9 (2011).

112. Squires, T. M. & Quake, S. R. Microfluidics: Fluid physics at the nanoliter scale. *Rev. Mod. Phys.* **77**, 977–1026 (2005).

113. Alexander, L., Allen, S. & Bindoff, N. L. Life at low reynolds number. *American* **45**, 1–36 (2013).

114. Thorsen, T., Roberts, R. W., Arnold, F. H. & Quake, S. R. Dynamic Pattern Formation in a Vesicle-Generating Microfluidic Device. *Phys. Rev. Lett.* **86**, 4163–4166 (2001).

115. Theberge, A. B. *et al.* Microdroplets in microfluidics: An evolving platform for discoveries in chemistry and biology. *Angew. Chemie - Int. Ed.* **49**, 5846–5868 (2010).

116. Fidalgo, L. M. *et al.* From Microdroplets to Microfluidics: Selective Emulsion Separation in Microfluidic Devices. *Angew. Chemie Int. Ed.* **47**, 2042–2045 (2008).

117. Chen, D. L., Gerdts, C. J. & Ismagilov, R. F. Using Microfluidics to Observe the Effect of Mixing on Nucleation of Protein Crystals. *J. Am. Chem. Soc.* **127**, 9672–9673 (2005).

118. Pekin, D. *et al.* Quantitative and sensitive detection of rare mutations using droplet-based microfluidics. *Lab Chip* **11**, 2156–2166 (2011).

119. Guttenberg, Z. *et al.* Planar chip device for PCR and hybridization with surface acoustic wave pump. *Lab Chip* **5**, 308–317 (2005).

120. Song, H., Chen, D. L. & Ismagilov, R. F. Reactions in droplets in microflulidic channels. *Angew. Chemie-International Ed.* **45**, 7336–7356 (2006).

121. Bibette, J., Calderon, F. L. & Poulin, P. Emulsions: basic principles. *Reports Prog. Phys.* **62**, 969–1033 (1999).

122. Bibette, J., Morse, D. C., Witten, T. A. & Weitz, D. A. Stability criteria for emulsions. *Phys. Rev. Lett.* **69**, 2439–2442 (1992).

123. Jullien, M.-C., Tsang Mui Ching, M.-J., Cohen, C., Menetrier, L. & Tabeling, P. Droplet breakup in microfluidic T-junctions at small capillary numbers. *Phys. Fluids* **21**, 072001 (2009).

124. Huebner, A. *et al.* Quantitative detection of protein expression in single cells using droplet microfluidics. *Chem. Commun.* **2**, 1218–1220 (2007).

125. Wang, B. L. *et al.* Microfluidic high-throughput culturing of single cells for selection based on extracellular metabolite production or consumption. *Nat. Biotechnol.* **32**, 473–478 (2014).

126. Bui, M.-P. N. *et al.* Enzyme Kinetic Measurements Using a Droplet-Based Microfluidic System with a Concentration Gradient. *Anal. Chem.* **83**, 1603–1608 (2011).

127. Piao, Y., Han, D. J., Azad, M. R., Park, M. & Seo, T. S. Enzyme incorporated microfluidic device for in-situ glucose detection in water-in-air microdroplets. *Biosens. Bioelectron.* **65**, 220–225 (2015).

128. Holtze, C. Large-scale droplet production in microfluidic devices—an industrial perspective. *J. Phys. D. Appl. Phys.* **46**, 114008 (2013).

129. Tendulkar, S. *et al.* A three-dimensional microfluidic approach to scaling up microencapsulation of cells. *Biomed. Microdevices* **14**, 461–469 (2012).

130. Tetradis-Meris, G. *et al.* Novel Parallel Integration of Microfluidic Device Network for Emulsion Formation. *Ind. Eng. Chem. Res.* **48**, 8881–8889 (2009).

131. Nisisako, T. & Torii, T. Microfluidic large-scale integration on a chip for mass production of monodisperse droplets and particles. *Lab Chip* **8**, 287–293 (2008).

132. Sun, B. J., Shum, H. C., Holtze, C. & Weitz, D. A. Microfluidic melt emulsification for encapsulation and release of actives. *ACS Appl. Mater. Interfaces* **2**, 3411–3416 (2010).

133. Bally, M. *et al.* Liposome and Lipid Bilayer Arrays Towards Biosensing Applications. *Small* **6**, 2481–2497 (2010).

134. Simon, A. *et al.* Formation and stability of a suspended biomimetic lipid bilayer on silicon submicrometer-sized pores. *J. Colloid Interface Sci.* **308**, 337–343 (2007).

135. Tsuji, Y. *et al.* Droplet-based lipid bilayer system integrated with microfluidic channels for solution exchange. *Lab Chip* **13**, 1476–81 (2013).

136. Han, X. *et al.* Nanopore Arrays for Stable and Functional Free-Standing Lipid Bilayers. *Adv. Mater.* **19**, 4466–4470 (2007).

137. Studer, A., Han, X., Winkler, F. K. & Tiefenauer, L. X. Formation of individual protein channels in lipid bilayers suspended in nanopores. *Colloids Surfaces B Biointerfaces* **73**, 325–331 (2009).

138. Kawano, R., Osaki, T., Sasaki, H. & Takeuchi, S. A Polymer-Based Nanopore-Integrated Microfluidic Device for Generating Stable Bilayer Lipid Membranes. *Small* **6**, 2100–2104 (2010).

139. Kawano, R. *et al.* Rapid Detection of a Cocaine-Binding Aptamer Using Biological Nanopores on a Chip. *J. Am. Chem. Soc.* **133**, 8474–8477 (2011).

140. Tsuji, Y. *et al.* Droplet-based lipid bilayer system integrated with microfluidic channels for solution exchange. *Lab Chip* **13**, 1476–81 (2013).

141. Syeda, R., Holden, M. a, Hwang, W. L. & Bayley, H. SI Screening Blockers Against a Potassium Channel. *J. Am. Chem. Soc.* **130**, SI 1-5 (2008).

142. Osaki, T., Suzuki, H., Le Pioufle, B. & Takeuchi, S. Multichannel Simultaneous Measurements of Single-Molecule Translocation in α-Hemolysin Nanopore Array. *Anal. Chem.* **81**, 9866–9870 (2009).

143. Suzuki, H., Tabata, K. V., Noji, H. & Takeuchi, S. Highly Reproducible Method of Planar Lipid Bilayer Reconstitution in Polymethyl Methacrylate Microfluidic Chip. *Langmuir* **22**, 1937–1942 (2006).

144. Ota, S., Suzuki, H. & Takeuchi, S. Microfluidic lipid membrane formation on microchamber arrays. *Lab Chip* **11**, 2485–7 (2011).

145. Stanley, C. E. *et al.* A microfluidic approach for high-throughput droplet interface bilayer (DIB) formation. *Chem. Commun. (Camb).* **46**, 1620–2 (2010).

146. Aghdaei, S., Sandison, M. E., Zagnoni, M., Green, N. G. & Morgan, H. Formation of artificial lipid bilayers using droplet dielectrophoresis. *Lab Chip* **8**, 1617–20 (2008).

147. El-Arabi, A. M., Salazar, C. S. & Schmidt, J. J. Ion channel drug potency assay with an artificial bilayer chip. *Lab Chip* **12**, 2409 (2012).

148. Rojko, N. *et al.* Imaging the lipid-phase-dependent pore formation of equinatoxin II in droplet interface bilayers. *Biophys. J.* **106**, 1630–1637 (2014).

149. Acharya, S. a, Portman, A., Salazar, C. S. & Schmidt, J. J. Hydrogel-stabilized droplet bilayers for high speed solution exchange. *Sci. Rep.* **3**, 3139 (2013).

150. Friddin, M. S. *et al.* Single-channel electrophysiology of cell-free expressed ion channels by direct incorporation in lipid bilayers. *Analyst* **138**, 7294–8 (2013).

151. Friddin, M. S., Morgan, H. & de Planque, M. R. R. Cell-free protein expression systems in microdroplets: Stabilization of interdroplet bilayers. *Biomicrofluidics* **7**, 014108 (2013).

152. Kawano, R. *et al.* Automated Parallel Recordings of Topologically Identified Single Ion Channels. *Sci. Rep.* **3**, 1995 (2013).

153. Zheng, B., Tice, J. & Ismagilov, R. F. Formation of Droplets of Alternating Composition in Microfluidic Channels and Applications to Indexing of Concentrations in Droplet-Based Assays NIH Public Access. *Anal. Chem.* **76**, 4977–4982 (2004).

154. Ahn, K., Agresti, J., Chong, H., Marquez, M. & Weitz, D. a. Electrocoalescence of drops synchronized by size-dependent flow in microfluidic channels. *Appl. Phys. Lett.* **88**, 1–4 (2006).

155. Chokkalingam, V., Herminghaus, S. & Seemann, R. Self-synchronizing pairwise production of monodisperse droplets by microfluidic step emulsification. *Appl. Phys. Lett.* **93**, 254101 (2008).

156. Frenz, L., Blouwolff, J., Griffiths, A. D. & Baret, J.-C. Microfluidic production of droplet pairs. *Langmuir* **24**, 12073–6 (2008).

157. Hong, J., Choi, M., Edel, J. B. & deMello, A. J. Passive self-synchronized two-droplet generation. *Lab Chip* **10**, 2702–9 (2010).

158. Hashimoto, M. *et al.* Formation of bubbles and droplets in parallel, coupled flow-focusing geometries. *Small* **4**, 1795–1805 (2008).

159. Hung, L.-H. *et al.* Alternating droplet generation and controlled dynamic droplet fusion in microfluidic device for CdS nanoparticle synthesis. *Lab Chip* **6**, 174–178 (2006).

160. Chokkalingam, V., Herminghaus, S. & Seemann, R. Self-synchronizing pairwise production of monodisperse droplets by microfluidic step emulsification. *Appl. Phys. Lett.* **93**, 254101 (2008).

161. Ahn, B., Lee, K., Lee, H., Panchapakesan, R. & Oh, K. W. Parallel synchronization of two trains of droplets using a railroad-like channel network. *Lab Chip* **11**, 3956–62 (2011).

162. Skelley, A. M., Kirak, O., Suh, H., Jaenisch, R. & Voldman, J. Microfluidic control of cell pairing and fusion. *Nat. Methods* **6**, 147–152 (2009).

163. Dura, B., Liu, Y. & Voldman, J. Deformability-based microfluidic cell pairing and fusion. *Lab Chip* **14**, 2783–2790 (2014).

164. Tan, W.-H. & Takeuchi, S. A trap-and-release integrated microfluidic system for dynamic microarray applications. *Proc. Natl. Acad. Sci. U.S.A.* **104**, 1146–51 (2007).

165. Huebner, A. *et al.* Static microdroplet arrays: a microfluidic device for droplet trapping, incubation and release for enzymatic and cell-based assays. *Lab Chip* **9**, 692–8 (2009).

166. Bai, Y. *et al.* A double droplet trap system for studying mass transport across a droplet-droplet interface. *Lab Chip* **10**, 1281–5 (2010).

167. Huebner, A. *et al.* Static microdroplet arrays: A microfluidic device for droplet trapping, incubation and release for enzymatic and cell-based assays. *Lab Chip* **9**, 692–698 (2009).

168. Martel, A. & Cross, B. Handling of artificial membranes using electrowetting-actuated droplets on a microfluidic device combined with integrated pA-measurements. *Biomicrofluidics* **6**, 12813–128137 (2012).

169. Villar, G., Graham, a. D. & Bayley, H. A Tissue-Like Printed Material. *Science (80-.).* **340**, 48–52 (2013).

170. Poulos, J. L., Nelson, W. C., Jeon, T.-J., Kim, C.-J. "Cj" & Schmidt, J. J. Electrowetting on dielectric-based microfluidics for integrated lipid bilayer formation and measurement. *Appl. Phys. Lett.* **95**, 013706 (2009).

171. Castell, O. K., Berridge, J. & Wallace, M. I. Quantification of membrane protein inhibition by optical ion flux in a droplet interface bilayer array. *Angew. Chem. Int. Ed. Engl.* **51**, 3134–8 (2012).

172. Korczyk, P. M., Derzsi, L., Jakieła, S. & Garstecki, P. Microfluidic traps for hard-wired operations on droplets. *Lab Chip* **13**, 4096–102 (2013).

173. Abate, A. R., Mary, P., van Steijn, V. & Weitz, D. a. Experimental validation of plugging during drop formation in a T-junction. *Lab Chip* **12**, 1516–21 (2012).

174. Yue, P., Feng, J. J., Liu, C. & Shen, J. A diffuse-interface method for simulating two-phase flows of complex fluids. *J. Fluid Mech.* **515**, 293–317 (2004).

175. Palumbo, P. *et al.* A general approach to the apparent permeability index. *J. Pharmacokinet. Pharmacodyn.* **35**, 235–48 (2008).

176. Goodchild, S. C. *et al.* Oxidation promotes insertion of the CLIC1 chloride intracellular channel into the membrane. *Eur. Biophys. J.* **39**, 129–138 (2009).

177. Goodchild, S. C., Angstmann, C. N., Breit, S. N., Curmi, P. M. G. & Brown, L. J. Transmembrane Extension and Oligomerization of the CLIC1 Chloride Intracellular Channel Protein upon Membrane Interaction. *Biochemistry* **50**, 10887–10897 (2011).

178. Lakowicz, J. R., Gryczynski, I. & Gryczynski, Z. High Throughput Screening with Multiphoton Excitation.pdf. *Journal of Biomolecular Screening* **4**, 355–361 (1999).

179. Zagnoni, M. & Cooper, J. M. A microdroplet-based shift register. *Lab Chip* **10**, 3069–73 (2010).

180. Oh, K. W., Lee, K., Ahn, B. & Furlani, E. P. Design of pressure-driven microfluidic networks using electric circuit analogy. *Lab Chip* **12**, 515–45 (2012).

181. Cornish, R. J. Flow in a Pipe of Rectangular Cross-Section. *Proc. R. Soc. A Math. Phys. Eng. Sci.* **120**, 691–700 (1928).

182. Niu, X., Gulati, S., Edel, J. B. & deMello, A. J. Pillar-induced droplet merging in

microfluidic circuits. *Lab Chip* **8**, 1837–41 (2008).

183. Schlicht, B. & Zagnoni, M. Droplet-interface-bilayer assays in microfluidic passive networks. *Sci. Rep.* **5**, 9951 (2015).

184. Bremond, N., Thiam, A. & Bibette, J. Decompressing Emulsion Droplets Favors Coalescence. *Phys. Rev. Lett.* **100**, 1–4 (2008).

185. Baroud, C. N., Gallaire, F. & Dangla, R. Dynamics of microfluidic droplets. *Lab Chip* **10**, 2032–45 (2010).

186. Thutupalli, S., Fleury, J.-B., Steinberger, A., Herminghaus, S. & Seemann, R. Why can artificial membranes be fabricated so rapidly in microfluidics? *Chem. Commun. (Camb).* **49**, 1443–5 (2013).

187. Baret, J.-C. Surfactants in droplet-based microfluidics. *Lab Chip* **12**, 422 (2012).

188. Baret, J.-C., Kleinschmidt, F., El Harrak, A. & Griffiths, A. D. Kinetic aspects of emulsion stabilization by surfactants: a microfluidic analysis. *Langmuir* **25**, 6088–93 (2009).

189. Krebs, T., Schroën, K. & Boom, R. Coalescence dynamics of surfactant-stabilized emulsions studied with microfluidics. *Soft Matter* **8**, 10650 (2012).

190. Zagnoni, M., Baroud, C. & Cooper, J. Electrically initiated upstream coalescence cascade of droplets in a microfluidic flow. *Phys. Rev. E* **80**, 046303 (2009).

191. Krämer, S. D. & Wunderli-Allenspach, H. Physicochemical properties in pharmacokinetic lead optimization. in *Farmaco* **56**, 145–148 (2001).

192. John N. Weinstein, Robert Blumenthal & Richard D. Klausner. Carboxyfluorescein leakage assay for lipoprotein-liposome interaction. *methods Enzymol.* **128**, 657–668 (1986).

193. Ishida, A., Otsuka, C., Tani, H. & Kamidate, T. Fluorescein chemiluminescence method for estimation of membrane permeability of liposomes. *Anal. Biochem.* **342**, 338–40 (2005).

194. Nisisako, T., Portonovo, S. a & Schmidt, J. J. Microfluidic passive permeability assay using nanoliter droplet interface lipid bilayers. *Analyst* **138**, 6793–800 (2013).

195. Faure, C. *et al.* Modeling leakage kinetics from multilamellar vesicles for membrane permeability determination: application to glucose. *Biophys. J.* **91**, 4340–9 (2006).

196. Song, L. *et al.* Structure of Staphylococcal alpha -Hemolysin, a Heptameric Transmembrane Pore. *Science (80-.).* **274**, 1859–1865 (1996).

197. Bayley, H. & Cremer, P. S. Stochastic sensors inspired by biology. *Nature* **413**, 226–230 (2001).

198. Walker, B., Krishnasastry, M., Zorn, L. & Bayley, H. Assembly of the oligomeric membrane pore formed by staphylococcal ??- hemolysin examined by truncation mutagenesis. *J. Biol. Chem.* **267**, 21782–21786 (1992).

199. Walker, B., Braha, O., Cheley, S. & Bayley, H. An intermediate in the assembly of a

pore-forming protein trapped with a genetically-engineered switch. *Chem. Biol.* **2**, 99–105 (1995).

200. Kawate T, G. E. Arresting and releasing Staphylococcal alpha-hemolysin at intermediate stages of pore formation by engineered disulfide bonds. *Protein Sci.* **12**, 997–1006 (2003).

201. Song, L. *et al.* Structure of Staphylococcal alpha -Hemolysin, a Heptameric Transmembrane Pore. *Science (80-.).* **274**, 1859–1865 (1996).

202. Berginc, K., Zakelj, S., Levstik, L., Ursic, D. & Kristl, A. Fluorescein transport properties across artificial lipid membranes, Caco-2 cell monolayers and rat jejunum. *Eur. J. Pharm. Biopharm.* **66**, 281–5 (2007).

203. Li, S., Hu, P. & Malmstadt, N. Confocal imaging to quantify passive transport across biomimetic lipid membranes. *Anal. Chem.* **82**, 7766–71 (2010).

204. Mälkiä, A., Murtomäki, L., Urtti, A. & Kontturi, K. Drug permeation in biomembranes: In vitro and in silico prediction and influence of physicochemical properties. *Eur. J. Pharm. Sci.* **23**, 13–47 (2004).

205. Kerns, E. H. High throughput physicochemical profiling for drug discovery. *Journal of Pharmaceutical Sciences* **90**, 1838–1858 (2001).

206. Artursson, P., Palm, K. & Luthman, K. Caco-2 monolayers in experimental and theoretical predictions of drug transport. *Adv. Drug Deliv. Rev.* **64**, 280–289 (2012).

207. Hanada, S. *et al.* Cell-based in vitro blood-brain barrier model can rapidly evaluate nanoparticles' brain permeability in association with particle size and surface modification. *Int. J. Mol. Sci.* **15**, 1812–25 (2014).

208. Jentsch, T. J., Stein, V., Weinreich, F. & Zdebik, A. A. Molecular Structure and Physiological Function of Chloride Channels. *Physiol. Rev.* **82**, 503–568 (2002).

209. Suzuki, M., Morita, T. & Iwamoto, T. Diversity of Cl- channels. *Cell. Mol. Life Sci.* **63**, 12–24 (2006).

210. Cromer, B., Morton, C., Board, P. & Parker, M. From glutathione transferase to pore in a CLIC. *Eur. Biophys. J.* **31**, 356–364 (2002).

211. Landry, D. W., Reitman, M., Cragoe, E. J. & Al-Awqati, Q. Epithelial chloride channel. Development of inhibitory ligands. *J. Gen. Physiol.* **90**, 779–798 (1987).

212. Singh, H. & Ashley, R. H. Redox regulation of CLIC1 by cysteine residues associated with the putative channel pore. *Biophys. J.* **90**, 1628–1638 (2006).

213. Tulk, B. M., Kapadia, S. & Edwards, J. C. CLIC1 inserts from the aqueous phase into phospholipid membranes, where it functions as an anion channel. *Am. J. Physiol. Cell Physiol.* **282**, C1103–C1112 (2002).

214. Warton, K. *et al.* Recombinant CLIC1 (NCC27) assembles in lipid bilayers via a pH-dependent two-state process to form chloride ion channels with identical characteristics to those observed in Chinese hamster ovary cells expressing CLIC1. *J. Biol. Chem.* **277**, 26003–26011 (2002).

215. Milton, R. H. *et al.* CLIC1 function is required for beta-amyloid-induced generation of reactive oxygen species by microglia. *J. Neurosci.* **28**, 11488–11499 (2008).

216. Della Bianca, V., Dusi, S., Bianchini, E., Dal Prà, I. & Rossi, F. β-amyloid activates the O2/·- forming NADPH oxidase in microglia, monocytes, and neutrophils. A possible inflammatory mechanism of neuronal damage in Alzheimer's disease. *J. Biol. Chem.* **274**, 15493–15499 (1999).

217. Novarino, G. *et al.* Involvement of the intracellular ion channel CLIC1 in microglia-mediated beta-amyloid-induced neurotoxicity. *J. Neurosci.* **24**, 5322–5330 (2004).

218. Parachikova, A. *et al.* Inflammatory changes parallel the early stages of Alzheimer disease. *Neurobiol. Aging* **28**, 1821–1833 (2007).

219. Shimohama, S. *et al.* Activation of NADPH Oxidase in Alzheimer's Disease Brains. *Biochem. Biophys. Res. Commun.* **273**, 5–9 (2000).

220. Valenzuela, S. M. *et al.* The nuclear chloride ion channel NCC27 is involved in regulation of the cell cycle. *J. Physiol.* **529 Pt 3**, 541–552 (2000).

221. Harrop, S. J. *et al.* Crystal Structure of a Soluble Form of the Intracellular Chloride Ion Channel CLIC1 (NCC27) at 1.4-?? Resolution. *J. Biol. Chem.* **276**, 44993–45000 (2001).

222. Valenzuela, S. M. *et al.* Molecular cloning and expression of a chloride ion channel of cell nuclei. *J. Biol. Chem.* **272**, 12575–12582 (1997).

223. Goodchild, S. C. *et al.* Metamorphic response of the CLIC1 chloride intracellular ion channel protein upon membrane interaction. *Biochemistry* **49**, 5278–5289 (2010).

224. Wilce, M. C. & Parker, M. W. Structure and function of glutathione S-transferases. *Biochim Biophys Acta* **1205**, 1–18 (1994).

225. Board, P. G. *et al.* Identification, characterization, and crystal structure of the omega class glutathione transferases. *J. Biol. Chem.* **275**, 24798–24806 (2000).

226. Littler, D. R. *et al.* The Intracellular Chloride Ion Channel Protein CLIC1 Undergoes a Redox-controlled Structural Transition. *J. Biol. Chem.* **279**, 9298–9305 (2004).

227. Tulk, B. M., Schlesinger, P. H., Kapadia, S. a. & Edwards, J. C. CLIC-1 functions as a chloride channel when expressed and purified from bacteria. *J. Biol. Chem.* **275**, 26986–26993 (2000).

228. Tonini, R. *et al.* Functional characterization of the NCC27 nuclear protein in stable transfected CHO-K1 cells. *FASEB J.* **14**, 1171–1178 (2000).

229. Singh, H., Cousin, M. a. & Ashley, R. H. Functional reconstitution of mammalian 'chloride intracellular channels' CLIC1, CLIC4 and CLIC5 reveals differential regulation by cytoskeletal actin. *FEBS J.* **274**, 6306–6316 (2007).

230. Berry, K. L., Bülow, H. E., Hall, D. H. & Hobert, O. A C. elegans CLIC-like protein required for intracellular tube formation and maintenance. *Science* **302**, 2134–2137 (2003).

231. Fanucchi, S., Adamson, R. J. & Dirr, H. W. Formation of an unfolding intermediate state of soluble chloride intracellular channel protein CLIC1 at acidic pH. *Biochemistry* **47**, 11674–11681 (2008).

232. Johansson, S. *et al.* Probing natural killer cell education by Ly49 receptor expression analysis and computational modelling in single MHC class I mice. *PLoS One* **4**, (2009).

233. Redhead, C., Sullivan, S. K., Koseki, C., Fujiwara, K. & Edwards, J. C. Subcellular distribution and targeting of the intracellular chloride channel p64. *Mol. Biol. Cell* **8**, 691–704 (1997).

234. Pitt-Rivers, R. & Impiombato, F. S. The binding of sodium dodecyl sulphate to various proteins. *Biochem. J.* **109**, 825–830 (1968).

235. Dunker, A. K. & Rueckert, R. R. Observations on molecular weight determinations on polyacrylamide gel. *J. Biol. Chem.* **244**, 5074–5080 (1969).

236. Ulmschneider, M. B. & Sansom, M. S. Amino acid distributions in integral membrane protein structures. *Biochim. Biophys. Acta* **1512**, 1–14 (2001).

237. Kongsuphol, P., Fang, K. B. & Ding, Z. Lipid bilayer technologies in ion channel recordings and their potential in drug screening assay. *Sensors Actuators B Chem.* **185**, 530–542 (2013).

238. Xu, J. *et al.* Ion-channel assay technologies: quo vadis? *Drug Discov. Today* **6**, 1278–1287 (2001).

239. Avdeef, A. & Testa, B. Physicochemical profiling in drug research: a brief survey of the state-of-the-art of experimental techniques. *Cell. Mol. Life Sci.* **59**, 1681–1689 (2002).

240. Ruell, J. A., Tsinman, K. L. & Avdeef, A. PAMPA—a drug absorption in vitro model. *Eur. J. Pharm. Sci.* **20**, 393–402 (2003).

241. Kuyper, C. L., Kuo, J. S., Mutch, S. A. & Chiu, D. T. Proton Permeation into Single Vesicles Occurs via a Sequential Two-Step Mechanism and Is Heterogeneous. *J. Am. Chem. Soc.* **128**, 3233–3240 (2006).

242. Nisisako, T., Portonovo, S. a & Schmidt, J. J. Microfluidic passive permeability assay using nanoliter droplet interface lipid bilayers. *Analyst* **138**, 6793–800 (2013).

243. Avdeef, A. *et al.* Caco-2 permeability of weakly basic drugs predicted with the Double-Sink PAMPA method. *Eur. J. Pharm. Sci.* **24**, 333–349 (2005).

244. Thutupalli, S., Herminghaus, S. & Seemann, R. Bilayer membranes in micro-fluidics: from gel emulsions to soft functional devices. *Soft Matter* **7**, 1312 (2011).

245. Czekalska, M. A. *et al.* A droplet microfluidic system for sequential generation of lipid bilayers and transmembrane electrical recordings. *Lab Chip* (2015). doi:10.1039/C4LC00985A

246. Cevc, G. & Richardsen, H. Lipid vesicles and membrane fusion. *Adv. Drug Deliv. Rev.* **38**, 207–232 (1999).

247. Matos, P. M. *et al.* Anionic lipids are required for vesicular stomatitis virus G protein-mediated single particle fusion with supported lipid bilayers. *J. Biol. Chem.* **288**, 12416–25 (2013).